universität wien

DIPLOMARBEIT

Titel der Diplomarbeit

Genetic Analysis of Homologous Recombination at *Arabidopsis thaliana* Telomeres

angestrebter akademischer Grad

Magister der Naturwissenschaften (Mag. rer.nat.)

Verfasserin / Verfasser:	Christian Sailer
Matrikel-Nummer:	0101214
Studienrichtung (lt. Studienblatt):	A490 Molekulare Biologie
Betreuerin / Betreuer:	Ortrun Mittelsten-Scheid

Wien, am 31.3.2008

Abstract

Telomeres are the end of linear chromosomes. The main function of telomeres is to protect the chromosome end from being recognized as a DNA Double Strand Break (DSB). In higher eukaryotes this is achieved by a T-loop structure. In this structure the single stranded 3' chromosome end invades the duplex telomeric DNA. It is thought that this process requires the Homologous Recombination (HR) machinery. Unlike a DNA repair event, the T-loop structure is not resolved. How this bi-modal behavior at telomeres is achieved is not understood. Proteins of the HR machinery, like the MRN (MRE11-RAD50-NBS1) complex, are located at telomeres. RAD51 as well as the BCDX2 (RAD51B-RAD51C-RAD51D-XRCC2) and CX3 (RAD51C-XRCC3) complexes are necessary for the strand invasion step of HR. Some studies also suggest a resolving role of the BCDX2 and CX3 complexes. Even though biochemical data on these two complexes exist, genetic data is missing. The role of these complexes in T-loop metabolism is unknown. In this thesis I utilized *Arabidopsis thaliana* as a model system to examine genetic requirements of telomeric recombination. Mutations in one of the five genes building the BCDX2 and CX3 complexes are viable, which is in contrast to mice, where mutations in *RAD51C* and *XRCC2* are embryo-lethal. In this thesis we present the first data on genetic interaction between genes encoding proteins of the BCDX2 and CX3 complexes. We also investigated the role of RAD51 and MRE11 in T-loop metabolism. To test for functional redundancies within the BCDX2 and CX3 complexes, we generated double and triple mutant combinations of recombination genes with *ku70*$^{-/-}$. This mutation results in extra-chromosomal telomeric circles (t-circles) that can be used to monitor HR at telomeres. I tested six different mutant combinations and obtained triple mutants for four of them. In all four triple mutant combinations, t-circles were present. However, I failed to obtain *rad51c-1 xrcc3-1 ku70-1* and *mre11-3 rad51c-1 ku70-1* combinations. Segregation analysis revealed a Non-Mendelian segregation in F2 populations derived from both crossings. Further analysis revealed a translocation to be the cause for the Non-Mendelian behavior in the *rad51c-1 xrcc3-1* combination. This translocation physically linked the two genes. In case of the *mre11-3 rad51c-1* combination we do not know the reason for the Non-Mendelian behavior yet. Further experiments will be needed to answer this question.

Introduction

1. Telomeres

1.1. Function of Telomeres

Telomeres are the ends of linear chromosomes. They consist of tandem repeats. During DNA replication the parental 3' chromosome end is replicated by the leading strand mechanism, whereas the parental 5' chromosome end is replicated by the lagging strand mechanism. Therefore the parental 5' chromosome end cannot be replicated in full as the sequence lost after degradation of the last RNA primer cannot be replaced. Consequently, telomeric DNA is lost with each round of the cell cycle. This phenomenon is referred to as the end replication problem. Additionally, telomeres can also be shortened by other mechanisms, which are referred to as Telomere Rapid Deletion (TRD) (Li and Lustig 1996; Watson and Shippen 2007).

Telomere loss due to the end replication problem or TRD is counteracted by telomerase. Telomerase is a reverse transcriptase which contains its own RNA template. This RNA template is complementary to the tandem repeats at the 3' chromosome end. In stem cells, and also in many cancer cells, telomeres can be elongated due to telomerase activity. In contrast, telomerase is usually inactive in somatic cells.

Since somatic cells do not have telomerase activity, telomeres shorten. After a certain number of cell divisions, animal cells undergo cellular senescence and cease dividing, because telomeres become too short to be functional. In cell culture, this phenomenon is known as the Hayflick limit. Since telomeres shorten in the course of human life, this phenomenon may be partially responsible for aging.

One main function of a telomere is to distinguish the chromosome end from the most dangerous DNA damage, a DNA Double Strand Break (DSB). Telomeres protect natural DNA ends from inappropriate repair. If telomeres shorten below a critical length, they are recognized as DNA DSB, triggering DNA repair events.

As a result of these DNA repair events, two chromosome ends fuse, forming a dicentric chromosome. During mitosis the two centromeres of this dicentric chromosome can attach to opposite spindle poles. The spindle tears the dicentric chromosome apart.

Breakage can occur anywhere along the fused chromosome. This sequence of events is called Breakage-Fusion-Bridge (BFB) cycle and was discovered by Barbara McClintock in maize. Broken ends fuse again resulting in another BFB cycle.

Due to formation of dicentric chromosomes, genomic information is no longer segregated equally between the two daughter cells. This effect becomes enhanced due to continuing BFB cycles. Therefore BFB cycles lead to genome instability. Severe genome instability usually results in cell senescence or cell death.

Cells containing mutations in the mechanisms protecting from the effects of genome instability (e.g. by avoidance of apoptosis (Hanahan and Weinberg 2000)) survive and proliferate. In animals survived genomic instabilities and mutations overriding the control mechanisms, like apoptosis and cell cycle arrest, but also telomeres below a critical length, can result in cancer.

1.2. Telomere Structure

In *Arabidopsis thaliana* telomeres consist of tandem TTTAGGG repeats ranging from 2kb to 4kb in length. Degradation of the RNA primer after DNA synthesis leaves a short 3' overhang. Since the nucleotide sequence of the 3' overhang is G-rich, this overhang is also referred to as the G-overhang. The C-strand is then further resected to make the G-overhang longer by an unidentified exonuclease (fig. 2-1).

Fig. 2-1: Repeat structure and 3' overhang of a telomere. The last base is unknown.

This G-overhang is a conserved feature across all species with linear chromosomes.

A major question in telomere biology is why is the chromosome end not recognized as a DNA DSB? Telomeres build up a special nucleoprotein structure with proteins associated especially with the telomeric tandem repeats. This special nucleoprotein structure is thought to protect the chromosome end from inappropriate DNA repair events. Organisms have evolved different protection structures. In *Tetrahymena sp.* for example a protein binds DNA at the very end of the telomere. In *Saccharomyces cerevisiae* the telomere associates with, for example, CDC13 proteins and as in *Tetrahymena sp.* CDC13 binds the very end of telomeric sequence. In higher eukaryotes proteins like the Telomeric Repeat Factors (TRF1 and 2) and the Protector Of

Telomeres 1 (POT1) are part of a protein complex referred to as Shelterin (de Lange 2005). Shelterin is specifically found at telomeres. It is believed that interaction between shelterin and the telomeric DNA leads to folding back of the 3' G-overhang, allowing it to invade internal duplex telomeric sequences. This structure is called the Telomere loop (T-loop, fig. 2-2) (Griffith, Comeau et al. 1999; Cesare, Quinney et al. 2003; de Lange 2004; Zellinger and Riha 2007).

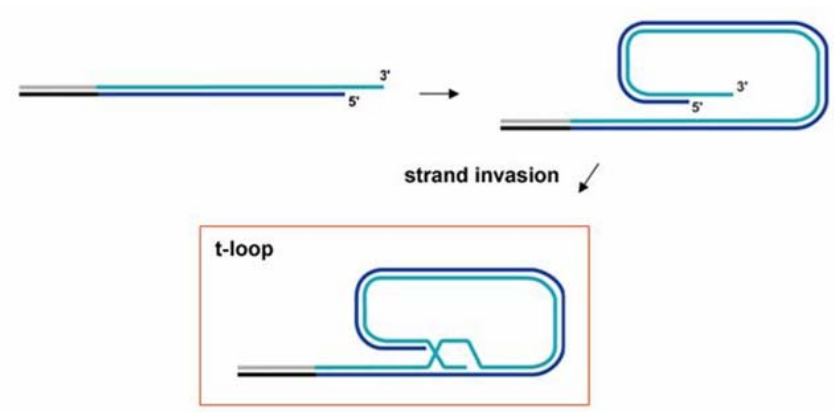

Fig. 2-2: Schematic representation of T-loop formation. First, the 3' G-overhang is formed by resection of the 5' end by an unidentified nuclease. Second, the telomere folds back and the 3' G-overhang invades homologous telomeric sequence. © Karel Riha

The formation of the T-loop is reminiscent of the first steps in Homologous Recombination (HR), namely strand invasion. In contrast to HR, the T-loop structure is not generally processed further. Although the T-loop structure is essential for chromosome end protection no data exists on its metabolism. This thesis addresses questions relating to T-loop metabolism.

Two faces appear in T-loop biology: First, the T-loop has to hide the telomere, which can be recognized as a DSB, from DNA repair factors (which includes HR machinery), and second, the HR machinery is needed to form the T-loop. The question arises, how this T-loop structure is distinguished from an HR intermediate (fig. 2-2). Why is it not resolved as normally happens in HR?

In order to address these questions, we need to know how homologous recombination functions. In the next chapter I will give a short overview of DSB repair by HR.

2. Homologous Recombination

2.1. Overview of Double Strand Break (DSB) Repair by Homologous Recombination (HR)

Homologous Recombination (HR) is a high fidelity mechanism for templated repair of DNA damage.

The repair of a DNA DSB by HR can be divided into five steps: (1) Recognition of the DSB, (2) strand resection, (3) strand invasion, (4) DNA synthesis and branch migration and (5) resolution (fig. 2-3).

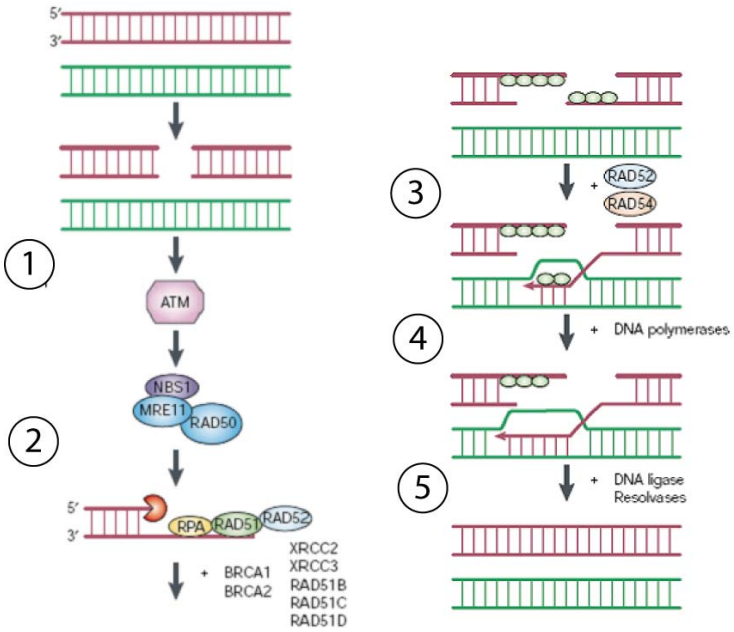

Fig. 2-3: Schematic overview of DSB repair by Homologous Recombination. 1) Recognition of the DSB, 2) strand resection, 3) strand invasion, 4) DNA synthesis and branch migration, 5) resolution. Figure adapted from van Gent, Hoeijmakers, Kanaar, 2001 ((van Gent, Hoeijmakers et al. 2001), fig. 3).

2.2. Recognition – The MRN complex and ATM

The MRN complex consists of the three proteins MRE11 (Meiotic REcombination), RAD50 (RADiation sensitive 50) and NBS1 (Nijmegen Breakage Syndrome). It is one of the first complexes that binds to a DSB. The importance of this complex is reflected by the rare genetic diseases Nijmegen Breakage Syndrome where *NBS1* is mutated and Ataxia Telangiectasia Like Disease (ATDL) where *MRE11* carries a mutation. These diseases are characterized by developmental neurological disorders and T-cell defects. It has been shown that the localization to DNA damage foci (accumulation of proteins in the cell at the sites of DSB) is dependent on Ataxia Telangiectasia Mutated (ATM). As ATM is a checkpoint kinase, this indicates that the MRN complex is involved in the DNA damage checkpoint response. The MRN complex is also found in DNA

replication foci, illustrating a role for this complex in normal DNA replication (reviewed in (D'Amours and Jackson 2002)).

2.3. End Resection

The 5' end has to be resected in order to gain a 3' overhang long enough for strand invasion of the homologous template.

Even though it has not been shown that the MRN complex is responsible for telomere strand resection to yield a 3' overhang, the MRE11 protein contains an exonuclease activity (which is 3' to 5'). The exonuclease activity of MRE11 is active on different substrates and is therefore thought to be involved in this first step of HR. In meiotic cells MRN was shown to be the exonuclease responsible for strand resection at a DSB (reviewed in (D'Amours and Jackson 2002)).

The nuclease responsible for strand resection in somatic cells during DSB repair is unknown.

2.4. Strand Invasion – RecA, RADA, RAD51 and Its Paralogs

The 3' overhang generated by an exonuclease needs proteins in order to be able to invade a homologous DNA double helix. These "recombinase" proteins belong to the RecA/RAD51 family.

2.4.1. RecA and the Evolution of the Five RAD51 Paralogs

In bacteria strand invasion is carried out by the RecA (Recombinase A) protein. RecA covers the single stranded DNA in a highly ordered fashion (reviewed in (D'Amours and Jackson 2002; West 2003; Schlacher and Goodman 2007)), forming a nucleoprotein filament. This nucleoprotein filament is essential for strand invasion. Orthologs of RecA are found in all three domains of life. It is RADA in archea and RAD51 in eukaryotes. The structure of the nucleoprotein filament is more highly conserved than the sequence of the proteins. Phylogenetic analysis revealed that orthologs in archea and eukaryotes can be split into two groups, the RADα and the RADβ group (Lin, Kong et al. 2006). The RADα group contains the archeal RADA and the eukaryotic DMC1 (Disrupted Meiotic cDNA1) and RAD51. In the RADβ group the archeal paralog RADB are found

as well as the other five eukaryotic paralogs RAD51B, RAD51C, RAD51D, XRCC2 (X-Ray Cross Complementing 2) and XRCC3 (fig. 2-4, (Lin, Kong et al. 2006)).

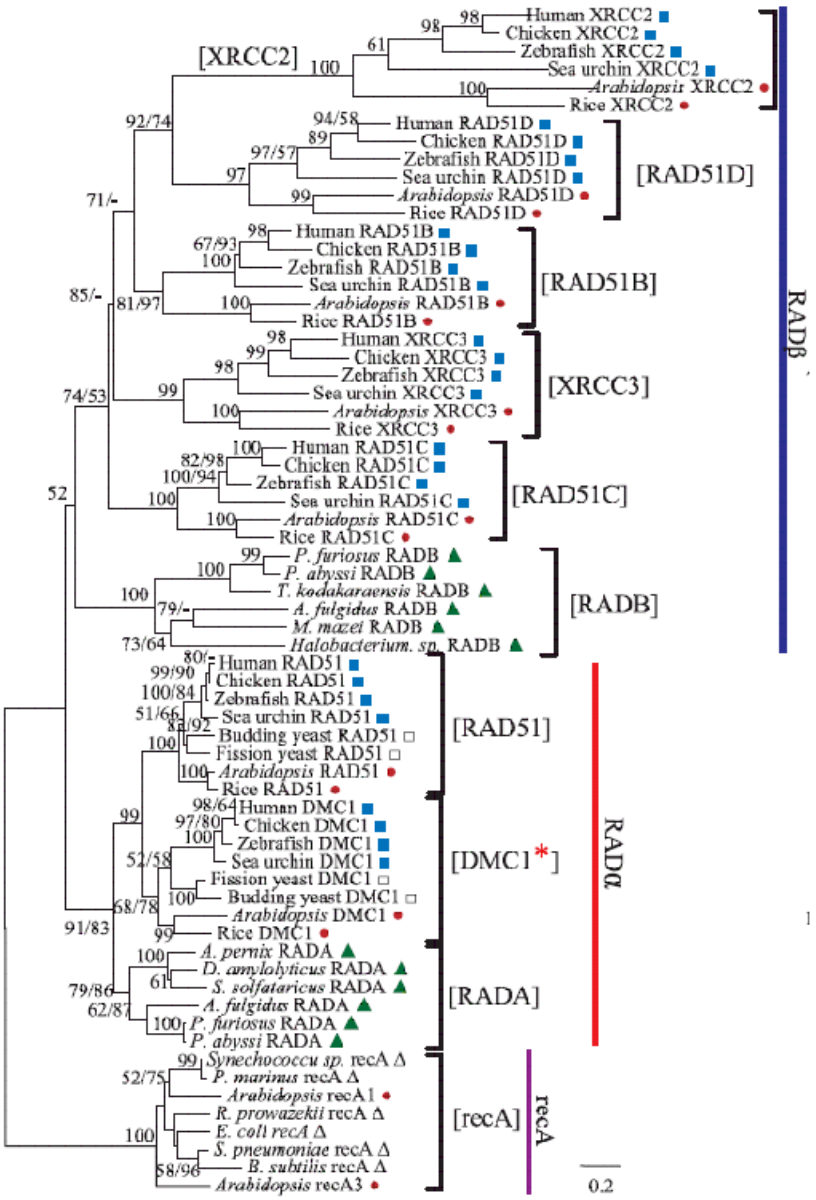

Fig. 2-4: Phylogeny of the RecA orthologs. Figure taken from Lin Z. et al. ((Lin, Kong et al. 2006), fig. 2A).

2.4.2. The BCDX2 and the CX3 Complex

There are seven RecA orthologs in eukaryotes. DMC1 is a meiosis specific protein and RAD51 covers the single stranded 3' overhang the same way as RecA and RADA. The loading of RAD51 onto the 3' overhang is a tightly regulated process. RAD51 alone has only a weak affinity for single stranded DNA (ssDNA) compared to double stranded DNA (dsDNA) (reviewed in (van Gent, Hoeijmakers et al. 2001)). Its assembly into a nucleoprotein filament is assisted by RPA, RAD52 and BRCA1 (reviewed in (van Gent, Hoeijmakers et al. 2001; West 2003)). The five RAD51 paralogs, RAD51B, RAD51C,

RAD51D, XRCC2 and XRCC3 also play a role in strand invasion. Their exact role is still not clear.

Pull down experiments and domain mapping have revealed that these five paralogs form two distinct complexes (Masson, Tarsounas et al. 2001; Miller, Sawicka et al. 2004). Different pull down experiments demonstrated that RAD51B associates with RAD51C, but not with RAD51D or XRCC2. RAD51C associates with RAD51B, RAD51D and XRCC3 (Masson, Tarsounas et al. 2001). Further experiments led to the model of complex formation and interaction partners shown in figure 2-5.

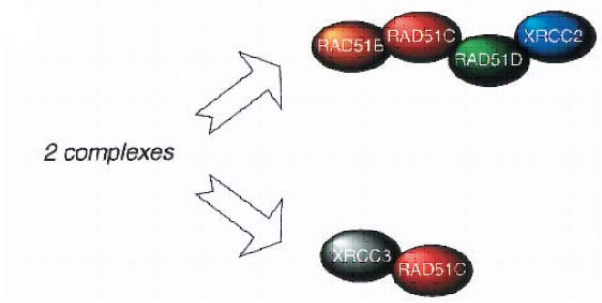

Fig. 2-5: Cartoon of the two RAD51 paralog complexes. This figure is taken form Masson et al. ((Masson, Tarsounas et al. 2001), fig. 3B)

One complex is named BCDX2 since it is formed by the proteins RAD51B, RAD51C, RAD51D and XRCC2. The other complex is named CX3 since it consists of the two proteins RAD51C and XRCC3. It is worth mentioning that RAD51C is part of both complexes.

The protein interactions proposed in fig. 2-5 by pull down experiments was later verified by domain mapping done by Miller KA et al (Miller, Sawicka et al. 2004) (fig. 2-6).

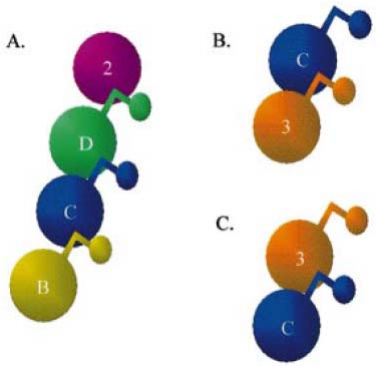

Fig. 2-6: Result of the domain mapping. ((Miller, Sawicka et al. 2004), fig. 7). A) Protein Order of the BCDX2 complex, B) and C) Two possibilities how RAD51C interacts with XRCC3. This figure is taken form their publication.

The CX3 complex can be built in two ways as shown in fig. 2-6.

2.5. Resolution – RuvC, MUS81, RAD51C and XRCC3

After the early steps in HR (DSB recognition, strand resection, strand invasion), DNA is synthesized, utilizing the invaded 3' end as a primer. The result of this process is intertwined DNA molecules. The structure formed is known as a Holliday junction. This Holliday Junction needs to be resolved to separate the two DNA molecules again. In bacteria this is accomplished by the RuvABC (Recombination/Repair after UV) complex in which RuvC has the structure specific endonuclease activity. So far, all attempts to find the Holliday Junction resolvase, and therefore an ortholog of RuvC, in eukarya have failed. There was a great deal of excitement about MUS81 (ethyl-Methanesulfonate Uv Sensitive clone 81, discovered in *S. cerevisiae*), which showed Holliday junction resolvase activity, but on the other hand, a much higher activity on 3' flap structures, which occur when the replication fork stalls ((Constantinou, Chen et al. 2002; Blais, Gao et al. 2004) and reviewed in (Haber and Heyer 2001; West 2003)). Another paper proposed a role for RAD51C in Holliday junction resolution (Liu, Masson et al. 2004).

This work was done in HeLa nuclear cell extracts. A later publication from the same group presented data demonstrating binding of recombinant RAD51C and XRCC3 proteins to a Holliday junction (Liu, Tarsounas et al. 2007). Data demonstrating actual Holliday junction cleavage with these recombinogenic proteins is still missing.

3. T-loop Resolution

The T-loop structure resembles the Holliday junction intermediate of HR. The question arose, how the T-loop is distinguished from an HR intermediate and therefore not further processed like a DSB is.

Fig. 2-7 schematically shows what happens, if the T-loop is resolved. As already briefly mentioned, telomeres shorten not only due to the end replication problem, but can be shortened more rapidly by TRD. One mechanism is the resolution of the T-loop. The T-loop is thought to be a well protected structure, but when this protection is lost, the T-loop is accessible to the HR machinery. Resolution of the Holliday junction results in a shortened telomere and an extrachromosomal circular DNA molecule (t-circle).

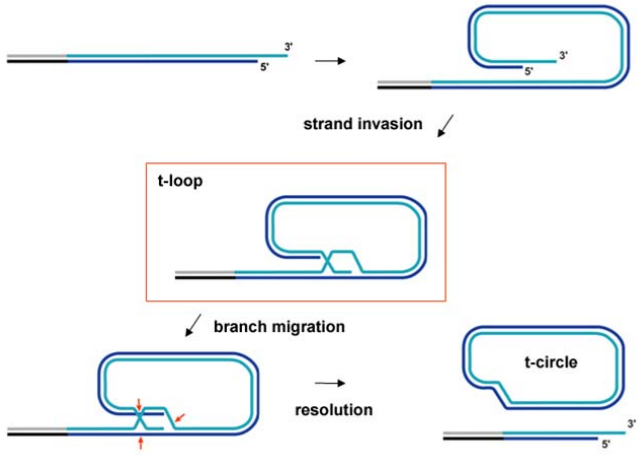

Fig. 2-7: Resolution of the T-loop results in a shortened telomere and an extrachromosomal circle of telomeric DNA, called a t-circle. © Karel Riha

In human cell cultures a mutation in Telomere Repeat binding Factor 2 (TRF2) results in rapid shortening of telomeres (Wang, Smogorzewska et al. 2004). T-circles were found in this $TRF2^{\Delta B}$ mutation. T-circles were also found in cells from Werner Syndrome patients (Li, Jog et al. 2008). In MEFs (Mouse Embryonic Fibroblasts) deletion of *Pot1a* results in elongated telomeres and in a p53 dependent cell senescence. But in a $p53^{-/-}$ background, the $pot1a^{\Delta/\Delta}$ mutation results in t-circle formation (Wu, Multani et al. 2006). In this double mutant t-circle formation is NBS1 dependent.

Recently, T-loop resolution was also described in *ku* mutants in *A. thaliana* (Zellinger, Akimcheva et al. 2007).

3.1. The KU heterodimer in *A. thaliana*

Ku has functionally conserved homologs throughout all three domains (reviewed in (Aravind and Koonin 2001; Downs and Jackson 2004)). Ku is a heterodimer formed by two subunits of 70 and 80 kDa (86 kDa in higher eukaryotes), referred to as KU70 and KU80, respectively. The heterodimer is ring shaped and binds (dsDNA) in a sequence independent manner through interaction with the phosphate backbone of the DNA helix, but not the bases of the DNA helix. Ku binds to DNA double stranded ends with either a blunt end or overhang. Originally identified as an autoantigen (Mimori, Akizuki et al. 1981), Ku is of central importance in DNA repair, antigen-receptor-gene rearrangement, mobile genetic elements, transcription, apoptosis and maintenance of telomeres. Ku is the first protein that binds to a DSB resulting in recruitment of the DNA-dependent protein kinase catalytic subunit (DNA-PK_{CS}), leading to repair of the DSB by Non-Homologous-End-Joining (NHEJ) (reviewed in (West 2003)). Even though lower

eukaryotes and plants lack DNA-PK_{CS}, Ku is still of central importance for NHEJ (reviewed (Downs and Jackson 2004; Fisher and Zakian 2005)).

The effect of *ku* mutants in telomere function varies in different organisms. Ku deficiency in *Saccharomyces cerevisiae, Schizosaccharomyces pombe* and *Homo sapiens* results in shortened telomeres and increased length of G-overhangs (table 1 in (Fisher and Zakian 2005)). This is in contrast to *Arabidopsis thaliana* where Ku deficiency results in increased length of G-overhangs (Riha and Shippen 2003) but also in longer telomeres (Bundock and Hooykaas 2002; Riha, Watson et al. 2002; Riha and Shippen 2003). Ku therefore blocks access of telomerase.

In *A. thaliana* Ku deficiency also results in formation of extrachromosomal t-circles, which is probably the result of a recombination event. Ku therefore blocks access of the recombination machinery to telomeres. T-circle formation occurs if either one of the subunits, KU70 or KU80, is knocked out (Zellinger, Akimcheva et al. 2007) (fig. 2-8).

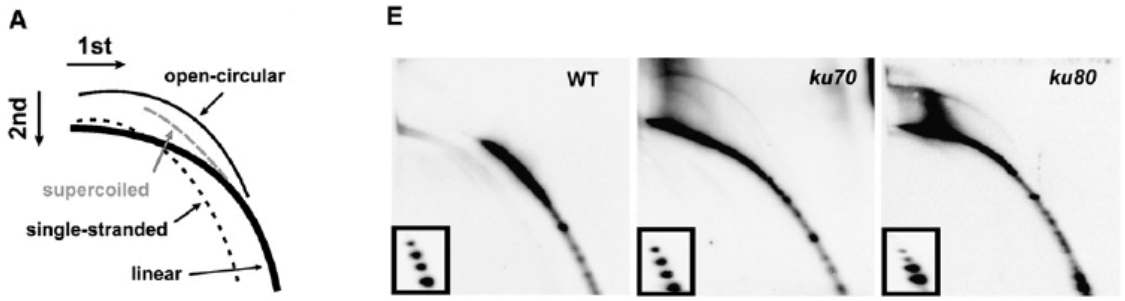

Fig. 2-8: 2D gels of Col-0 wild type (wt) plants and *ku* mutants. A) shows a cartoon of DNA migration in a 2D gel. E) shows the result on Col-0 wt and *ku70*$^{-/-}$ and *ku80*$^{-/-}$ mutants. Figures taken from figure 1 in Zellinger et al. (Zellinger, Akimcheva et al. 2007) and modified with Photoshop.

To test whether genes involved in HR are required for t-circle excision, Barbara Zellinger created double mutants of *ku70*$^{-/-}$ with mutants in the 5 RAD51 paralogs. No t-circle suppression was found in the double mutants, nor does it look like there is any decrease in t-circle formation.

This result is in contrast to Wang et al, who showed that *XRCC3* is essential for t-circle formation in a human cell line (Wang, Smogorzewska et al. 2004).

Figure 2-9 summerizes the current T-loop formation and resolution model.

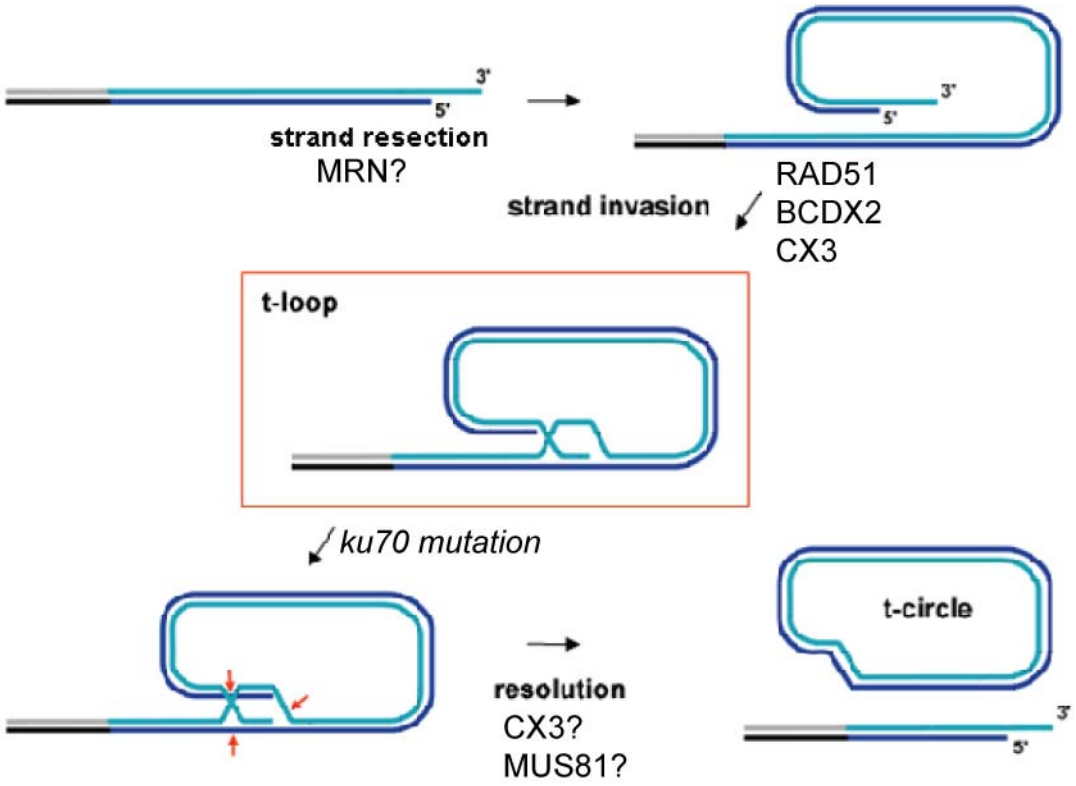

Fig. 2-9: Cartoon of T-loop formation and resolution. The 5' strand is resected with a possible involvement of the MRN complex, yielding a 3' overhang which is covered by RAD51. The BCDX2 and CX3 complex assist in strand invasion. The resulting structure is called T-loop and is depicted in the red square. This structure is protected and stable. A *ku70* mutation leads to loss of T-loop protection and results in further processing by the HR machinery and resolution. The protein responsible for T-loop resolution is unknown. Possible candidates are the CX3 complex or MUS81. T-loop resolution results in an extrachromosomal t-circle and a shortened telomere.

4. Working Hypothesis and Aims

Our working hypothesis was that t-circle formation is the result of a homologous recombination event.

The goal of this diploma thesis was to find suppressor mutants for *ku70*$^{-/-}$ dependent t-circle formation in a candidate gene approach.

I optimized genotyping for the candidate genes to make it more efficient.

Candidate genes were analyzed for a possible role in telomere biology and t-circle formation. *FAS1* (FASciata 1), which has a role in chromatin formation, *APOLLO*, an exonuclease found at telomeres, *BARD1*, a possible regulator of strand invasion and *MUS81* an endonuclease with Holliday junction resolvase activity.

To investigate possible redundancies between RAD51-like recombination genes that have been tested before in double mutants with *ku70*$^{-/-}$ (Zellinger, Akimcheva et al.

2007), I generated various triple mutant combinations. These combinations were propagated to F2 and the triple mutants analyzed for the presence of t-circles.

Results

1. Genes Genetically Tested for their Role in T-circle Excision

Mutants in 11 genes were used for reverse genetics in this thesis. Their positions in the *A. thaliana* genome are depicted in fig. 3-1.

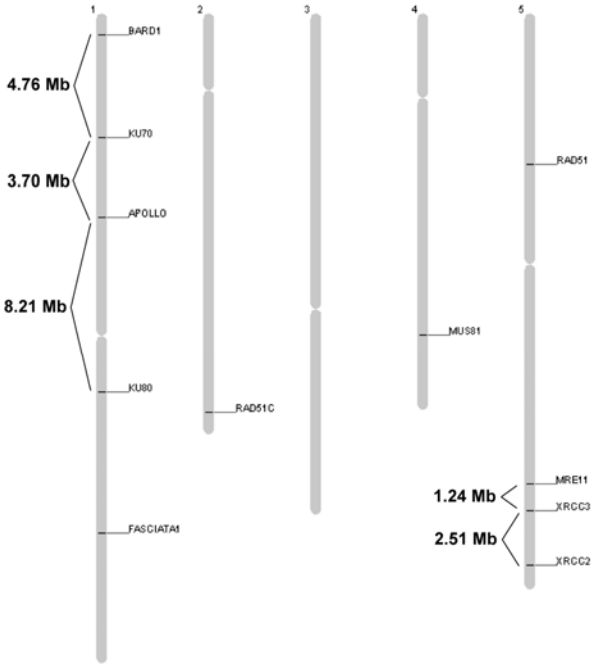

Fig. 3-1: Physical map of genes used in this thesis. The distances between some genes are indicated. The map was drawn utilizing an online tool: http://www.arabidopsis.org/jsp/ChromosomeMap/tool.jsp

Table 3-1 gives a short overview of the name and the physical location of the gene and a very short ontology.

Name	Location	Ontology
KU70	At1g16970	DSB repair by NHEJ
KU80	At1g48050	DSB repair by NHEJ
FAS1	At1g65470	Subunit of CAF1, chromatin assembly
Apollo	At1g27410	Exonuclease positioned at telomeres
BARD1	At1g04020	Subunit of E3 ligase built with BRCA1
MUS81	At4g30870	Resolvase?
MRE11	At5g54260	Exonuclease, HR
RAD51	At5g20850	ssDNA binding, HR
RAD51C	At2g45280	Part of the BCDX2 and CX3 complexes, HR, resolvase?
XRCC2	At5g64520	Part of the BCDX2 complex, HR
XRCC3	At5g57450	Part of the CX3 complex, HR, resolvase?

Table 3-1: List of genes used in this thesis, position in the *A. thaliana* genome and brief ontology. DSB – Double Strand Break, NHEJ – Non-Homologous End Joining, CAF1 – Chromatin Assembly Factor 1, BRCA1 – BReast CAncer susceptibility 1, HR – Homologous Recombination, ssDNA – single stranded DNA

2. FASCIATA1 (FAS1) in End Protection

2.1. Function of FAS1

Fasciata1 is the *A. thaliana* ortholog of human p150 and yeast CAC1, which are the largest subunit of the Chromatin Assembly Factor 1 (CAF1). CAF1 is a chromatin chaperone. It facilitates the assembly of nucleosome cores (Ridgway and Almouzni 2000). CAF-1 activity is regulated by phosphorylation in a cell cycle dependent manner. This shows a role of CAF-1 during DNA replication. But CAF-1 driven repair coupled chromatin assembly is stimulated several fold by DNA damage, suggesting a role for CAF-1 after DNA repair (Ridgway and Almouzni 2000). In *S. cerevisiae* CAC1, CAC2 and MSI1 (largest, middle and smallest subunit of CAF-1, respectively) mutants show derepression of silenced genes (van Nocker 2003). In *A. thaliana* FAS mutants show fasciation of the stem, hence the name.

2.2. Mutant Allele Used

The FAS1 gene has the annotated number At1G65470.

The allele *fas1-4* was found in a T-DNA insertion line screen in C24 ecotype in Bernd Reiss' lab. The T-DNA insertion mutant *fas1-4* plants are dwarfed, almost sterile and show a very strong fasciation (Kirik, Pecinka et al. 2006). Assays for determining Intra-Chromosomal Homologous Recombination (ICHR) showed that the frequency of these events is at least a 100 fold higher in *fas1-4* mutants compared to wild type. DAPI staining of nuclei revealed a reduction of chromocenter size and a more blurred picture of heterochromatin, which is not due to different DNA methylation, but due to altered chromatin conformation (Kirik, Pecinka et al. 2006).

Because T-loop formation and t-circle excision are intra-chromatid recombination events, we tested whether the mutation affects telomere structure.

2.3. Terminal Restriction Fragment Analysis

The length of a telomere can be measured with a Terminal Restriction Fragment (TRF) analysis.

2.3.1. Principle of a Terminal Restriction Fragment Analysis

In a Terminal Restriction Fragment (TRF) assay, the DNA is digested by an endonuclease, which doesn't cut in telomeric sequence. The digested DNA is then loaded onto a 0.8% agarose gel and run at low voltage for several hours. After an ethidiumbromide stain to check for equal loading the gel is Southern blotted and the telomeres are detected with a radioactively labeled telomeric probe (see materials and methods). The length variation of the telomeres in the whole plant can be seen from such a blot. Comparisons between TRFs from wild type (wt) and mutant plants will reveal a change in telomere length. If this is the case, this hints to a direct involvement of the studied gene in telomere biology.

2.3.2. TRF of *fas1-4*

Fas1-4 mutants can be easily distinguished by eye. But we could not distinguish between wt and heterozygous plants, since we do not have a genotyping system for this gene. *Fas1-4* is a recessive mutation, so we expect no effect in heterozygotes.

Fig. 3-2 shows the result of the TRF. The left two lanes represent Col-0 wt telomeres and the middle ones represent C24 telomeres. The ecotype C24 has longer telomeres than Col-0, ranging from 2.5kb up to 7kb, compared to 2kb to 5kb respectively. We couldn't detect a clear change in telomere length. Telomeres from G1 *fas1-4* mutants seem to be as long as the C24 wt telomeres (right lanes in fig. 3-2), even though this blot suggests a slight shortening.

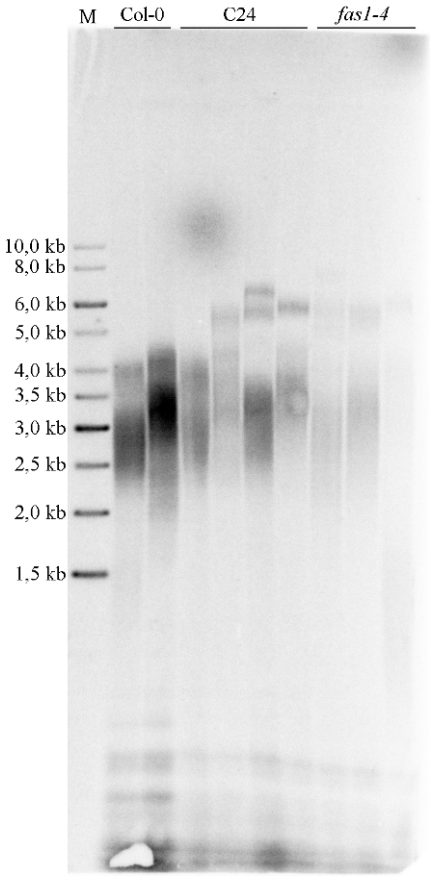

Fig. 3-2: TRF of wild type Col-0, wild type C24 and *fas1-4* (ecotype C24). Telomere lengths of the *fas1-4* mutant plants are in the wild type range (2.5kb – 7kb). Each lane represents telomere lengths from a single plant. The blot was hybridized with a G-strand probe. M – marker, sizes as indicated

We still cannot exclude a small effect on telomere size that can become apparent only after several generations. This was not tested since *fas1-4* mutant plants only produce very few seeds. We did not test for germination of these seeds and if G2 *fas1-4* mutants also produce seeds.

2.4. Telomeric Circle Amplification Analysis

We used this assay to study the effect of the *fas1-4* mutation on telomeric recombination.

2.4.1. Principle of a Telomeric Circle Amplification Assay

In the TCA a C-strand primer is annealed to the denatured t-circles. The C-strand is then amplified with a phi29-DNA-polymerase. Phi29-DNA-polymerase has a very high processivity, a helicase activity and a strong strand displacement activity. Therefore, as polymerizing along the circular molecule, it displaces its own product, resulting in a very long DNA (up to 100kb) molecule. The high molecular weight DNA is separated from the bulk DNA in an alkaline gel and detected by Southern Blot with a telomeric probe. Fig. 3-3 shows a schematic representation of the process.

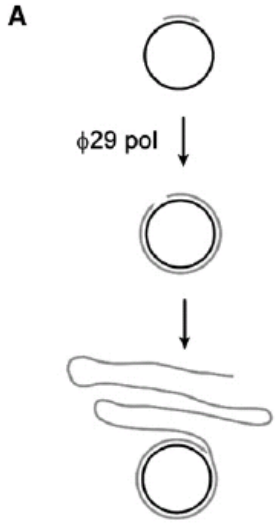

Fig. 3-3: Scheme of TCA. Cartoon taken from Zellinger et al, 2007, Molecular Cell (Zellinger, Akimcheva et al. 2007)

2.4.2. TCA of *fas1-4*

If t-circles are present, the TCA results in a high molecular signal (arrow in fig. 3-4). The signal is very prominent in *ku70*$^{-/-}$ mutants.

I hypothesized that the loosened chromatin structure and the hyper-recombination phenotype are sufficient to enable t-circle formation in the *fas1-4* mutant.

We did not see a change in telomere length but t-circles could still be formed. Fig. 3-4 shows the result.

There was no clear enhancement of t-circles in the *fas1-4* mutant. *Ku70*$^{-/-}$ (left in fig. 3-4) served as positive control. A faint signal was detected in the *fas1-4* mutants. I never compared it to the C24 wt plants, since I only had seeds from heterozygous plants. We lack a genotyping set up, so I could not distinguish between wild type a heterozygote. Wild type and Heterozygotes would have needed to be tested in order to exclude an effect on t-circle formation in heterozygotes.

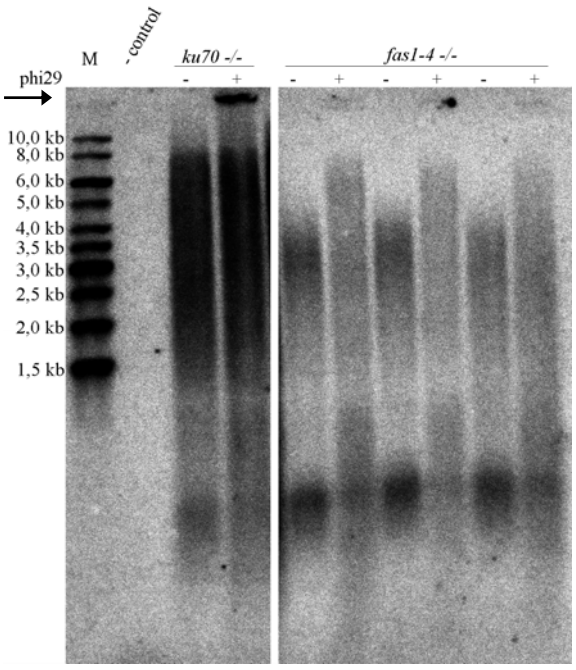

Fig. 3-4: TCA of *fas1-4*. A faint t-circles signal was detected in those mutants. *Ku70*$^{-/-}$ serves as a positive control. + and – indicate presence or absence of phi29-DNA-polymerase. One sample is derived from 2-3 plants of the same genotype and split into two reactions, + and – phi29-DNA-polymerase. Smears are hybridized telomeres. M – marker, sizes as indicated, - control – no DNA, phi29 – phi29-DNA-polymerase

Taking the TRF and TCA result together suggests that simple enhancement of ICHR and a less tight heterochromatic structure are not sufficient to allow prominent t-circle formation. Crossing this mutation to *ku* or *tert* mutants would be interesting to see an effect on telomere length.

3. Analysis of the Role of Recombination Genes in T-loop Metabolism and t-Circle Excision

3.1. Introduction

Up to date it is not known which proteins are involved in T-loop formation and resolution in *A. thaliana*. To address this problem we used a candidate reverse genetics approach. Genes shown to have exo- or endonuclease activity and mutants known to exhibit a recombination phenotype were chosen. The mutant of *Apollo*, which has been shown to have an exonuclease activity and bind to telomeres (van Overbeek and de Lange 2006), was tested if it exhibits a telomere phenotype. Mutants in *BARD1*, which is thought to be a regulator during strand invasion, and *MUS81*, an endonuclease, were crossed to *ku70*$^{-/-}$, a mutant showing t-circle formation, to test for their involvement in t-circle formation.

In the following sections I will describe T-DNA insertion mutants and genotyping of these mutants.

3.1.1. T-DNA Insertion Lines

Currently it is not possible to knock out a targeted gene from a plant's genome by directed excision. That's why insertion mutants are used for genetic analysis. Those lines are generated by infecting the plant with *Agrobacterium tumefaciens* which will incorporate its T-DNA (transfer DNA) randomly into the genome of the transfected plant. In fact the T-DNA used for insertion mutagenesis is not the original T-DNA but was depleted for the genes necessary for Nopalin synthesis.

Usually, more than one copy of the T-DNA is inserted in one locus and these insertions can have different orientations. Frequently micro-deletions and micro-insertions occur during the insertion event at the insertion site. Sometimes, even translocations can happen. The process of T-DNA insertion is not understood in complete detail.

The ends of the T-DNA are defined by sequence, called left border (LB) and right border (RB). The border sequences are used for mapping the insertion site and also for PCR-based genotyping. One T-DNA copy spans about 4500bp and contains a lot of stop codons in all reading frames, which disrupts translation of any gene in which the T-DNA is inserted. Therefore, and for the events described above, the translation machinery cannot read over a T-DNA in most cases, which results in disruption of gene function. The splicing machinery can also be impaired at this locus, due to rearrangements during the insertion event. For these reasons, it is not important, if the T-DNA integrated in an intron or an exon. Sometimes, a transcript can still be made, resulting in a functional, partially functional, differentially functional or non-functional protein. If a new mutant is characterized, RT-PCR and Northern blots need to be utilized to check for transcripts from the locus carrying the insertion. If no transcripts are detected, the mutant line is described as a null-mutation, which is comparable to knock out obtained by excision.

Stock centers maintain mapped insertion lines covering the whole genome of *Arabidopsis thaliana*. The annotated number of T-DNA insertion lines reflects the stock centre in which it was produced and maintained. Here we used SALK lines from the Salk institute for biological studies in San Diego, USA. We sometimes also used GABI-Kat lines from the Bielefeld University, Germany. The *ku* mutants we used were generated in the Wisconsin Arabidopsis gene knock out facility, which already closed down.

3.1.2. Genotyping

It is very important to know the genotype of the material used for the experiments, since only then conclusions about genetics and phenotypes can be drawn.

Having a T-DNA insertion line in hands, genotyping can be easily based on PCR. As presented in the following cartoon, three different primers are needed for genotyping. Two primers (1 and 2 in fig. 3-5) are gene specific and placed the way that the amplification product would span the insertion site. Due to the large size of the T-DNA, the Taq-polymerase is unable of efficient DNA synthesis across the whole insert. Therefore, a product from primers 1 and 2 will only be obtained, if the insert is not present, indicating the presence of the wild type (wt) allele.

One primer (3 in fig. 3-5), is specific for the T-DNAs LB and directs towards the disrupted gene. An amplification product of primers 1 and 3 will only be obtained if the T-DNA insertion is present, indicating the presence of the mutant allele.

If a lot of plants need to be genotyped (e.g. a sterile mutant has to be out-segregated from a heterozygous plant), all three different primers can be used in the same PCR reaction to speed up genotyping. This multiplex PCR cuts down labor and time to half. For a situation as depicted in fig. 3-5, primer 2 will compete with primer 3. Therefore the PCR conditions need to be optimized.

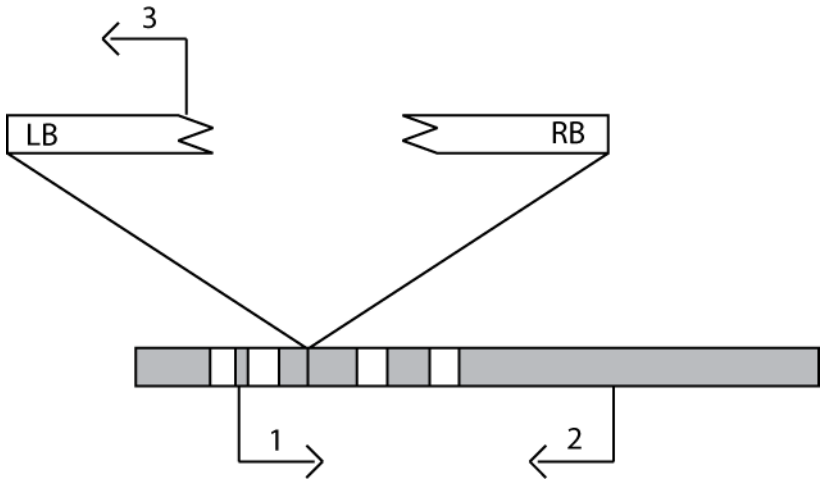

Fig. 3-5: Cartoon of genotyping an insertion mutant. LB – Left Border, RB – Right Border, 1,2,3 – different primers, grey boxes – exons

Optimizations were always done the way that DNA from a heterozygous plant was used as template to test the primer combinations for the wt-allele (primers 1 and 2), and for two possible left borders (primers 1 and 3 and 2 and 3), as well as for the multiplex

PCR. The negative control contained no primers. The multiplex set up was further tested on DNA from wt, heterozygous and mutant plants. Temperature and cycle number were the conditions optimized.

If the conditions for both competing primers are equal, equal amounts of an amplification product from primers 1 and 2 as well as from primers 1 and 3 should be generated. The primers have to be placed the way that those resulting fragments are of different size, at least 200bp for clear separation in an agarose gel electrophoresis. If this is the case, then two bands of different size and of the same intensity should be seen on a gel, if the plant was heterozygous for a T-DNA insertion. Only one band of the appropriate size should be seen if the plant was either wild type or mutant.

3.2. APOLLO

3.2.1. Function of APOLLO

Apollo is an Artemis-like nuclease which has a 5' – 3' exonuclease activity for blunt ends and 3' overhangs. Artemis and Apollo belong to the β-CASP metallo-β-lactamase family of caretaker proteins (Lenain, Bauwens et al. 2006). Apollo interacts with TRF2 and localizes to telomeres via shelterin. The knock down results in a cell arrest and triggers a DNA damage signal via p53 and p21 (van Overbeek and de Lange 2006). The knock out of Apollo leads to severe growth defects in human cell cultures and increased telomere fusions (Lenain, Bauwens et al. 2006). Apollo is therefore thought to take part in global genome integrity and telomere protection. The localization to telomeres and the exonuclease activity make Apollo a candidate to be involved T-loop biology. So far, this protein has not been characterized in plants.

I hypothesized that APOLLO has a role in telomere maintenance in *A. thaliana*.

3.2.2. Identification of *atAPOLLO*

No ortholog of Apollo was described or annotated so far for *A. thaliana*. Therefore a blast search with the human Apollo (hSNM1B) was performed in the lab to find an ortholog in plants. 8 hits with an expectancy value below 0.05 were found (fig. 3-6).

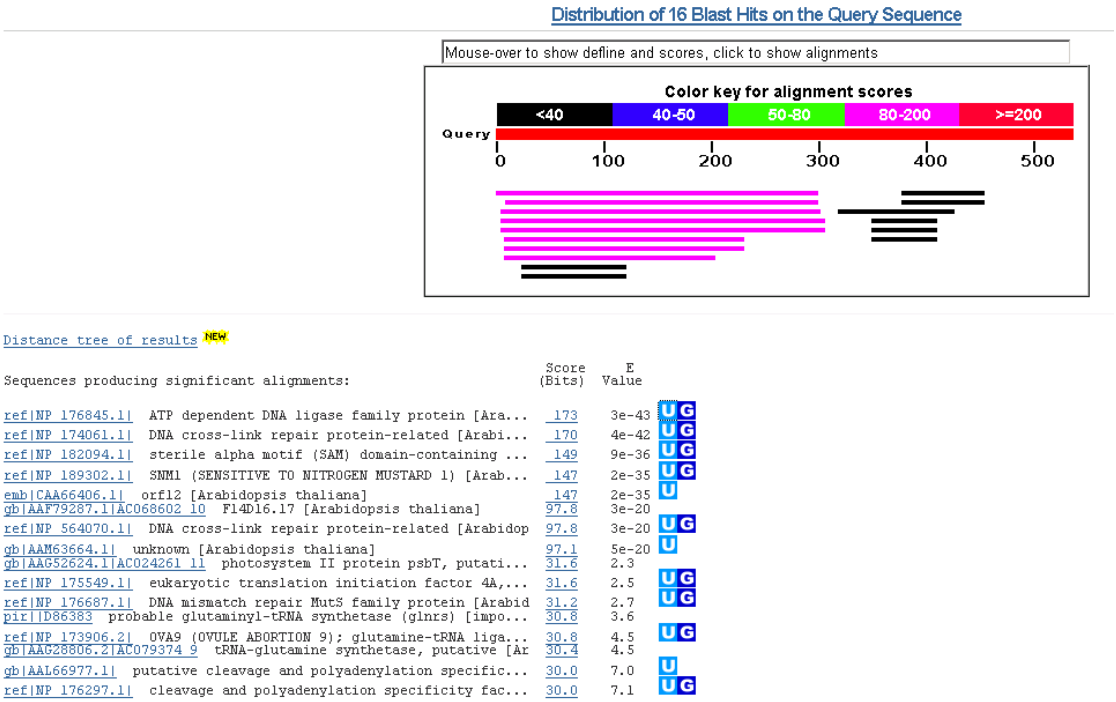

Distance tree of results NEW

Sequences producing significant alignments:	Score (Bits)	E Value
ref|NP_176845.1| ATP dependent DNA ligase family protein [Ara...	173	3e-43
ref|NP_174061.1| DNA cross-link repair protein-related [Arabi...	170	4e-42
ref|NP_182094.1| sterile alpha motif (SAM) domain-containing ...	149	9e-36
ref|NP_189302.1| SNM1 (SENSITIVE TO NITROGEN MUSTARD 1) [Arab...	147	2e-35
emb|CAA66406.1| orf12 [Arabidopsis thaliana]	147	2e-35
gb|AAF79287.1|AC068602_10 F14D16.17 [Arabidopsis thaliana]	97.8	3e-20
ref|NP_564070.1| DNA cross-link repair protein-related [Arabidop	97.8	3e-20
gb|AAM63664.1| unknown [Arabidopsis thaliana]	97.1	5e-20
gb|AAG52624.1|AC024261_11 photosystem II protein psbT, putati...	31.6	2.3
ref|NP_175549.1| eukaryotic translation initiation factor 4A,...	31.6	2.5
ref|NP_176687.1| DNA mismatch repair MutS family protein [Arabid	31.2	2.7
pir||D86383 probable glutaminyl-tRNA synthetase (glnrs) [impo...	30.8	3.6
ref|NP_173906.2| OVA9 (OVULE ABORTION 9); glutamine-tRNA liga...	30.8	4.5
gb|AAG28806.2|AC079374_9 tRNA-glutamine synthetase, putative [Ar	30.4	4.5
gb|AAL66977.1| putative cleavage and polyadenylation specific...	30.0	7.0
ref|NP_176297.1| cleavage and polyadenylation specificity fac...	30.0	7.1

Fig. 3-6: Result of BLAST search for an *A. thaliana* ortholog of APOLLO.

The first hit showed 33% sequence identity and referred to the gene At1g66730. Searching the TAIR (The Arabidopsis Information Resource, www.arabidopsis.org) webpage revealed a protein with a putative metallo-β-lactamase domain and a predicted length of 1417 amino acids (aa). The second hit showed 34% sequence identity. It referred to the gene At1g27410, which was described as a DNA repair metallo-beta-lactamase containing an InterPro domain. Its predicted length was 422 aa. This was closer to the human protein length of 532 aa.

I named this gene *atAPOLLO*.

Figure 3-7 shows the protein alignment of human APOLLO with atAPOLLO.

```
 Score =  165 bits (418),  Expect = 1e-38
 Identities = 117/336 (34%), Positives = 156/336 (46%), Gaps = 54/336 (16%)

Query  11   IAVDFWSLRRAGTARLFFLSHMHSDHTVGLSSTWAR-PLYCSPITAHLLHRHL---QVSK  66
            I+VD W   R G+ + +FL+H+HSDHT GLS  W++ PLYCS  TA L         +S
Sbjct  6    ISVDRW---RNGS-QAYFLTHIHSDHTRGLSGGWSQGPLYCSRTTASLFPSRFPGFDLSL  61

Query  67   QWIQALEVGESHVLPLDEIGQET-MTVTLLDANHCPGSVMFLFEGYFGTILYTGDFRYTP  125
              +  L    S  L     G    + +  +DA+HCPGS+MFLF G FG  LYTGDFR+
Sbjct  62   LRVVPLFSWTSLSLRSPSSGSTVRLHLMAIDAHHCPGSIMFLFRGDFGCFLYTGDFRWDS  121

Query  126  SMLKEPALTLGKQIHT-----LYLDNTNCNPALVLPSRQEAAHQIVQLIRKHPQHNIKIG  180
               E   TL   I       LYLDNT CNP    PSR  A   +  +I  HP H+I I
Sbjct  122  DASDEARTTLVAAIDEFPVDILYLDNTYCNPIYSFPSRLVAVQLVADIIASHPSHDIIIA  181

Query  181  LYSLGKESLLEQLA--LEFQTWVVLSPRRLELVQLLGLADVFTVEEKAGRIHAVDHMEIC  238
            + SLGKE LL  ++  L  + WV   P RL  + LLG  D+FT +    R+ AV
Sbjct  182  VDSLGKEDLLVHVSRILNIKIWV--WPERLRTMHLLGFQDIFTTDTSLTRVRAVPRYSFS  239

Query  239  HSNMLRWNQTHPTIAILPT-----------------------------------SRKIH  262
               +   N   PTI I+P+                                   +  +H
Sbjct  240  IQTLEGLNTMCPTIGIMPSGLPWVKRPFKGDDKLSGSFLTASMKNETVSAKKELEAAAVH  299

Query  263  SSHPDIHVIPYSDHSSYSELRAFVAALKPCQVVPIV  298
               H  ++ + YSDHS Y E+  F+  +KP  +  IV
Sbjct  300  KFHDYMYSVHYSDHSCYEEIGEFIKLVKPKSMKGIV  335
```

Fig. 3-7: Alignment of human Apollo (hSNM1B) (top line) and the identified *A. thaliana* ortholog (bottom line).

3.2.3. Mutant Allele Used

The gene At1g27410 consists of 5 exons. I looked for an insertion line available for this gene at the SIGnAL homepage (http://signal.salk.edu/), and found a GABI-Kat line (GABI_23D05, ecotype Col-0). Using the Lasergene and Vector NTI software I annotated the T-DNA insertion into exon 3, based on the sequence data from the LB available on the SIGnAL homepage (http://signal.salk.edu/cgi-bin/tdnaexpress). I named the mutant allele *apollo-1* as no mutant line for an Apollo ortholog was described so far.

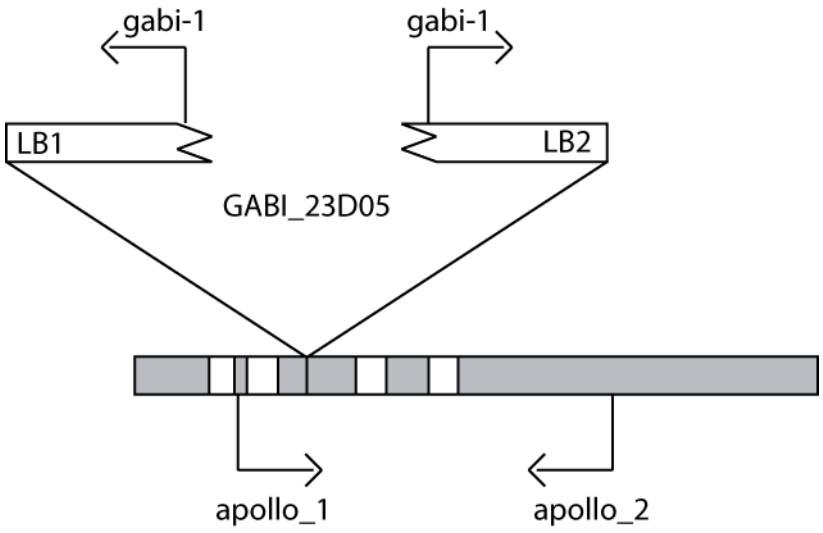

Fig.3-8: *atAPOLLO*; *apollo-1* – 1mm ≡ 20bp, LB – Left Border, primers used as indicated, grey boxes – exons

For primer design I assumed the most frequent case of at least a double inverted insertion with two LBs, as indicated in fig. 3-8. Gabi-1 is the T-DNA specific primer.

3.2.4. Genotyping Situation

As described in the introduction, several T-DNA copies can be inserted in inverse orientation, resulting in a second LB. The second LB (fig. 3-8) is found experimentally during PCR optimization. This situation is the most frequent case.

For PCR-based genotyping this means, that a third combination is possible: apollo_2 and gabi-1.

The genotyping can be split into two reactions: one reaction to detect the wt allele (apollo_1 and apollo_2 in fig. 3-8) and one reaction to detect the mutant allele (apollo_1 and gabi-1 or apollo_2 and gabi-1). But it is also possible to run only one genotyping reaction with all three primers, resulting in competition of apollo_2 and gabi-1 as well as apollo_1 and gabi-1. In this multiplex set up, the primers have to be placed the way that amplification product lengths of apollo_1 and apollo_2 and apollo_1 and gabi-1 have to be of different size, so that they can be easily separated in a gel electrophoresis (usually $\geq$ 200bp). If the amplification product lengths of apollo_1 and gabi-1 and of apollo_2 and gabi-1 are of similar size (< 50bp), they cannot be separated well enough on a gel electrophoresis, appearing as one band.

3.2.5. Genotyping Optimization

According to the available sequence information the wt allele should be detected by primers apollo_1 and apollo_2 by producing an amplification product of 991bp. As can be seen on the gels in fig. 3-9 this band migrated just below the 1000bp marker-band. Combination of the primers apollo_1 and gabi-1 were designed to detect the presence of LB1 by giving an amplification product of 655bp in length, if the insertion was placed correctly. Indeed, this primer combination resulted in a band migrating just above 500bp. If there is a second LB present, apollo_2 and gabi-1 should yield a product of 1262bp. The assumption of a double inverted insertion turned out to be correct, since a product was gained and the band migrated clearly above the 1000bp and below the 1500bp marker band (fig. 3-9). This proves that the T-DNA inserted in exon three. If there are deletions, insertions or base changes at the T-DNA insertion site remains unknown, since I didn't sequence the LB junction sites.

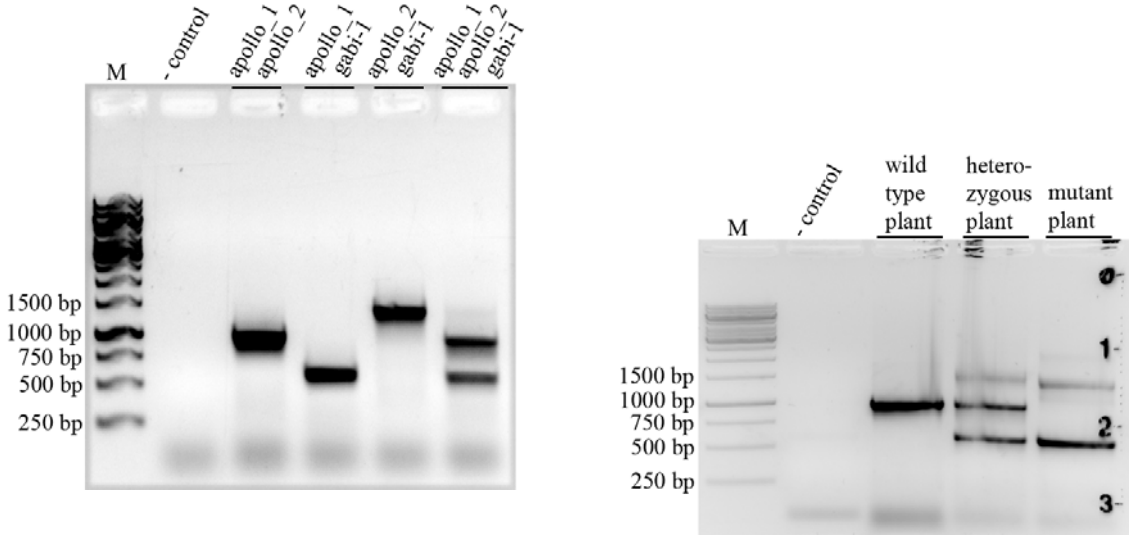

Fig. 3-9: Genotyping optimization of *APOLLO-1*: The left side shows different primer combinations on DNA from a heterozygous plant, whereas on the right side different templates (as indicated) were used in a multiplex set up. M – marker, - control – no DNA, sizes as indicated, primers used as indicated

In the multiplex set up the reaction for LB2, which yields the longer product, was out-competed by the reaction for LB1, which gives the smaller fragment. A shadow can still be seen above the wt band (left part of fig. 3-9). The multiplex set up was then tested on all three possible genotypes. As expected, the mutant resulted in two bands, corresponding in size to the two LBs present, with the larger product being low competing against the smaller product. On the heterozygous template three bands were visible, but the largest fragment still had the lowest intensity, showing that this reaction performed weaker compared to the other two reactions taking place (right part of fig. 3-9).

3.2.6. Terminal Restriction Fragment Analysis

As described briefly under 3.2.1. Function of Apollo, APOLLO is associated with telomeres via TRF2 in humans (Lenain, Bauwens et al. 2006; van Overbeek and de Lange 2006). To see if depletion of Apollo leads to telomeric phenotypes also in *A. thaliana*, I examined telomere length by TRF analysis.

The mutant allele used is on Col-0 background. Therefore wt Col-0 plants were grown and processed together with the *apollo-1*$^{-/-}$ mutant plants. The Col-0 wt telomere length is between 2kb and 4.5kb (first two lanes next to the marker in fig. 3-10). As can be seen from figure 3-10 all of the five sampled *apollo-1*$^{-/-}$ plants have telomere lengths in the wt range.

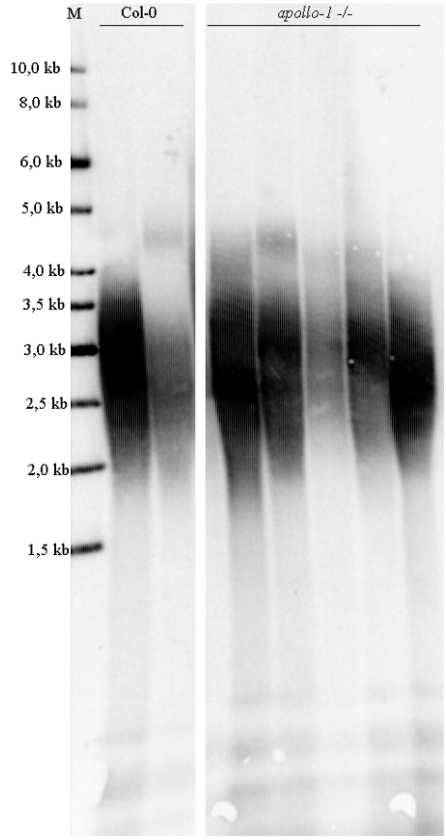

Fig. 3-10: TRF of *apollo-1*. Telomere lengths of this mutant are in the wild type range. Each lane represents a single plant. The blot was hybridized with a G-strand probe. M – marker, sizes as indicated.

There was no obvious effect of the *apollo-1* mutation on telomeres. It is possible that this mutation only shows an effect on already deregulated telomeres, which will be tested by crossing this mutation to *tert* and *ku* mutants.

3.3. BARD1

3.3.1. Function of BARD1

BRCA1 associated RING domain 1 (BARD1) interacts specifically with BRCA1 (BReast CAncer type 1 susceptibility gene). About 75% of the cells BRCA1 are associated with BARD1 *in vivo* (reviewed in (Baer and Ludwig 2002)). Together they form a heterodimer which is stabilized by a 4-helix bundle and coordinates 4 Zn^{2+} ions. The SNPs (Singele Nucleotide Polymorphisms) found in BRCA1 which are associated with breast cancer lie in the metal ion coordinating residues of BRCA1. The BRCA1/BARD1 heterodimer has an E3 ligase activity, which selects the substrate for ubiquitination. The formed E3 ligase is part of the non-HECT E3 ligases and the RING motif is essential for its enzymatic activity (reviewed in (Baer and Ludwig 2002)). Controlled protein turnover is important for correct cell function, especially during the

cell cycle. Since repair proteins like RAD51 are found together with BRCA1 and BARD 1 in discrete nuclear bodies with the onset of DNA synthesis, it is accepted that BRCA1 and BARD1 play a role in DNA repair. This is strongly supported by experiments in plants. Mutants in *BARD1* in *A. thaliana* exhibit a hypo-recombinogenic phenotype (Reidt, Wurz et al. 2006). Under genotoxic stress, induction of DNA repair by HR is less strongly induced than it is in wild type plants.

In order to test if the hypo-recombinogenic phenotype of *bard1* mutants is sufficient to reduce t-circle formation, I crossed *BARD1*$^{+/-}$ to *KU80*$^{+/-}$.

3.3.2. Mutant Allele Used

BARD1 has the annotated number At1G04020 and consist of 13 exons. Two T-DNA insertion lines are available, SALK_097601 with the insertion located in the first intron and termed *bard1-1*, and SALK_031862 with the insertion located in the third exon and termed *bard1-2* (Reidt, Wurz et al. 2006). I have designed primers for both alleles but the genotyping was not optimized for the multiplex set up.

3.3.3. Crossing of *BARD1*$^{+/-}$ to *KU80*$^{+/-}$

For crossing mutants in *BARD1* with mutants in *KU* we choose *KU80*, since it is further away from *BARD1* (16.7Mb) than *KU70* is (4.8Mb) (fig.3-11).

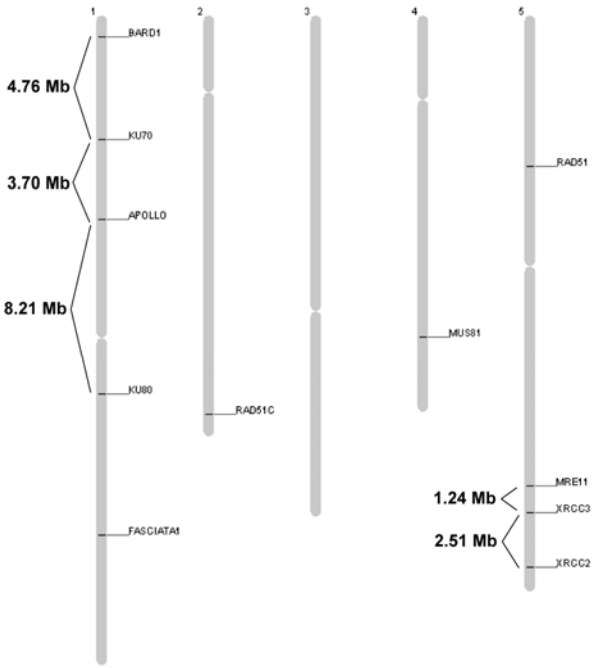

Fig. 3-11: Physical map of genes used in this thesis. The distances between some genes are indicated. The map was drawn utilizing an online tool: http://www.arabidopsis.org/jsp/ChromosomeMap/tool.jsp

Heterozygotes of *BARD1* and *KU80* were crossed (fig. 3-12).

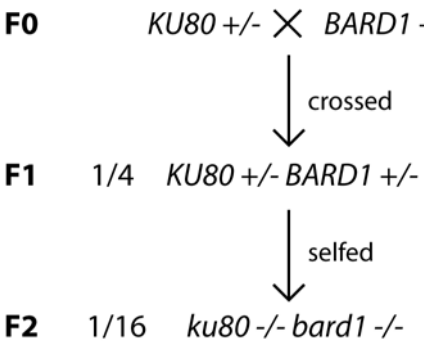

Fig. 3-12: Crossing scheme for *BARD1*$^{+/-}$ an *KU80*$^{+/-}$

Double heterozygous plants were selected for in the F1 generation and selfed. Seeds were obtained from F1 but the F2 population was not analyzed by the end of this thesis.

3.4. MUS81

3.4.1. Function of MUS81

MUS81 endonuclease was shown to cleave Holliday junctions *in vitro* and is therefore the hottest candidate for a eukaryotic homolog of the bacterial RuvC and RusA (reviewed in (Haber and Heyer 2001; West 2003)). Closer biochemical studies showed that the Mus81-Eme1 complex (Eme1 is essential for the catalytic activity of Mus81) has higher activity on structures resembling stalled replication forks (Haber and Heyer 2001; Constantinou, Chen et al. 2002; Blais, Gao et al. 2004). Nonetheless the complex shows Holliday junction resolution activity. Recombinant and tagged Mus81-Eme1 complexes exhibit both activities, but the activity on 3' flap structures and Y-shaped structure is much higher than activity on synthetic Holliday junctions (Blais, Gao et al. 2004). Down-regulation of MUS81 by RNA interference results in reduced somatic recombination, a phenotype that can be rescued by expressing the Holliday junction resolvase RusA (Blais, Gao et al. 2004). RusA doesn't show any activity on 3' flap structures. This argues that Mus81 does not only repair stalled replication forks by Synthesis-Dependent Strand Annealing (SDSA, a process in which endonuclease activity is needed on 3' flap structures), it actually argues against it and suggests an *in vivo* role as Holliday junction resolvase. Also mutants in *RAD51,* double mutants in *RAD51* and *RAD54*, all of which are needed in the early steps of homologous recombination, suppress the *mus81* mutant phenotype argue for a role of the Mus81-Eme1 complex as a Holliday junction resolvase. On the other hand *mus81 req* double

mutants show a synthetic lethality. This is true for all orthologs of this complex from *S. cerevisiae* and *S. pombe* (reviewed in (Haber and Heyer 2001) to *A. thaliana* (Hartung, Suer et al. 2006). This would either suggest an essential role in repair of stalled replication forks. Also MUS81 localizes to foci of DNA damage mainly in cells which are in S-phase (Blais, Gao et al. 2004).

The data known so far gives MUS81 a more important role in DNA replication due to repair of stalled replication forks, but it does not exclude a function as a Holliday junction resolvase, an activity that is also needed in a possible repair pathway of a stalled replication fork. Even though MUS81 might not be the eukaryotic Holliday junction resolvase as RuvC and RusA are in the prokaryotic system.

With the TCA system established and used in our lab, we have the possibility to look for a resolving function of MUS81 in plants and at the same time check for a role of MUS81 in telomere biology.

With the TCA MUS81 can be tested if it is a key endonuclease in t-circle formation. T-circle suppression should therefore occur in the *ku70*$^{-/-}$ *mus81*$^{-/-}$ double mutant.

3.4.2. Mutant Allele Used

The *atMUS81* gene has the annotated number At4g30870 and consists of 15 exons. Two mutant alleles, *mus81-1* and *mus81-2* (SALK_107515, ecotype Col-0) have already been characterized (Hartung, Suer et al. 2006). We also used a new, uncharacterized allele *mus81-3* (SALK_002176, ecotype Col-0). The gene and the two alleles used (*mus81-2*, *mus81-3*) are depicted in fig. 3-13. The primers indicated on the left borders of the insertion are LBc-1, the T-DNA specific primer for SALK lines, which was used in the lab before. The other gene specific primers have been designed by me.

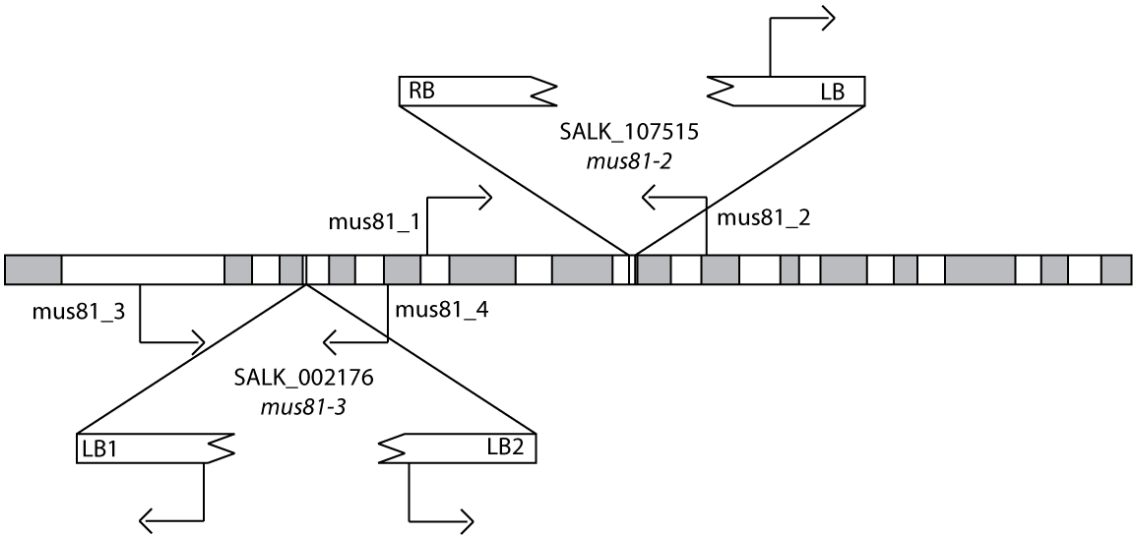

Fig. 3-13: *atMUS81*; insertion mutants *mus81-2* & *mus81-3*. 1mm ≡ 20bp, RB – Right Border, LB – Left Border, primers used as indicated, grey boxes – exons

Genotyping was not optimized for a multiplex set up. Therefore, genotyping was split in detection of the wt allele and detection of the mutant allele.

3.4.3. Crossing of *MUS81*$^{+/-}$ to *KU70*$^{+/-}$

MUS81-3$^{+/-}$ were obtained and crossed, but the crossing was unsuccessful and is therefore not depicted in figure 3-14.

No *MUS81-2*$^{+/-}$ but *mus81-2*$^{-/-}$ plants were obtained directly from seeds from the stock centre. Since the *mus81-2*$^{-/-}$ plants are fertile, I crossed them to *KU70*$^{+/-}$ plants. This increased the probability from 0.25 to 0.5 to get double heterozygous plants in the F1 generation, which were then selected and selfed (fig.3-14).

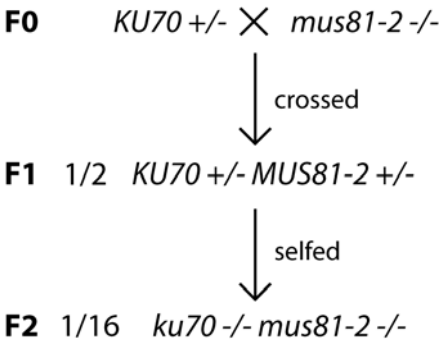

Fig. 3-14: Crossing scheme for *KU70*$^{+/-}$ with *mus81-2*$^{-/-}$

KU70$^{+/-}$ plants were chosen for crossing, because *ku70*$^{-/-}$ plants exhibit an altered telomere structure, which may obscure downstream analysis of mus81 mutants.

To follow the genetics in the crossed plants, segregation analysis was performed.

3.4.4. Segregation Analysis

3.4.4.1. Principle

Segregation Analysis was performed to see if the combination of mutants shows a defect in segregation. Segregation from double heterozygous plants results in Mendel's 9:3:3:1 ratio of phenotypes. This ratio refers to the crossing of two different recessive mutations and the analysis of the phenotype in the F2 generation. If the genes segregated independently, 9 plants show the wild type phenotype, 3 plants show the mutant phenotype of one gene, 3 plants show the mutant phenotype of the other gene, and 1 plant shows the mutant phenotype of both genes in the F2 generation. As shown in table 3-2 those 4 different phenotypes result from 9 different genotypes.

	AB	**aB**	**Ab**	**ab**
AB	AABB	AaBB	AABb	AaBb
aB	AaBB	aaBB	AaBb	aaBb
Ab	AABb	AaBb	AAbb	Aabb
ab	AaBb	aaBb	Aabb	aabb

Table 3-2: Mendelian segregation of two independent loci. Uppercase letters – wild type allele, lowercase letters – mutant allele, white – wt phenotype, blue – mutant phenotype of gene A, orange – mutant phenotype of gene B, green – mutant phenotype of both genes

Segregation analysis compares the observed number of genotypes to the expected one. With a Chi^2 distribution test (goodness of fit), the significance of a change is tested (see materials and methods). I used the standard error probability of 5%. For 9 possible genotypes we have 8 degrees of freedom (8 other possibilities). For these parameters the critical value for χ^2 is 15.51 (http://de.wikibooks.org/wiki/Mathematik:_Statistik:_Tabelle_der_Chi-Quadrat-Verteilung). A χ^2 – value greater than 15.51 means, that there is a significant change between the Mendelian and the observed segregation pattern. The higher the number of plants sampled with a Chi^2 test, the more confident is the result of the Chi^2 test.

3.4.4.2. Segregation Analysis of ku70-/- mus81-/-

Crossing of *KU70*$^{+/-}$ x *mus81-2*$^{-/-}$ resulted in F1 double heterozygous plants, which were selected and selfed to obtain the F2 generation. The F2 population was genotyped. No double mutant was obtained and segregation analysis revealed a Non-Mendelian segregation. This change was significant as can be seen by the χ^2 value of 38.68, which

is greater than the critical value of 15.51. In fact I found only one *mus81-2*$^{-/-}$ in this F2 population (highlighted in table 3-3).

wt		**Number of plants**		**Probability**	
n=78		**Expected**	**Observed**	**Expected**	**Observed**
MUS81-2$^{+/+}$	***KU70***$^{+/+}$	4.88	5	0.063	0.064
MUS81-2$^{+/+}$	***KU70***$^{+/-}$	9.75	6	0.125	0.077
MUS81-2$^{+/-}$	***KU70***$^{+/+}$	9.75	22	0.125	0.282
MUS81-2$^{+/-}$	***KU70***$^{+/-}$	19.5	22	0.250	0.282
mus81-2$^{-/-}$	***KU70***$^{+/+}$	4.88	0	0.063	0.000
mus81-2$^{-/-}$	***KU70***$^{+/-}$	9.75	1	0.125	0.013
MUS81-2$^{+/+}$	***ku70***$^{-/-}$	4.88	8	0.063	0.103
MUS81-2$^{+/-}$	***ku70***$^{-/-}$	9.75	14	0.125	0.179
mus81-2$^{-/-}$	***ku70***$^{-/-}$	4.88	0	0.063	0.000

χ^2 = 38,68

Table 3-3: Segregation of F2 *mus81-2*$^{-/-}$ x *KU70*$^{+/-}$. Green – mutants, yellow – heterozygotes, n – number of plants analyzed

We wanted to know if the observed alteration in segregation is due to the combination of the mutants, or if this alteration is due to Non-Mendelian segregation of the single loci. Therefore the single loci were analyzed independently from the same dataset (tables 3-4 and 3-5).

	Number of plants		**Probability**	
n=81	**Expected**	**Observed**	**Expected**	**Observed**
KU70$^{+/+}$	20.25	27	0.25	0.333
KU70$^{+/-}$	40.5	29	0.50	0.358
ku70$^{-/-}$	20.25	25	0.25	0.309

χ^2 = 6.63

Table 3-4: Segregation of *KU* in the F2 population of *mus81-2*$^{-/-}$ x *KU70*$^{+/-}$. Green – mutants, yellow – heterozygotes, n – number of plants analyzed

Interestingly, the Mendelian ratio of 1:2:1 has switch to nearly 1:1:1 (table 3-4). For 2 degrees of freedom, the critical value is 5.99. As can be seen from the χ^2 value is 6.63, this change is significant.

	Number of plants		**Probability**	
n=81	**Expected**	**Observed**	**Expected**	**Observed**
MUS81-2$^{+/+}$	20.25	19	0.25	0.235
MUS81-2$^{+/-}$	40.5	61	0.50	0.753
mus81-2$^{-/-}$	20.25	1	0.25	0.012

χ^2 = 28.75

Table 3-5: Segregation of *MUS81-2* in the F2 population of *mus81-2*$^{-/-}$ x *KU70*$^{+/-}$. Green – mutants, yellow – heterozygotes, n – number of plants analyzed

Table 3-5 shows the segregation of *MUS81-2*. Even though there were Mendelian amounts of *MUS81-2*$^{+/+}$ found, only 1 instead of 20 *mus81-2*$^{-/-}$ plants were segregated.

On cost of these *mus81-2*$^{-/-}$ mutant plants, more *MUS81-2*$^{+/-}$ plants were obtained (61 instead of 41, highlighted in table 3-5). This could point to some advantage of heterozygotes, but a Non-Mendelian segregation was not reported in the published study (Hartung, Suer et al. 2006).

Because this dataset is based on analysis of 78 F2 plants, the segregation pattern should be verified by analysis of another F2 population in the future.

4. Analysis of T-circle Excision in Combinations of Mutants in RAD51 family members

4.1. *ku70*$^{-/-}$: The Genetic Background

The *ku70*$^{-/-}$ mutation in *A. thaliana* results in increased G-overhang length and longer telomeres (Riha, Watson et al. 2002; Riha and Shippen 2003). The elongated telomeres reach a homeostatic length in third generation (G3) mutants (Watson and Shippen 2007). Using 2D gels and the newly developed TCA assay, Zellinger et al. showed the existence of telomeric circles (t-circles) in *ku70*$^{-/-}$ mutants (Zellinger, Akimcheva et al. 2007).

To test whether genes involved in HR are required for t-circle excision, Barbara Zellinger created double mutants of *ku70*$^{-/-}$ with the 5 RAD51 paralogs and also with *MIM* and *MRE11*. Fig. 3-15 shows the result of the TCAs in these double mutants. As comparison and as a positive control *ku70*$^{-/-}$ mutants are shown for each TCA. No t-circle suppression was found in the double mutants, nor does it look like there is any decrease in t-circle formation.

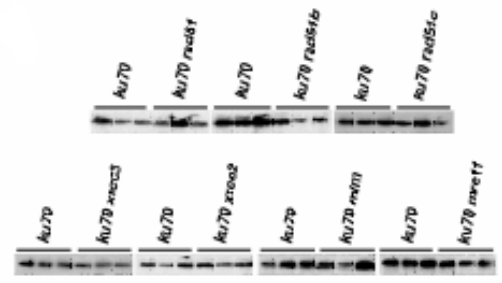

Fig. 3-15: Double mutants of *ku70*$^{-/-}$ with *RAD51* paralogs still produce t-circles. Figure taken from Zellinger et al., 2007, supplemental

This result is in contrast to Wang et al, who showed that *XRCC3* is essential for t-circle formation in a human cell line (Wang, Smogorzewska et al. 2004).

To test for possible redundancies between RAD51, the MRN complex and the BCDX2 and CX3 complexes, I generated various triple mutant combinations.

4.2. Genes chosen for Triple Mutant Combinations

Fig. 3-16 shows highlighted in yellow the genes chosen for triple mutant combinations on a physical map. *KU70* is annotated on chromosome I. Since *RAD51C* is part of both the BCDX2 and the CX3 complex, we used the *rad51c-1* mutation in combination with *rad51-1*, *mre11-3*, *xrcc2-1* and *xrcc3-1*, all of which are on chromosome V. Of these four different triple mutant combinations all three different genes are on three different chromosomes and should segregate independently, resulting in Mendelian 9:3:3:1 segregation pattern.

The other two combinations generated were *ku70*$^{-/-}$ with *xrcc2-1* and *rad51-1* mutations and *ku70*$^{-/-}$ with *mre11-3* and *rad51-1* mutations. Even though *RAD51*, *MRE11* and *XRCC2* are on chromosome V, we expected Mendelian segregation since *RAD51* is more than 50cM apart from *MRE11*. We did not combine *ku70*$^{-/-}$ with *mre11-3* and *xrcc2-1*, *mre11-3* and *xrcc3-1* or *xrcc2-1* and *xrcc3-1*, since they are close together on chromosome V (1.2Mb and 2.5Mb respectively) and we expected a tight genetic linkage between those genes.

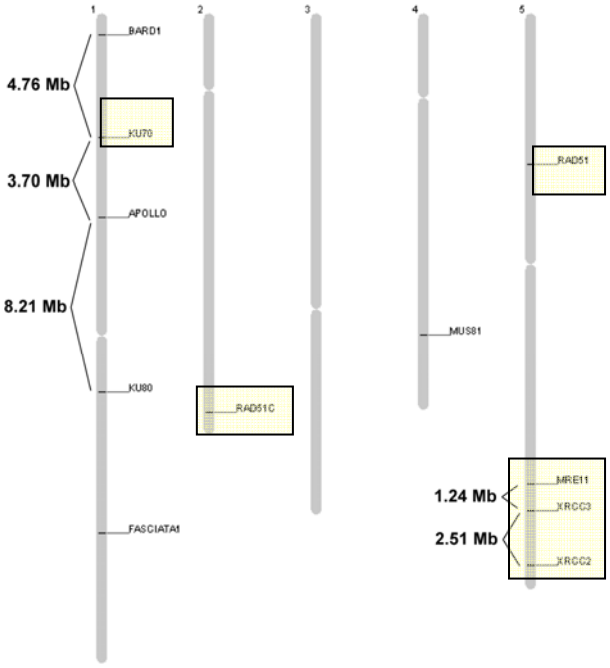

Fig. 3-16: Physical map of genes used in this thesis. Highlighted in yellow are the genes used in triple mutant combinations. Physical distances between selected genes are indicated. The map was drawn utilizing an online tool: http://www.arabidopsis.org/jsp/ChromosomeMap/tool.jsp

4.3. Crossing Strategy

Figure 3-17 shows the crossing scheme by which triple mutants were obtained. *Ku70*$^{-/-}$ mutants are fully fertile. But *rad51*$^{-/-}$, *rad51c*$^{-/-}$, *xrcc3*$^{-/-}$ and *mre11*$^{-/-}$ show a sterility phenotype. Martina Schirato, our technician who did all these crossings, used a *ku70*$^{-/-}$ mutant heterozygous for one gene (A in fig. 3-17) and a *ku70*$^{-/-}$ mutant heterozygous for the other gene (B in fig. 3-17) for crossing. Therefore all plants in the F1 generation were already *ku70*$^{-/-}$ mutants. With the probability of 1/4 *ku70*$^{-/-}$ double heterozygous plants (*ku70*$^{-/-}$ *gene A*$^{+/-}$ *gene B*$^{+/-}$ in fig. 3-17) were obtained (table 3-6). Those plants were then selfed and propagated to F2 generation. In F2 *ku70*$^{-/-}$ was already mutated for the 3rd generation (G3), meaning that the telomeres have reached their homeostatic length (Watson and Shippen 2007). 1/16 of the plants in the F2 generation should be triple mutants.

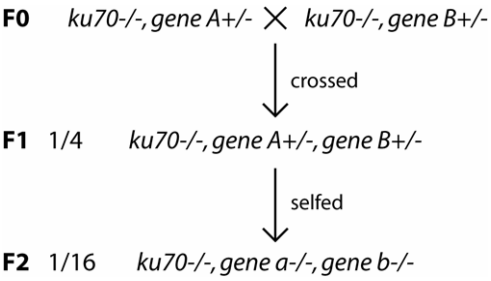

	AB	aB
AB	AABB	AaBB
Ab	AABb	AaBb

Table 3-6: Segregation pattern of the F1 generation resulting form the crossing strategy used. Highlighted is the looked for genotype. Uppercase letters – wild type allele, lowercase letters – mutant allele

Fig. 3-17: Crossing scheme. A, B genes of interest

Due to the sterility phenotype of *rad51*$^{-/-}$, *rad51c*$^{-/-}$, *xrcc3*$^{-/-}$ and *mre11*$^{-/-}$, triple mutant combinations had to be out-segregated from *ku70*$^{-/-}$ *gene A*$^{+/-}$ *gene B*$^{+/-}$ plants. *Xrcc2*$^{-/-}$ does not show a sterility phenotype, but in order to have the same conditions for all triple mutant combinations, a *ku70*$^{-/-}$ *XRCC2*$^{+/-}$ plant was used for crossing. In order to be able to handle these amounts of plants, genotyping optimization into a multiplex PCR approach was essential.

4.4. Optimization of Genotyping for *KU70*

4.4.1. Mutant Allele Used

AtKU70 has the annotated number At1g16970. Fig. 3-18 shows a drawn to scale cartoon of the gene structure. The gene consists of 18 exons. In the allele *ku70-1* (ecotype Wassilewskija) the insertion was located at the 3' end of exon 10 resulting in a 25bp deletion (black box in fig. 3-18) (Riha, Watson et al. 2002).

Primers ku70_2 and ku70_11 are gene-specific whereas the primer LB-cd6 is specific for the T-DNA (Riha, Watson et al. 2002). Those primers have already been in use in the laboratory for genotyping *atKU70*.

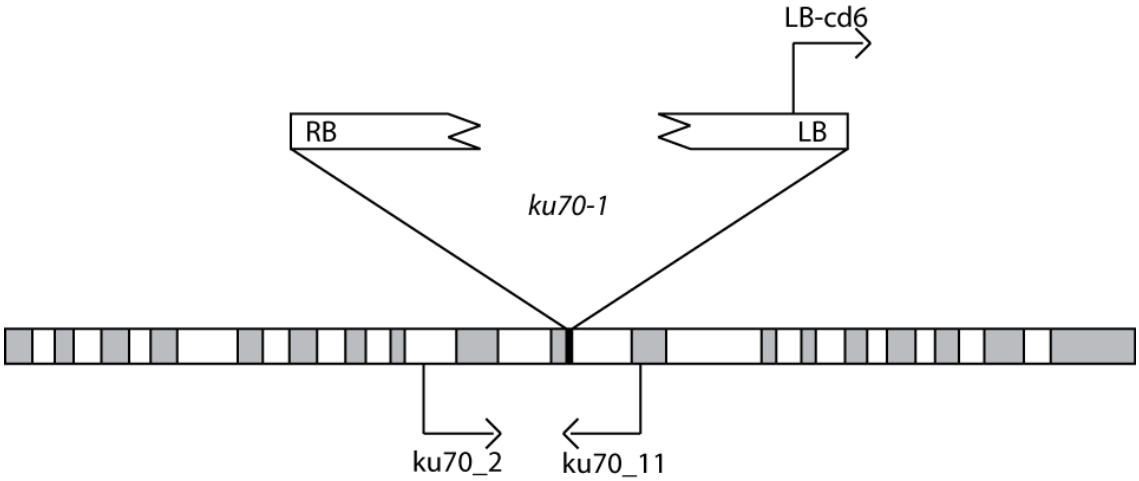

Fig. 3-18: *atKU70*; *ku70-1* (1mm ≡ 30bp); Names and positions of primers as indicated, name of the allele as indicated, LB – Left Border, RB – Right Border, grey boxes – exons, black box – 25 bp deletion

4.4.2. Genotyping

Combining the two gene specific primers ku70_2 and ku70_11 yielded a 939bp long product. As seen on the gel (fig. 3-19) this band migrated just below 1000bp. If ku70_2 and LB-cd6 were combined, no product was obtained indicating the absence of a LB facing the 5'end of the gene (figs 3-18 & 3-19). A 639bp long product was yielded by combining ku70_11 and LB-cd6, indicating the presence of a LB facing the 3' end of the gene. The band migrated between 500bp and 750bp on the agarose gel (figs 3-18 & 3-19). If all three primers (two gene-specific and one T-DNA specific) were combined, two products of different length were obtained (left part in fig. 3-19).

The multiplex PCR approach was tested on the three possible genotypes. Clear distinction of the three different genotypes was achieved (right part in fig. 3-19).

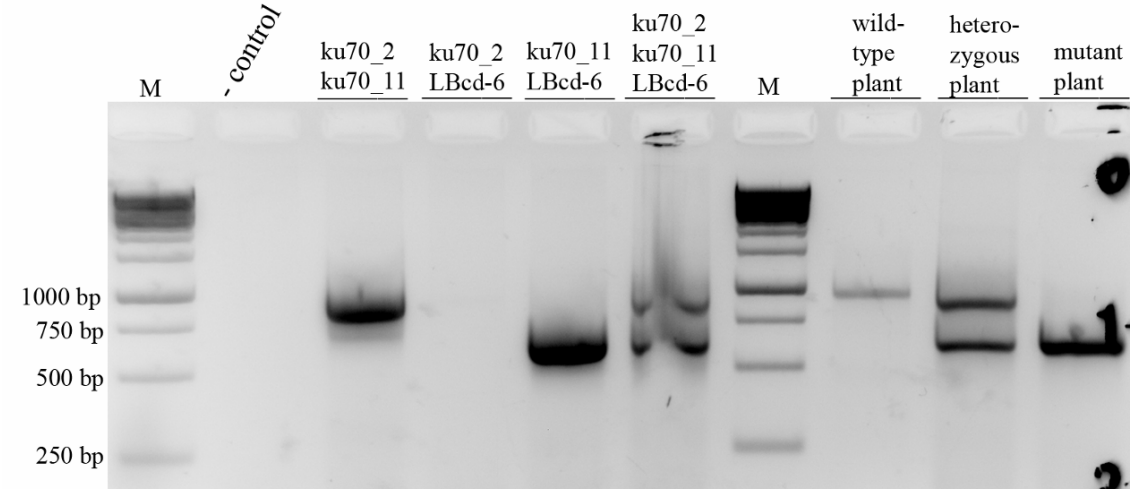

Fig. 3-19: Genotyping Optimization of *KU70-1*: The left side shows different primer combinations on DNA from a heterozygous plant, whereas on the right side different templates (as indicated) were used with the multiplex set up. M – marker, - control – no DNA, sizes as indicated, primers used as indicated

Therefore, this combination of primers worked ideally and robustly for genotyping *KU70*.

4.5. Triple Mutant *ku70-1 rad51c-1 rad51-1*

First the gene onthologies and the genotyping optimizations will be described.

4.5.1. RAD51

4.5.1.1. RAD51 function

RAD51 is the eukaryotic ortholog of the bacterial recombination protein RecA and the archeal recombination protein RadA. In higher eukaryotes, *RAD51* has evolved into five additional paralogs, *RAD51B, RAD51C, RAD51D, XRCC2* and *XRCC3* (Lin, Kong et al. 2006), three of which will be discussed below. RAD51 is a key protein for homologous recombination. After strand resection, in which the MRN complex might be involved (reviewed in (D'Amours and Jackson 2002)), RAD51 covers the ssDNA (a 3' overhang) forming a nucleoprotein filament in a highly ordered right handed helical structure that is more highly conserved throughout the three domains of life than its sequence is (reviewed in (West 2003)). By forming the nucleoprotein filament the ssDNA becomes recombinogenic. Formation of this recombinogenic nucleoprotein filament is highly regulated involving Replication Protein A (RPA), RAD52, RAD54 but also BRCA1 and BRCA2. Knock outs in *S. cerevisiae* result in impaired DSB repair and in mice the null mutation is embryo-lethal (Bennett and Knight 2005). In plants the *rad51*$^{-/-}$ null mutation is not lethal but results in complete sterility due to chromosome instabilities

during meiosis (Li, Chen et al. 2004). Since *rad51*$^{-/-}$ plants can be obtained, the function of this protein can be studied genetically in plants. The *A. thaliana* ortholog is also more closely related to the human ortholog than is the *S. cerevisiae* one.

4.5.1.2. Mutant Allele Used

The gene has the annotated number At5g20850, consists of nine exons and the T-DNA insertion is annotated in intron 4. We used the *rad51-1* mutant allele in our experiments. Since no sequence information of the T-DNA border was given in the publication by Li et al (Li, Chen et al. 2004) and we did not sequence the borders it was not exactly known where the T-DNA insertion lies and therefore I did not draw a cartoon of the gene. The GABI-Kat insertion line (ecotype Col-0) has the number 134A01.

4.5.1.3. Genotyping Optimization

The primers we used were published in Li W. et al (Li, Chen et al. 2004). I tested those primers first in a two primer set up to check for amplification product size useful for a possible multiplex set up. Combination of three of the published primers worked reliably and gave a very clear genotyping in a multiplex set up (fig. 3-20). Primers pcr_rad51_1 and pcr_rad51_2 detected the wild type allele and resulted in an amplification product of about 900bp in length, and primers pcr_rad51_1 and rad51TDNA detected the mutant allele giving an amplification product of about 300bp in length. Figure 3-20 shows the multiplex set up on different templates. There was one clear band on a wild type and on a mutant template and two clear bands of correct size on a heterozygous template. Therefore, clear and reliable genotyping was possible with this multiplex PCR set up.

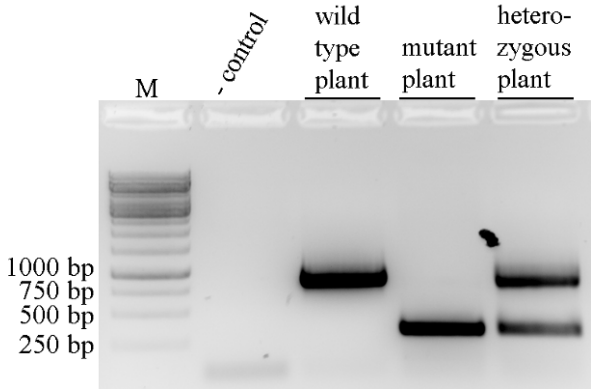

Fig. 3-20: Genotyping optimization of *RAD51-1*. A multiplex set up was used on different templates (as indicated). M – marker, - control – no DNA, sizes as indicated

4.5.2. RAD51C

4.5.2.1. Function of RAD51C

RAD51C is one of the five RAD51 paralogs (Lin, Kong et al. 2006) in higher eukaryotes. It is part of the BCDX2 (RAD51B-RAD51C-RAD51D-XRCC2) and CX3 (RAD51C-XRCC3) complexes (Masson, Tarsounas et al. 2001; Miller, Sawicka et al. 2004). The BCDX2 and the CX3 complexes are thought to be mediators of RAD51 nucleoprotein filament formation (reviewed in (van Gent, Hoeijmakers et al. 2001)). But there is also biochemical data that suggests involvement of RAD51C together with XRCC3 in Holliday junction (HJ) resolution (Liu, Masson et al. 2004). But this is data from cell extracts and so far this data has not been reproduced with reconstituted recombinant complexes. The same author did HJ binding studies with reconstituted recombinant RAD51C-XRCC3. The recombinant proteins bind the HJ and build a low molecular protein-Holliday junction complex, but fails to build the high molecular protein-Holliday junction complex as bacterial RuvA and the cell extract does (Liu, Tarsounas et al. 2007). Results on HJ resolvase activity with the reconstituted recombinant proteins are still missing. RAD51C was also shown to stabilize RAD51 as a nucleoprotein filament (Bennett and Knight 2005). In mice the knock out results in embryo lethality (Kuznetsov, Pellegrini et al. 2007), whereas plant *rad51c*$^{-/-}$ mutants are fully viable but they are sterile due to defects in segregation during meiosis (Abe, Osakabe et al. 2005; Bleuyard, Gallego et al. 2005). Therefore, mutants can be used for functional analysis of the *RAD51C* gene in *A. thaliana*.

4.5.2.2. Mutant Allele Used

The gene has the annotated number At2g45280 and consists of nine exons (fig.3-21).

There is at least a double inverted T-DNA insertion at the 3’ end of exon three, deleting 45bp, most of which lies in intron 3 (Abe, Osakabe et al. 2005; Bleuyard, Gallego et al. 2005). Since there was another description of the same allele, placing the insertion in the second intron (Li, Yang et al. 2005), I sequenced the amplification product from the mutant allele. I found that the T-DNA was inserted at the border of exon 3 and intron 3. Using a primer placed in the middle of exon 3 facing the 3’ end of the gene together with the T-DNA specific primer LBc-1 yielded a product, excluding the possibility of the insertion sitting in exon 2 (data not shown).

The primer rad51c_5 has been used in the lab before. LBc-1 is a T-DNA specific primer for SALK lines.

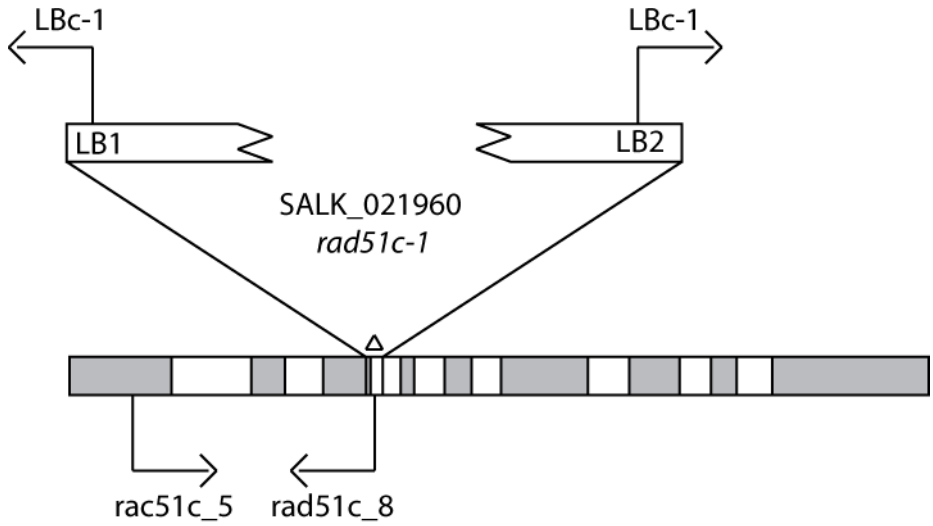

Fig. 3-21: *atRAD51C*; *rad51c-1* (1mm ≡ 20bp); Gene structure as well as position of gene-specific and T-DNA specific primer, and position of the insertion, the name of the allele and the number of the SALK line (ecotype Col-0) are indicated. LB – Left Border, gray boxes – exons, the triangle marks a 45bp deletion

4.5.2.3. Genotyping Situation

Deletions and insertions are also very frequent in T-DNA insertion lines as described in the introduction. A deletion can be used as an additional discrimination marker for the PCR-based genotyping in a multiplex set up. As depicted in fig. 3-21 the second gene specific primer, primer 2 in fig. 3-22, is placed inside the sequence that is deleted when the T-DNA insertion has happened. Therefore, primer 2 can only bind in the wt situation, making the genotyping reaction less prone to artefacts.

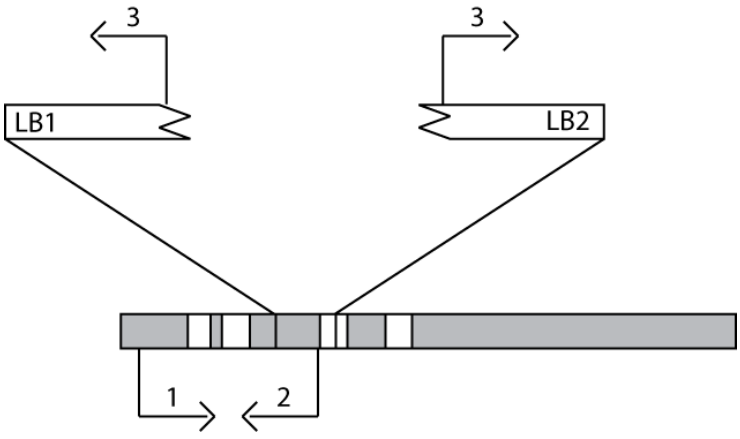

Fig. 3-22: Cartoon of a genotyping set up, if a deletion is present. LB – Left Border; RB – Right Border; 1,2,3 – different primers; grey boxes – exons; for description see text

Furthermore, placing primer 2 inside the deleted sequence, an amplification product between primers 2 and 3 is not possible, reducing the competitions between the primers in the genotyping reaction.

Primer rad51c_8 was designed and placed in the deletion site during this thesis to improve genotyping.

4.5.2.4. Genotyping Optimization

The two gene specific primers rad51c_5 and rad51c_8 (fig. 3-21) yielded a 639bp long product which was seen as a band between 600bp and 700bp on the agarose gel (fig. 3-23). Rad51c_5 and LBc-1 should yield an 807bp long fragment and indeed a band of about 800bp was detected. Primer rad51c_8 was placed in the deletion site, facing primer rad51c_5, but no LB (primer LBc-1, fig. 3-21). Therefore, no product was expected and none was observed, proving the presence of the deletion and the function of the additional discrimination effect. The multiplex set up resulted in two products of different size, corresponding to the wt allele and the mutant allele, respectively. Since the two products were only 168bp different in size a higher percentage agarose gel (1.6%) was necessary to separate them clearly (left part of fig. 3-23).

This multiplex set up was tested on different templates, representing the three genotypes possible. The wt and the mutant template yielded only one band, corresponding to the sizes determined with the different primer combinations described above. The heterozygous template yielded two bands, corresponding to the two alleles (right part of fig. 3-23).

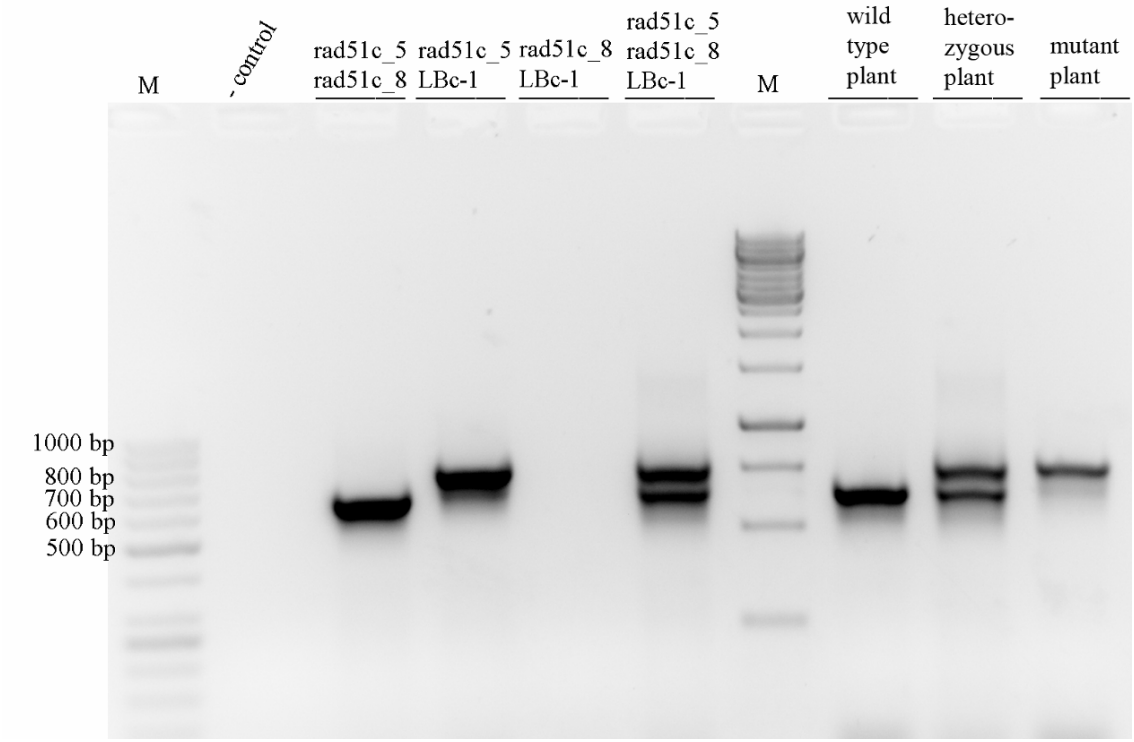

Fig. 3-23: Genotyping optimization of *RAD51C-1*: The left side shows different primer combinations on DNA from a heterozygous plant, whereas on the right side different templates (as indicated) were used with in a multiplex set up. M – marker, - control – no DNA, sizes as indicated, primers used as indicated

This primer combination gave a robust and sensitive genotyping of *RAD51C*.

4.5.3. Analysis of the *ku70*$^{-/-}$ *rad51*$^{-/-}$ *rad51c*$^{-/-}$ Triple Mutant

With this combination of mutants we impaired both the BCDX2 and CX3 complex and knocked out *RAD51*. Fig. 3-24 shows a cartoon depicting the combination.

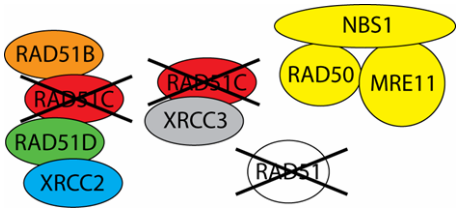

Fig. 3-24: Schematic representation of the impairment of the major recombination complexes in a triple mutant with *ku70*$^{-/-}$.

With the following analysis I tested if RAD51 acts redundantly with RAD51C.

4.5.3.1. Segregation Analysis

As can be seen from table 3-7 the population segregated Mendelian. χ^2 of 3.73 is below the critical value of 15.51, meaning that the observed segregation fitted very well with the expected one. Triple mutant plants did not show any obvious phenotype besides sterility, which was described for the single mutants of *rad51*$^{-/-}$ and *rad51c*$^{-/-}$ (Li, Chen

et al. 2004; Abe, Osakabe et al. 2005; Bleuyard, Gallego et al. 2005; Li, Yang et al. 2005).

ku70$^{-/-}$		Number of plants		Probability	
n=107		Expected	Observed	Expected	Observed
RAD51C$^{+/+}$	*RAD51*$^{+/+}$	6,69	7	0,063	0,065
RAD51C$^{+/+}$	*RAD51*$^{+/-}$	13,38	16	0,125	0,150
RAD51C$^{+/-}$	*RAD51*$^{+/+}$	13,38	16	0,125	0,150
RAD51C$^{+/-}$	*RAD51*$^{+/-}$	26,75	26	0,250	0,243
rad51c$^{-/-}$	*RAD51*$^{+/+}$	6,69	5	0,063	0,047
rad51c$^{-/-}$	*RAD51*$^{+/-}$	13,38	12	0,125	0,112
RAD51C$^{+/+}$	*rad51*$^{-/-}$	6,69	5	0,063	0,047
RAD51C$^{+/-}$	*rad51*$^{-/-}$	13,38	18	0,125	0,168
rad51c$^{-/-}$	*rad51*$^{-/-}$	6,69	6	0,063	0,056

$\chi^2 = 3.73$

Table 3-7: Segregation of F2 *ku70*$^{-/-}$ *RAD51C*$^{+/-}$ x *ku70*$^{-/-}$ *RAD51*$^{+/-}$. Green – mutants, yellow – heterozygotes, n – number of plants analyzed

4.5.3.2. T-circles

If *RAD51* is redundant with *RAD51C*, t-circle formation should be suppressed in the *ku70*$^{-/-}$ *rad51*$^{-/-}$ *rad51c*$^{-/-}$ triple mutant.

The out-segregated double mutants *ku70*$^{-/-}$ *rad51c*$^{-/-}$ and *ku70*$^{-/-}$ *rad51*$^{-/-}$ served as additional positive controls and are an independent reproduction of previous results on double mutants (Zellinger, Akimcheva et al. 2007).

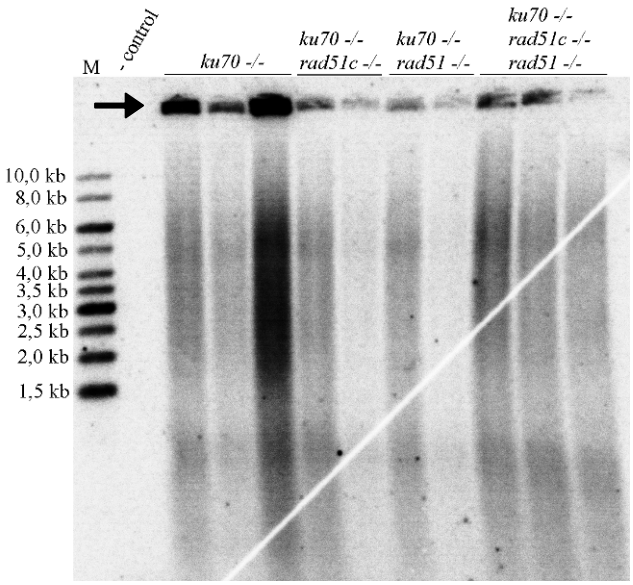

Fig. 3-25: TCA of out-segregated genotypes from the *ku70*$^{-/-}$ *RAD51C*$^{+/-}$ x *ku70*$^{-/-}$ *RAD51*$^{+/-}$ cross. Out-segregated *ku70*$^{-/-}$ and double mutants with *ku70*$^{-/-}$ serve as a control. T-circles are still present in the triple mutant. Each lane represents a different sample derived from a pool of 2-3 plants of the same genotype. The arrow points to the high molecular weight signal derived from t-circles. White stripe is due to a small failure of the detector. Smears seen below the high molecular weight signal are derived from TRFs. M – marker, sizes as indicated; - control – no DNA

As can be seen in figure 3-25 t-circles were still generated in the *ku70*$^{-/-}$ *rad51*$^{-/-}$ *rad51c*$^{-/-}$ triple mutant. *RAD51* is not redundant with *RAD51C*.

The result of the triple mutant is the first data on genetic interaction between BCDX2, CX3 and RAD51.

4.6. Triple Mutant *ku70-1 rad51c-1 xrcc2-1*

For gene onthology and genotyping optimization of *RAD51C* see chapter 4.5.2.

4.6.1. XRCC2

4.6.1.1. Function of XRCC2

XRCC2 is part of the BCDX2 complex which is thought to be a mediator of RAD51 nucleoprotein filament formation (reviewed in (van Gent, Hoeijmakers et al. 2001)). Biochemical data suggests a role in branch migration and Holliday junction resolution in context of the BCDX2 complex (Liu, Masson et al. 2004) but this has not been proven with reconstituted recombinant complexes. Knock outs in mice result in embryonic lethality (Thacker and Zdzienicka 2004). Surprisingly *xrcc2*$^{-/-}$ plants are fully viable and fully fertile (Bleuyard, Gallego et al. 2005). Therefore, genetic analysis on this gene can be done in the *A. thaliana* system.

4.6.1.2. Mutant Allele Used

The gene has the annotated number At5g64520 and we used the *xrcc2-1* mutant allele (SALK_029106, (Bleuyard, Gallego et al. 2005)). Fig. 3-26 shows a drawn to scale cartoon of this gene and indicates the position of the T-DNA insertion and the primers used. This allele is not a complete null mutation since a truncated transcript is produced that may result in a truncated protein. This was not tested by Western blots (Bleuyard, Gallego et al. 2005).

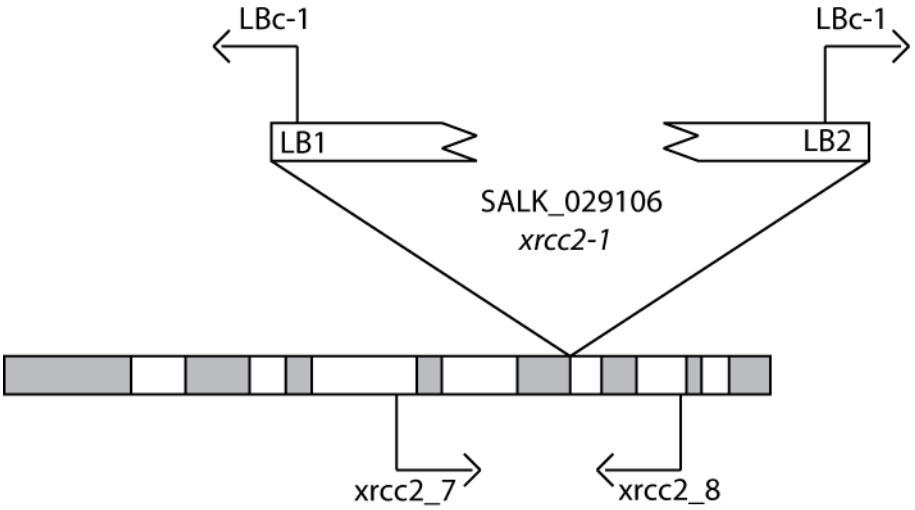

Fig. 3-26: *atXRCC2*; *xrcc2-1* (1mm ≡ 20bp); LB – Left Border, primers used as indicated, gray boxes – exons

4.6.1.3. Genotyping Optimization

Fig. 3-27 shows the optimization of different primers on a heterozygous template. Primers xrcc2_7 and xrcc2_8 detected the wild type allele and resulted in an amplification product of 531bp. One LB of the mutant allele was detected with xrcc2_7 and LBc-1 and resulted in a 607bp long amplification product. The reaction with primers xrcc2_8 and LBc-1 gave a product which was seen as a band of 205bp showing the existence of a second LB. The wt allele amplification product and the amplification product from LB1 were only 76bp apart, making it necessary to use a higher percentage agarose gel (2%) to separate them. In the multiplex set up the band from LB1 was faint but still detectable. Above this band appeared a chimeric band which was most likely the result of the presence of the wild type allele. This chimeric band was used as an additional discrimination mark between mutants and heterozygotes.

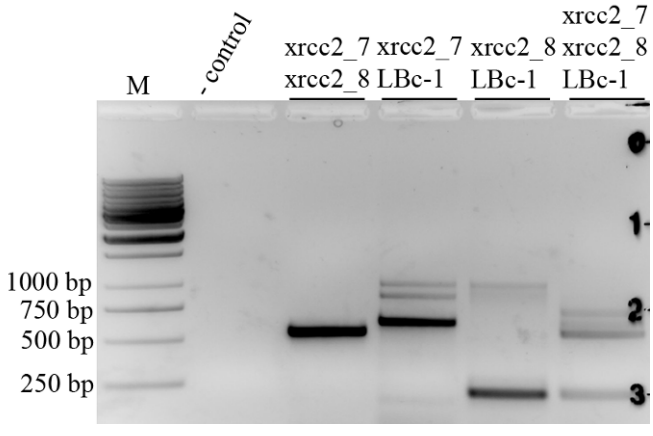

Fig. 3-27: Optimization gel for *XRCC2-1* genotyping. The gel shows different primer combinations on DNA from a heterozygous plant. M – marker, - control – no DNA, sizes as indicated, primers used as indicated

This genotyping worked well and reliable in a multiplex PCR set up.

4.6.2. Analysis of the *ku70*$^{-/-}$ *rad51c*$^{-/-}$ *xrcc2*$^{-/-}$ Triple Mutant

With this combination of mutants the CX3 complex is impaired and the BCDX2 complex is strongly impaired, as schematically shown in fig. 3-28

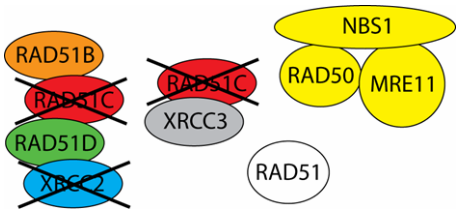

Fig. 3-28: Schematic representation of the impairment of the major recombination complexes in a triple mutant with *ku70*$^{-/-}$.

With the following analysis I tested for a residual function of the RAD51D-XRCC2 part (Liu, Masson et al. 2004) of the BCDX2 complex in t-circle formation.

4.6.2.1. Segregation Analysis

The segregation analysis showed almost perfect correlation to Mendelian segregation, as can be seen by a χ^2 value of 1.68 (Table 3-8), which below the critical value of 15.51.

ku70$^{-/-}$		**Number of plants**		**Probability**	
n=126		**Expected**	**Observed**	**Expected**	**Observed**
RAD51C$^{+/+}$	***XRCC2***$^{+/+}$	7,88	8	0,063	0,063
RAD51C$^{+/+}$	***XRCC2***$^{+/-}$	15,75	16	0,125	0,127
RAD51C$^{+/-}$	***XRCC2***$^{+/+}$	15,75	13	0,125	0,103
RAD51C$^{+/-}$	***XRCC2***$^{+/-}$	31,50	32	0,250	0,254
rad51c$^{-/-}$	***XRCC2***$^{+/+}$	7,88	8	0,063	0,063
rad51c$^{-/-}$	***XRCC2***$^{+/-}$	15,75	15	0,125	0,119
RAD51C$^{+/+}$	***xrcc2***$^{-/-}$	7,88	5	0,063	0,040
RAD51C$^{+/-}$	***xrcc2***$^{-/-}$	15,75	17	0,125	0,135
rad51c$^{-/-}$	***xrcc2***$^{-/-}$	7,88	8	0,063	0,063
					χ^2 = 1.68

Table 3-8: Segregation of F2 *ku70*$^{-/-}$ *RAD51C*$^{+/-}$ x *ku70*$^{-/-}$ *XRCC2*$^{+/-}$. Green – mutants, yellow – heterozygotes, n – number of plants analyzed

4.6.2.2. T-circles

Fig. 3-29 shows the TCA on selected genotypes of this population. As already shown previously (Zellinger, Akimcheva et al. 2007), the *ku70*$^{-/-}$ *rad51c*$^{-/-}$ and *ku70*$^{-/-}$ *xrcc2*$^{-/-}$ double mutants produce t-circles. In the *ku70*$^{-/-}$ *rad51c*$^{-/-}$ *xrcc2*$^{-/-}$ triple mutant t-circles were still produced.

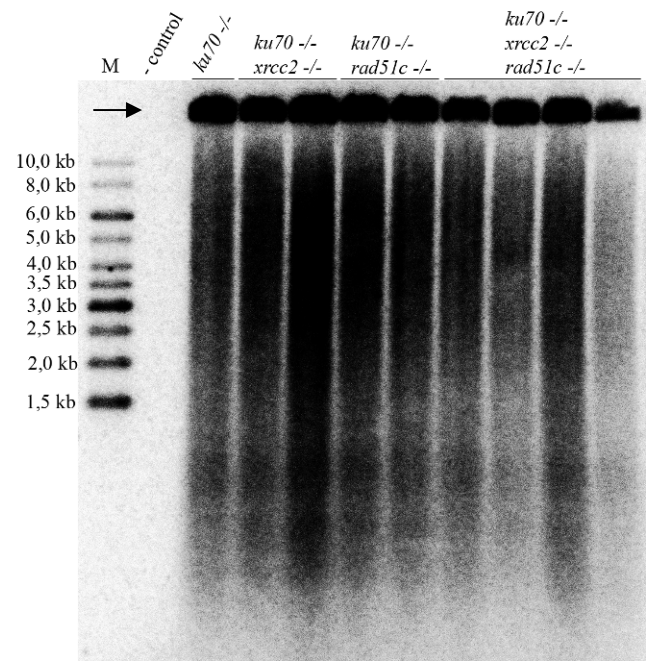

Fig. 3-29: TCA of out-segregated genotypes from the *ku70*$^{-/-}$ *XRCC2*$^{+/-}$ x *ku70*$^{-/-}$ *RAD51C*$^{+/-}$ cross. T-circles are still present in the triple mutant. Each lane represents a different sample derived from a pool of 2-3 plants of the same genotype. Smears seen below the high molecular weight signal are derived from TRFs. The arrow points to the high molecular weight signal derived from t-circles. M – marker, sizes as indicated; - control – no DNA

No residual complex parts, as RAD51D-XRCC2, are present in the *ku70*$^{-/-}$ *rad51c*$^{-/-}$ *xrcc2*$^{-/-}$ triple mutant. The presence of t-circles indicates that no residual activity of the BCDX2 complex is responsible for the t-circle formation observed in the *ku70*$^{-/-}$ *rad51*$^{-/-}$ *rad51c*$^{-/-}$ triple mutant. The BCDX2 complex might therefore not be important for t-circle formation.

4.7. Triple Mutant *ku70-1 xrcc2-1 rad51-1*

For gene onthologies and genotyping optimization of *RAD51* see chapter 4.5.1 and for *XRCC2* see chapter 4.6.1.

4.7.1. Analysis of the *ku70*$^{-/-}$ *xrcc2*$^{-/-}$ *rad51*$^{-/-}$ Triple Mutant

With this combination the BCDX2 complex is impaired, the CX3 complex is fully functional and *RAD51* is knocked out. Fig. 3-30 schematically shows the impairment of the analyzed complexes.

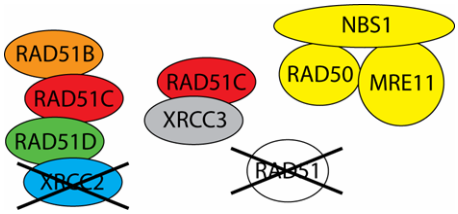

Fig. 3-30: Schematic representation of the impairment of the major recombination complexes in a triple mutant with *ku70*$^{-/-}$.

To test if RAD51 can act redundantly with XRCC2, the *xrcc2-1* and *rad51-1* mutations were combined.

4.7.1.1. Segregation Analysis

Segregation Analysis of $RAD51C^{+/-}$ $XRCC2^{+/-}$ showed almost double as many $xrcc2^{-/-}$ $rad51^{-/-}$ plants (14) and only half of $XRCC2^{+/+}$ $RAD51^{+/+}$ plants (3) as would expected by Mendelian segregation (6.44, table 3-9). This was the reason for the high χ^2-value of 14.53, which is below the critical value of 15.53. Therefore, this change from Mendelian segregation is not significant. In order to improve accuracy of the observed segregation pattern, more plants than 103 would have to be analyzed. The other segregated genotypes were in the expected range.

It turned out during genotyping, that the plants were segregated from a triple heterozygous plant ($KU70^{+/-}$ $XRCC2^{+/-}$ $RAD51^{+/-}$). It doesn't make a difference for segregation analysis, since only two loci are looked at for analysis.

Still 3 triple mutant plants could be recovered, which was enough for TCA analysis. Seeds from $ku70^{-/-}$ $XRCC2^{+/-}$ $RAD51^{+/-}$ and $KU70^{+/+}$ $XRCC2^{+/-}$ $RAD51^{+/-}$ were collected for further verification of the data in F3.

$KU70^{+/-}$		Number of plants		Probability	
n=103		Expected	Observed	Expected	Observed
$XRCC2^{+/+}$	$RAD51^{+/+}$	6,44	3	0,063	0,029
$XRCC2^{+/+}$	$RAD51^{+/-}$	12,88	8	0,125	0,078
$XRCC2^{+/-}$	$RAD51^{+/+}$	12,88	11	0,125	0,107
$XRCC2^{+/-}$	$RAD51^{+/-}$	25,75	23	0,250	0,223
$xrcc2^{-/-}$	$RAD51^{+/+}$	6,44	7	0,063	0,068
$xrcc2^{-/-}$	$RAD51^{+/-}$	12,88	13	0,125	0,126
$XRCC2^{+/+}$	$rad51^{-/-}$	6,44	6	0,063	0,058
$XRCC2^{+/-}$	$rad51^{-/-}$	12,88	17	0,125	0,165
$xrcc2^{-/-}$	$rad51^{-/-}$	6,44	14	0,063	0,136

$\chi^2 = 14.53$

Table 3-9: Segregation of $KU70^{+/-}$ $RAD51C^{+/-}$ $XRCC2^{+/-}$. Green – mutants, yellow – heterozygotes, light yellow bars – changes from Mendelian segregation

4.7.1.2. T-circles

We utilized the TCA to test if RAD51 can act redundantly to XRCC2 in t-circle formation. The TCA showed the presence of t-circles in $ku70^{-/-}$ $xrcc2^{-/-}$ $rad51^{-/-}$ triple mutants (fig. 3-31). This is consistent with the previous results including *rad51-1*, showing that *RAD51* is not essential for t-circle formation.

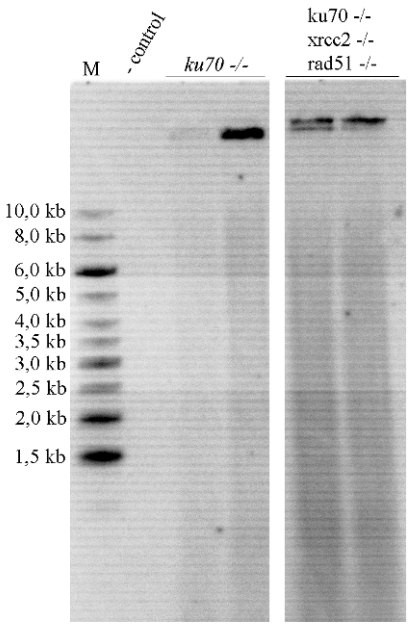

Fig. 3-31: TCA of *ku70*$^{-/-}$ *xrcc2*$^{-/-}$ *rad51*$^{-/-}$ triple mutant. *ku70*$^{-/-}$ serves as positive control. Each lane represents a different sample derived from a pool of 2-3 plants of the same genotype. Smears seen below the high molecular weight signal are derived from TRFs. The arrow points to the high molecular weight signal derived from t-circles. M – marker, sizes as indicated; - control – no DNA

RAD51 is not redundant to *XRCC2*. Results presented above showed that *RAD51* is also not redundant with *RAD51C*. Taken together the data from the 3 experiments described above, suggests that the BCDX2 complex has no important function in t-circle formation.

4.8. Triple mutant *ku70-1 mre11-3 rad51-1*

For the *RAD51* gene onthology and genotyping optimization see chapter 4.5.1.

4.8.1. MRE11

4.8.1.1. Function of MRE11

MRE11 is the core of the MRN complex (MRE11, RAD50, NBS1). MRE11 has a 3'-5' dsDNA exonuclease activity, but also a ssDNA endonuclease activity (reviewed in (D'Amours and Jackson 2002)). The MRN complex (MRX in yeast, MRE11, RAD50, XRS2) is important for DNA repair during replication and is involved in checkpoint signalling, which will not be discussed here. It has been shown that the MRN complex is required for maintenance of telomere length in yeast, mammals and plants (Kanaar, Hoeijmakers et al. 1998; Joenje and Patel 2001; West 2003). Due to its nuclease activity the MRN complex is thought to be involved in the formation of ssDNA 3' overhangs, which are necessary for strand invasion and is therefore involved in T-loop formation (Haber 1998; Shen, Xiao et al. 2003; West 2003). NBS1 is required for t-circle formation in *pot1a*$^{\Delta/\Delta}$ mutants in mice (Wu, Multani et al. 2006). *Mre11*$^{-/-}$ null mutant

mice result in early embryo lethality. In plants *mre11*$^{-/-}$ plants are viable but fully sterile (Bundock and Hooykaas 2002; Puizina, Siroky et al. 2004). Therefore, plants offer the possibility to study this gene in the context of an organism and perform genetic analysis on it. As in *S. cerevisiae* and vertebrates, the MRN complex is important for genome stability. This is also true for *A. thaliana*. *Atmre11*$^{-/-}$ plants show anaphase bridges in somatic cells with a frequency of 16.2% compared to 0.3% in wild type plants (Puizina, Siroky et al. 2004). 1.7% also show chromosome fragmentation. Plants show a growth phenotype, being smaller in size than wild type, but the size can vary and leaves show sort of a wrinkled phenotype (Puizina, Siroky et al. 2004). The alleles *MRE11-1* and *MRE11-2* show lengthened telomeres and some plants also show fasciation, hinting to chromosomal instabilities (Bundock and Hooykaas 2002).

4.8.1.2. Mutant Allele Used

AtMRE11 has the annotated number At5g54260 and as shown in fig. 3-32, consists of 23 exons. The *mre11-3* mutant allele (SALK_054418, ecotype Col-0) used here produces a truncated protein, which seems to be not functional (Puizina, Siroky et al. 2004). The mutant line has an at least double inverted T-DNA insertion (indicated by the two LBs), carrying a 170bp deletion (indicated by the triangle in fig. 3-32) deleting exon 10 completely (Puizina, Siroky et al. 2004).

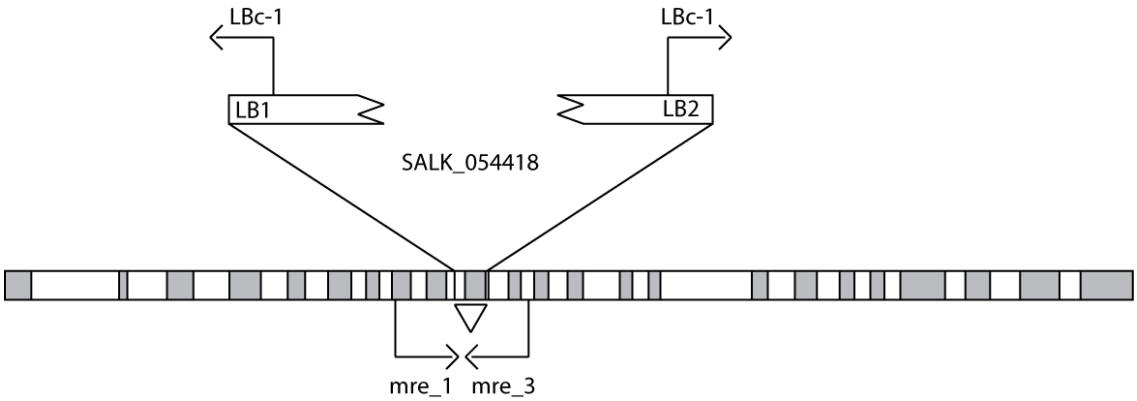

Fig. 3-32: *atMRE11*; *mre11-3* (1mm ≡ 30bp); Primers were used in the lab for genotyping *MRE11-3* before. LBc-1 – T-DNA specific primer, LB – Left Border, gray boxes – exons, triangle – 170bp deletion, complete exon 10 is deleted

4.8.1.3. Optimization of Genotyping

Fig. 3-33 shows the result of the optimization reaction. Detection of the wt allele by primers mre_1 and mre_3 resulted in an amplification product of 701bp in length. To identify the mutant allele, two set ups were possible. LB1 was detected by the 470bp

long product of primers mre_1 and LBc-1. Combining mre_3 and LBc-1 resulted in a product of 490bp in length, which indicated the presence of a second LB. In the multiplex set up, the two products of the mutant allele appeared as one strong band (left part in fig. 3-33). They also out-competed the wt allele reaction to a certain extent, but not completely, that's why the wt-allele could still be detected in the multiplex set up. There were two bands above the wt allele product which were chimeras from the different products in this reaction.

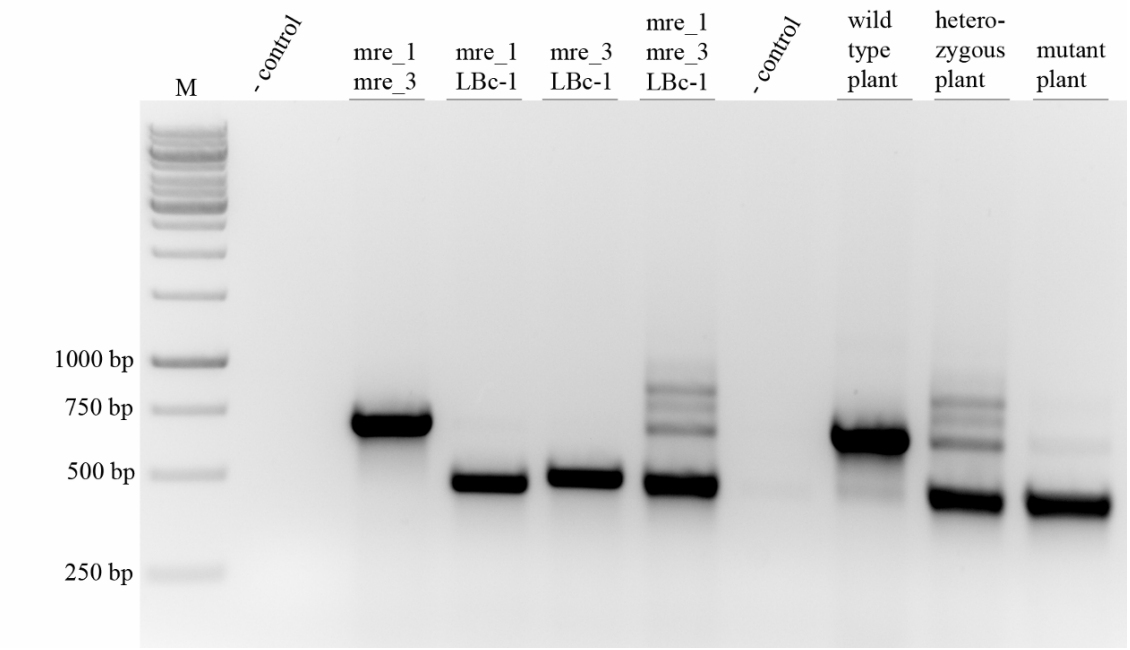

Fig. 3-33: Genotyping optimization of *MRE11-3*: The left side shows different primer combinations on DNA from a heterozygous plant, whereas on the right side different templates (as indicated) were used in a multiplex set up. M – marker, - control – no DNA, sizes as indicated, primers used as indicated

The test on the three possible genotypes showed that even though the wt-allele reaction competed weaker compared to the mutant-allele reaction, a clear distinction between the genotypes could be drawn (right part of fig. 3-33).

4.8.2. Analysis of the *ku70*$^{-/-}$ *mre11*$^{-/-}$ *rad51*$^{-/-}$ Triple Mutant

This combination of mutants leaves the BCDX2 and CX3 complexes fully functional, abolishes the function of the MRN complex and knocks out *RAD51* (fig. 3-34).

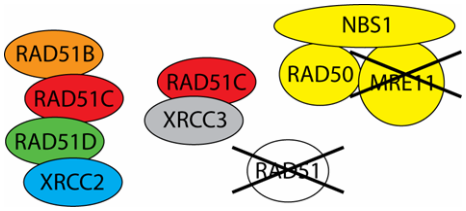

Fig. 3-34: Schematic representation of the impairment of the major recombination complexes in a triple mutant with *ku70*$^{-/-}$.

With the following analysis I tested for the role of the MRN complex and RAD51 in t-circle formation.

4.8.2.1. Segregation Analysis

The triple mutant was obtained and the segregation of this population was Mendelian as seen by the χ^2-value of 10.77, which is below the critical value of 15.51 (table 3-10).

***ku70*$^{-/-}$**		**Number of plants**		**Probability**	
n=124		**Expected**	**Observed**	**Expected**	**Observed**
***MRE11*$^{+/+}$**	***RAD51*$^{+/+}$**	7,75	5	0,063	0,040
***MRE11*$^{+/+}$**	***RAD51*$^{+/-}$**	15,50	24	0,125	0,194
***MRE11*$^{+/-}$**	***RAD51*$^{+/+}$**	15,50	16	0,125	0,129
***MRE11*$^{+/-}$**	***RAD51*$^{+/-}$**	31,00	30	0,250	0,242
***mre11*$^{-/-}$**	***RAD51*$^{+/+}$**	7,75	9	0,063	0,073
***mre11*$^{-/-}$**	***RAD51*$^{+/-}$**	15,50	19	0,125	0,153
***MRE11*$^{+/+}$**	***rad51*$^{-/-}$**	7,75	5	0,063	0,040
***MRE11*$^{+/-}$**	***rad51*$^{-/-}$**	15,50	11	0,125	0,089
***mre11*$^{-/-}$**	***rad51*$^{-/-}$**	7,75	4	0,063	0,032

χ^2 = 10.77

Table 3-10: Segregation of F2 *ku70*$^{-/-}$ *MRE11*$^{+/-}$ x *ku70*$^{-/-}$ *RAD51*$^{+/-}$. Green – mutants, yellow - heterozygotes

4.8.2.2. T-circles

We tested for a role of MRE11 and RAD51 in t-circle formation by utilizing the TCA. As can be seen in figure 3-35 t-circles were formed in the triple mutant. This showed that neither *RAD51* nor *MRE11* are important for t-circle formation.

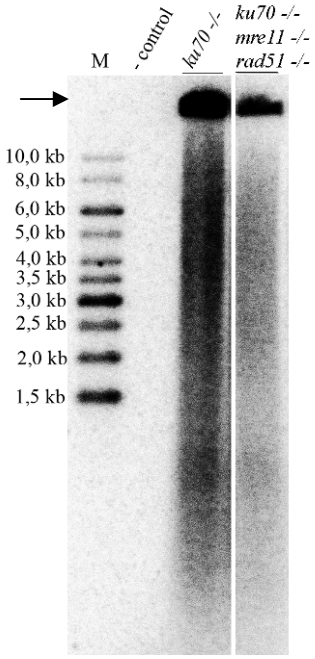

Fig. 3-35: TCA of *ku70*$^{-/-}$ *mre11-3*$^{-/-}$ *rad51*$^{-/-}$ triple mutant. *ku70*$^{-/-}$ serves as positive control. Each lane represents a different sample derived from a pool of 2-3 plants of the same genotype. Smears seen below the high molecular weight signal are derived from TRFs. The arrow points to the high molecular weight signal derived from t-circles. M – marker, sizes as indicated; - control – no DNA

4.9. Summary on Obtained Triple Mutants

In the four triple mutant combinations analyzed so far, t-circles were still generated. In comparison with the previous results from double mutants (Zellinger, Akimcheva et al. 2007), we now can exclude a redundant function between *RAD51* and *RAD51C*, as well as between *RAD51* and *XRCC2*. Residual function of RAD51D-XRCC2 (Liu, Masson et al. 2004) can also be excluded. We suggest that the BCDX2 complex has no important role in t-circle formation. Both the MRN complex and RAD51 are not required for t-circle formation. Resolving redundancy between MRN and the BCDX2 and CX3 complexes cannot be excluded so far.

The following combinations should address the question of redundancy between MRN and BCDX2 and CX3 complexes, redundancy between BCDX2 and CX3 as well as the role of the CX3 complex in t-circle formation.

4.10. Triple Mutant *ku70-1 mre11-3 rad51c-1*

For gene onthologies and genotyping optimization of *RAD51C* see chapter 4.5.1 and for *MRE11* see chapter 4.8.1.

4.10.1. Analysis of the *ku70*$^{-/-}$ *mre11*$^{-/-}$ *rad51c*$^{-/-}$ Triple Mutant

This combination of mutants abolishes the function of the MRN complex and impairs the BCDX2 and the CX3 complex (fig. 3-36).

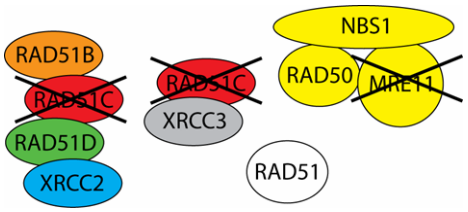

Fig. 3-36: Schematic representation of the impairment of the major recombination complexes in a triple mutant with *ku70*$^{-/-}$.

With this combination of mutants I tested if the activity of the MRN complex is important for the activity of the BCDX2 and CX3 complexes in t-circle formation.

4.10.1.1. Segregation Analysis

No triple mutant was obtained and segregation analysis was employed to test for anomalies in segregation (table 3-11). The analysis revealed that less

ku70$^{-/-}$ *MRE11*$^{+/+}$ *RAD51C*$^{+/+}$ plants were obtained (2 instead of 7 to 8) and that the genotypes containing *mre11*$^{-/-}$ were drastically reduced (only 5 in total instead of 23-24). There was also an obvious change in the numbers of genotypes containing *rad51c*$^{-/-}$. The expected 1:2 ratio between *MRE11*$^{+/+}$ *rad51c*$^{-/-}$ (21 observed, 7-8 expected) and *MRE11*$^{+/-}$ *rad51c*$^{-/-}$ (21 observed, 15-16 expected) was changed to 1:1. The χ^2-value 54.16, which is above the critical value of 15.51, indicates a significant change from Mendelian segregation.

ku70$^{-/-}$		**Number of plants**		**Probability**	
n=124		**Expected**	**Observed**	**Expected**	**Observed**
MRE11$^{+/+}$	*RAD51C*$^{+/+}$	7,75	2	0,063	0,016
MRE11$^{+/+}$	***RAD51C***$^{+/-}$	15,50	18	0,125	0,145
MRE11$^{+/-}$	***RAD51C***$^{+/+}$	15,50	18	0,125	0,145
MRE11$^{+/-}$	*RAD51C*$^{+/-}$	31,00	39	0,250	0,315
mre11$^{-/-}$	*RAD51C*$^{+/+}$	7,75	3	0,063	0,024
mre11$^{-/-}$	*RAD51C*$^{+/-}$	15,50	2	0,125	0,016
MRE11$^{+/+}$	*rad51c*$^{-/-}$	7,75	21	0,063	0,169
MRE11$^{+/-}$	*rad51c*$^{-/-}$	15,50	21	0,125	0,169
mre11$^{-/-}$	*rad51c*$^{-/-}$	7,75	0	0,063	0,000

χ^2 = 54.16

Table 3-11: Segregation of F2 *ku70*$^{-/-}$ *MRE11*$^{+/-}$ x *ku70*$^{-/-}$ *RAD51C*$^{+/-}$. Yellow bars highlight the changes in the segregation pattern. Green – mutants, yellow – heterozygotes

No recovery of a *ku70*$^{-/-}$ *mre11*$^{-/-}$ *rad51c*$^{-/-}$ triple mutant could be explained by lethality. But the 4 fold decrease in segregated *ku70*$^{-/-}$ *MRE11*$^{+/+}$ *RAD51C*$^{+/+}$ plants suggest that lethality of the *ku70*$^{-/-}$ *mre11*$^{-/-}$ *rad51c*$^{-/-}$ triple mutant is not the only reason. A 6.2 fold decrease in segregated *mre11*$^{-/-}$ containing genotypes was striking. If the *ku70*$^{-/-}$ *mre11*$^{-/-}$ *rad51c*$^{-/-}$ triple mutant is synthetically lethal this is still a 4.7 fold decrease.

In order to figure out if the Non-Mendelian segregation is due to the combination of the mutations or if there is a defect already in the segregation of a single locus, I performed an independent segregation analysis of the single loci from the same dataset.

Analysis of the single locus showed a clear bias against *mre11*$^{-/-}$ (table 3-12). The other two genotypes were more abundant as expected. *MRE11*$^{+/+}$ showed a 1.4 fold increase, *MRE11*$^{+/-}$ a 1.3 fold increase, whereas *mre11*$^{-/-}$ decreased 6.2 fold. This change was clearly significant as seen by the χ^2-value of 30.06.

ku70$^{-/-}$	Number of plants		Probability	
n=126	Expected	Observed	Expected	Observed
MRE11$^{+/+}$	31,25	43	0,25	0,341
MRE11$^{+/-}$	62,50	78	0,50	0,619
mre11$^{-/-}$	31,25	5	0,25	0,040

χ^2 = 30.06

Table 3-12: Segregation of *MRE11* single locus. Yellow bar highlights the most striking change in the segregation pattern. Green – mutants, yellow - heterozygotes

RAD51C also segregated Non-Mendelian (table 3-13). The χ^2-value of 6.61 was above the critical value of 5.99 for these parameters (2 degrees of freedom, error probability of 0.05). But in contrast to *MRE11*, this locus showed a bias towards *rad51c*$^{-/-}$ (1.3 fold increase) on cost of *RAD51C*$^{+/+}$ (1.4 fold decrease).

ku70$^{-/-}$	Number of plants		Probability	
n=124	Expected	Observed	Expected	Observed
RAD51C$^{+/+}$	31,25	23	0,25	0,183
RAD51C$^{+/-}$	62,50	59	0,50	0,468
rad51c$^{-/-}$	31,25	42	0,25	0,333

χ^2 =6.11

Table 3-13: Segregation of *RAD51C* single locus. Yellow bar highlights the most striking change in the segregation pattern. Green – mutants, yellow - heterozygotes

Interestingly, the two loci seemed to behave inversely (*mre11*$^{-/-}$ go down, *rad51c*$^{-/-}$ go up).

After segregation analysis of the single loci it was clear, that the Non-Mendelian segregation is due to Non-Mendelian segregation of the single loci and does not need to be caused by combining *MRE11* and *RAD51C*, even though this possibility still cannot be ruled out.

Populations of this combination were regrown three times, but no more *mre11*$^{-/-}$ were observed. This was judged by the leaf phenotype (Puizina, Siroky et al. 2004) of *mre11*$^{-/-}$ plants by eye. Since none have been observed, and our interest was in the triple mutant, genotyping was not performed. Therefore the number for the segregation analysis is still low and refers only to one population. Nonetheless the bias against *mre11*$^{-/-}$ plants was reproduced.

4.10.1.2. Growth Phenotype of Mutant Combinations

The five plants carrying *mre11*$^{-/-}$ showed a growth phenotype as can be seen in fig. 3-37. *Ku70*$^{-/-}$ *MRE11*$^{+/-}$ *RAD51C*$^{+/-}$ plants had wild type appearance and seemed to be fully fertile (right plant in fig. 3-37). The three *ku70*$^{-/-}$ *mre11*$^{-/-}$ double mutants obtained

showed the leaf phenotype and the variation in size which are usual for *mre11*$^{-/-}$ (Puizina, Siroky et al. 2004). But the two *ku70*$^{-/-}$ *mre11*$^{-/-}$ *RAD51C*$^{+/-}$ plants obtained (table 3-11) were severely retarded in growth, showed a dwarfed phenotype and flowered late (left plant in fig. 3-37). By time of finishing this thesis this phenotype remained unreproduced, since no more *mre11*$^{-/-}$ plants could be generated in the populations regrown from the same seed stock.

Since the number of plants was too low, and the plants were very small, no DNA from the two *ku70*$^{-/-}$ *mre11*$^{-/-}$ *RAD51C*$^{+/-}$ plants was extracted for TCA analysis.

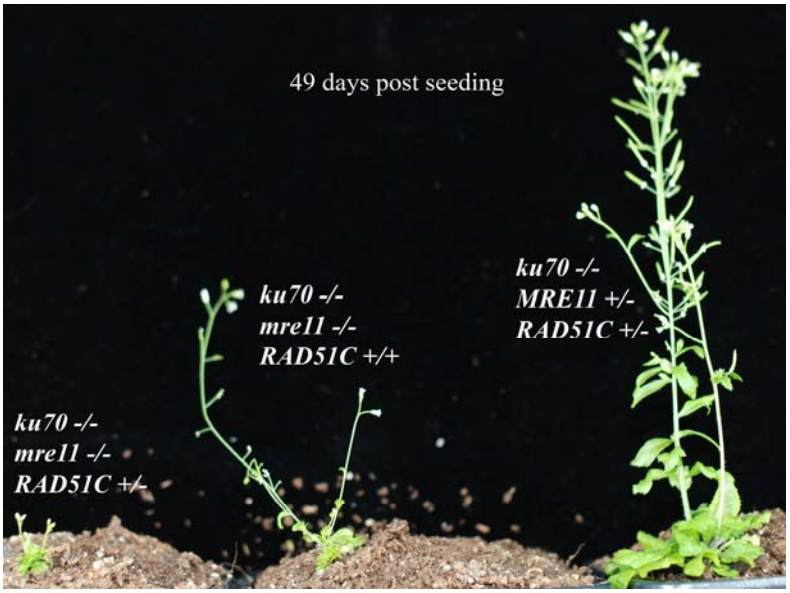

Fig. 3-37: Phenotypes of *ku70*$^{-/-}$ *MRE11*$^{+/-}$ *RAD51C*$^{+/-}$, *ku70*$^{-/-}$ *mre11*$^{-/-}$ *RAD51C*$^{+/+}$ and *ku70*$^{-/-}$ *mre11*$^{-/-}$ *RAD51C*$^{+/-}$ plants (r. to l.). The genotypes are indicated next to the corresponding plant.

Since those genotypes are on *ku70*$^{-/-}$ background, we were interested if the Non-Mendelian segregation is *KU*-dependent. Therefore a control cross was performed and brought to F2 generation, which, by time of finishing this thesis, has not been grown and analyzed.

4.10.1.3. Lethality of the Male Gametophyte

The bias against *mre11*$^{-/-}$ plants and non-recovery of a *ku70*$^{-/-}$ *mre11*$^{-/-}$ *rad51c*$^{-/-}$ triple mutant suggested involvement of lethality. We used Alexander staining as a test for lethality of the male gametophyte. It was performed on *MRE11*$^{+/-}$ *RAD51C*$^{+/-}$ plants from the F1 generation of the control cross (fig. 3-38).

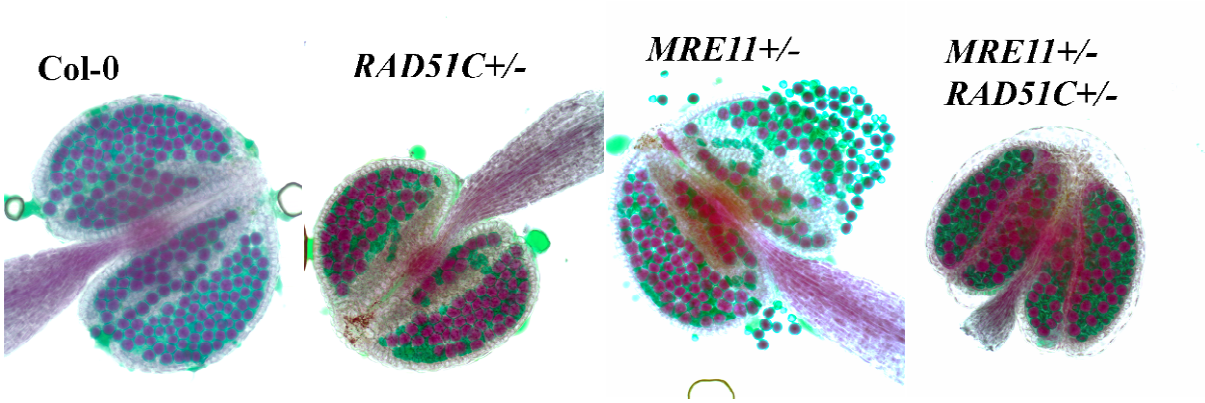

Fig. 3-38: Alexander stainings of Col-0. Out-segregated F1 *RAD51C*$^{+/-}$ *MRE11*$^{+/-}$ and *MRE11*$^{+/-}$ *RAD51C*$^{+/-}$. Viable pollen are purple, dead pollen are green.

The Alexander stain (Alexander 1969) is a mixture of dyes staining the pollen wall and the cytoplasm differentially. If pollen is dead, there is no cytoplasm left and only the pollen wall can be stained, appearing green. In viable pollen the cytoplasm is stained as well, appearing purple, making viable pollen appear purple with a green border.

Wild type Col-0 shows full pollen viability. *RAD51C*$^{+/-}$ shows few dead pollen. *MRE11*$^{+/-}$ clearly shows some pollen lethality and in the *MRE11*$^{+/-}$ *RAD51C*$^{+/-}$ double heterozygote pollen viability is clearly reduced.

Combining *MRE11-3* and *RAD51C-1* resulted in reduced pollen viability in double heterozygous plants. They showed Non-Mendelian segregation, which was most likely due to Non-Mendelian segregation of the single locus. By the time of finishing this thesis it was still unclear whether this is *KU* dependent and to what extend pollen lethality plays a role.

4.11. Triple Mutant *ku70-1 rad51c-1 xrcc3-1*

For the *RAD51C* gene onthology and genotyping optimization see chapter 4.5.2.

4.11.1. XRCC3

4.11.1.1. Function of XRCC3

XRCC3 is part of the CX3 complex and was implicated with a Holliday junction resolving function in HeLa cell extracts (Liu, Masson et al. 2004; Liu, Tarsounas et al. 2007). It was shown in human HT116 colon carcinoma cells that the formation of extra-chromosomal t-circles depends on XRCC3 (Wang, Smogorzewska et al. 2004). *Xrcc3*$^{-/-}$

plants are fully viable but male sterile (Bleuyard and White 2004). Again, plants offer the possibility to study the function of this gene utilizing genetic analysis.

4.11.1.2. Mutant Allele Used

The gene has the annotated number At5g57450 and consists of one exon (fig. 3-39). *XRCC3-1* (SALK_045564, ecotype Col-0) carries at least a double inverted T-DNA insertion (Bleuyard and White 2004).

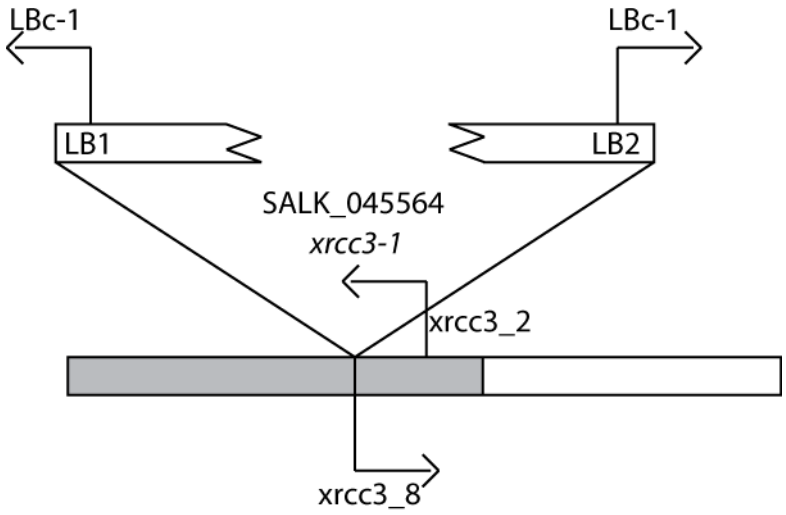

Fig. 3-39: *atXRCC3*; *xrcc3-1* (1mm ≡ 20bp); LB – Left Border, primers used and position of primers as indicated, gray box – exon

Sequencing analysis by Bleuyard et al. revealed that the *xrcc3-1* allele has single base pair changes both at the 5' end and at the 3' end of the T-DNA insertion (Bleuyard and White 2004). Primers were designed in both directions to span over those single base pair changes to lead to a discriminating mismatch in the genotyping reaction. The combination of xrcc3_8 and LBc-1 was successful and is shown in figures 3-39 & -40. After optimization only unspecific background bands were observed (lane xrcc3_8, LBc-1 lane in fig. 3-40), which disappeared when a multiplex set up was employed. LBc-1 competed better than xrcc3_8 on a heterozygous template, resulting in a weaker wt band (lane xrcc3_2, xrcc3_8, LBc-1 and lane heterozygous plant in fig. 3-40). Since the 230bp wt and the 365bp mutant product were less than 200bp apart and very small, a high percentage (2%) agarose gel was needed for clear separation (left part of fig. 3-40).

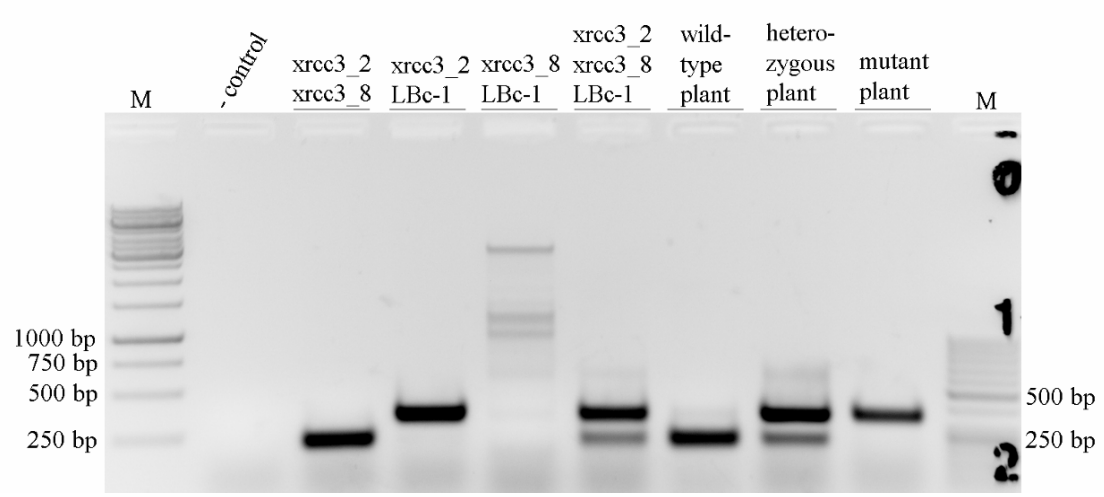

Fig. 3-40: Optimization for *XRCC3-1* genotyping: The left side shows different primer combinations on DNA from a heterozygous plant, whereas on the right side different templates (as indicated) were used with the three primer set up. M – marker, - control – no DNA, sizes as indicated, primers used as indicated

The test of the multiplex set up on different templates revealed that this primer combination is suitable and reliable for genotyping *XRCC3-1* (right part of fig. 3-40).

4.11.2. Analysis of the *ku70*$^{-/-}$ *rad51c*$^{-/-}$ *xrcc3*$^{-/-}$ Triple Mutant

This combination of mutants leaves the MRN complex intact, impairs the BCDX2 complex and completely knocks out the CX3 complex (fig. 3-41).

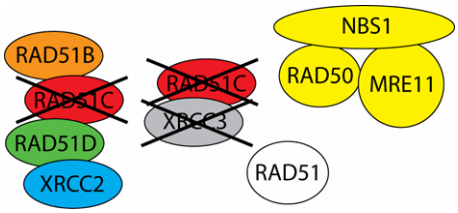

Fig. 3-41: Schematic representation of the impairment of the major recombination complexes in a triple mutant with *ku70*$^{-/-}$.

With the following analysis I aimed to test if the CX3 complex is the essential complex in t-circle formation in *A. thaliana*.

4.11.2.1. Segregation Analysis

The triple mutant for this combination was never obtained. The population was regrown several times and three different set ups for genotyping were employed to exclude the possibility of faulty genotyping. I analyzed 364 plants, and still could not find a *ku70*$^{-/-}$ *rad51c*$^{-/-}$ *xrcc3*$^{-/-}$ triple mutant. In fact, segregation analysis showed that every genotype was off Mendelian expectancies (table 3-14). For example, only two *ku70*$^{-/-}$ *RAD51C*$^{+/+}$ *XRCC3*$^{+/+}$ plants were generated, which is an 11.4 fold reduction. *Ku70*$^{-/-}$ *RAD51C*$^{+/+}$ *XRCC3*$^{+/-}$ and *ku70*$^{-/-}$ *RAD51C*$^{+/-}$ *XRCC3*$^{+/+}$ plants were also found

to be below expectancy with a 4.1 fold and a 4.6 fold reduction, respectively. In contrast 178 *ku70*$^{-/-}$ *RAD51C*$^{+/-}$ *XRCC3*$^{+/-}$ plants were almost twice as many as expected (91 plants), a 2.0 fold increase. Even more severe was the change of the 1:2 ratio of *rad51c*$^{-/-}$ *XRCC3*$^{+/+}$ to *rad51c*$^{-/-}$ *XRCC3*$^{+/-}$ and vice versa. This ratio was inverted and increased dramatically. For *rad51c*$^{-/-}$ *XRCC3*$^{+/+}$ to *rad51c*$^{-/-}$ *XRCC3*$^{+/-}$ it became 11.8 to 1, for *RAD51C*$^{+/+}$ *xrcc3*$^{-/-}$ to *RAD51C*$^{+/-}$ *xrcc3*$^{-/-}$ the ratio became 11.3 to 1 instead of the expected 1:2 ratio. This change of the segregation behaviour was very significant (χ^2 = 486.99). Such Non-Mendelian segregation could not be explained by lethality of the *rad51c*$^{-/-}$ *xrcc3*$^{-/-}$ combination alone.

ku70$^{-/-}$		**Number of plants**		**Probability**	
n=364		**Expected**	**Observed**	**Expected**	**Observed**
RAD51C$^{+/+}$	***XRCC3***$^{+/+}$	22,75	2	0,063	0,006
RAD51C$^{+/+}$	***XRCC3***$^{+/-}$	45,50	11	0,125	0,028
RAD51C$^{+/-}$	***XRCC3***$^{+/+}$	45,50	10	0,125	0,030
RAD51C$^{+/-}$	***XRCC3***$^{+/-}$	91,00	178	0,250	0,489
rad51c$^{-/-}$	***XRCC3***$^{+/+}$	22,75	71	0,063	0,195
rad51c$^{-/-}$	***XRCC3***$^{+/-}$	45,50	6	0,125	0,017
RAD51C$^{+/+}$	***xrcc3***$^{-/-}$	22,75	79	0,063	0,217
RAD51C$^{+/-}$	***xrcc3***$^{-/-}$	45,50	7	0,125	0,019
rad51c$^{-/-}$	***xrcc3***$^{-/-}$	22,75	0	0,063	0

χ^2 = 486.99

Table 3-14: Segregation of F2 *ku70*$^{-/-}$ *RAD51C*$^{+/-}$ x *ku70*$^{-/-}$ *XRCC3*$^{+/-}$. Green – mutants, yellow - heterozygotes

Now we wanted to know if, as in the *ku70*$^{-/-}$ *MRE11*$^{+/-}$ x *ku70*$^{-/-}$ *RAD51C*$^{+/-}$ cross, this change is due to Non-Mendelian segregation of the single loci. Therefore I took the same dataset and performed an independent segregation analysis of the single loci. As it turned out, the single loci segregated Mendelian (tables 3-15 & 3-16 with χ^2 = 3.20 and χ^2 = 2.34, respectively, both below the critical value of 5.99).

ku70$^{-/-}$	**Number of plants**		**Probability**	
n=368	**Expected**	**Observed**	**Expected**	**Observed**
RAD51C$^{+/+}$	92	92	0,25	0,250
RAD51C$^{+/-}$	184	198	0,50	0,538
rad51c$^{-/-}$	92	78	0,25	0,212

χ^2 = 3.20

Table 3-15: Segregation of *RAD51C* single locus of F2 *ku70*$^{-/-}$ *RAD51C*$^{+/-}$ x *ku70*$^{-/-}$ *XRCC3*$^{+/-}$. Green – mutants, yellow – heterozygotes

ku70$^{-/-}$	Number of plants		Probability	
n=367	Expected	Observed	Expected	Observed
XRCC3$^{+/+}$	91,8	83	0,25	0,226
XRCC3$^{+/-}$	183,5	198	0,50	0,538
xrcc3$^{-/-}$	91,8	86	0,25	0,234

$\chi^2 = 2.34$

Table 3-16: Segregation of *XRCC3* single locus of F2 *ku70*$^{-/-}$ *RAD51C*$^{+/-}$ x *ku70*$^{-/-}$ *XRCC3*$^{+/-}$. Green – mutants, yellow - heterozygotes

In contrast to the *ku70*$^{-/-}$ *MRE11*$^{+/-}$ *RAD51C*$^{+/-}$ segregation pattern, this segregation pattern is due to combining *RAD51C-1* and *XRCC3-1*.

The next question we addressed was if the Non-Mendelian segregation of *RAD51C*$^{+/-}$ *XRCC3*$^{+/-}$ could be due to the *ku70*$^{-/-}$ mutant background. So I performed control crosses with *RAD51C*$^{+/-}$ and *XRCC3*$^{+/-}$ and brought this cross to the F2 generation to see if the observed Non-Mendelian segregation pattern is *KU*-dependent.

4.11.2.2. Segregation Analysis of the control *RAD51C*$^{+/-}$ *XRCC3*$^{+/-}$ F2 population

Segregation analysis showed the same distortions from Mendelian segregation on wild type background as on *ku70*$^{-/-}$ background (table 3-17). The change from Mendelian segregation was significant as indicated by a χ^2-value of 151.29, which is greater than the critical value of 15.51. In contrast to the population on *ku70*$^{-/-}$ background, no wild type plant could be obtained. *RAD51C*$^{+/-}$ *XRCC3*$^{+/-}$ were almost twice as abundant as expected (1.9 fold increase), and the 1:2 ratios again were inverted. For *rad51c*$^{-/-}$ *XRCC3*$^{+/+}$ to *rad51c*$^{-/-}$ *XRCC3*$^{+/-}$ it became 5.5 to 1, and 4.6 to 1 for *RAD51C*$^{+/+}$ *xrcc3*$^{-/-}$ to *RAD51C*$^{+/-}$ *xrcc3*$^{-/-}$.

Wt		Number of plants		Probability	
n=146		**Expected**	**Observed**	**Expected**	**Observed**
***RAD51C*$^{+/+}$**	***XRCC3*$^{+/+}$**	9,13	0	0,063	0,000
***RAD51C*$^{+/+}$**	***XRCC3*$^{+/-}$**	18,25	8	0,125	0,055
***RAD51C*$^{+/-}$**	***XRCC3*$^{+/+}$**	18,25	6	0,125	0,041
***RAD51C*$^{+/-}$**	***XRCC3*$^{+/-}$**	35,50	67	0,250	0,459
***rad51c*$^{-/-}$**	***XRCC3*$^{+/+}$**	9,13	22	0,063	0,151
***rad51c*$^{-/-}$**	***XRCC3*$^{+/-}$**	18,25	4	0,125	0,027
***RAD51C*$^{+/+}$**	***xrcc3*$^{-/-}$**	9,13	32	0,063	0,219
***RAD51C*$^{+/-}$**	***xrcc3*$^{-/-}$**	18,25	7	0,125	0,048
***rad51c*$^{-/-}$**	***xrcc3*$^{-/-}$**	9,13	0	0,063	0,000

$\chi^2 = 151.29$

Table 3-17: Segregation of F2 from crosses *RAD51C*$^{+/-}$ x *XRCC3*$^{+/-}$ and *XRCC3*$^{+/-}$ x *RAD51C*$^{+/-}$ summarized by genotype, since the direction of the cross had no influence on segregation. Green – mutants, yellow – heterozygotes

In order to see if the Non-Mendelian segregation is due to the combination of the mutations or due to Non-Mendelian segregation of the single loci, an independent segregation analysis of the single loci form the same dataset was performed.

	Number of plants		Probability	
n=147	**Expected**	**Observed**	**Expected**	**Observed**
***RAD51C*$^{+/+}$**	36,75	40	0,25	0,272
***RAD51C*$^{+/-}$**	73,50	81	0,50	0,551
***rad51c*$^{-/-}$**	36,75	26	0,25	0,177

$\chi^2 = 4.20$

Table 3-18: Segregation of *RAD51C* single locus of F2 from crosses *RAD51C*$^{+/-}$ x *XRCC3*$^{+/-}$ and *XRCC3*$^{+/-}$ x *RAD51C*$^{+/-}$ summarized by genotype. Green – mutants, yellow - heterozygotes

	Number of plants		Probability	
n=145	**Expected**	**Observed**	**Expected**	**Observed**
***XRCC3*$^{+/+}$**	36,25	28	0,25	0,193
***XRCC3*$^{+/-}$**	72,50	78	0,50	0,538
***xrcc3*$^{-/-}$**	36,25	39	0,25	0,269

$\chi^2 = 2.50$

Table 3-19: Segregation of *XRCC3* single locus of F2 from crosses *RAD51C*$^{+/-}$ x *XRCC3*$^{+/-}$ and *XRCC3*$^{+/-}$ x *RAD51C*$^{+/-}$ summarized by genotype. Green – mutants, yellow - heterozygotes

Segregation analysis of the single loci showed Mendelian segregation (tables 3-18 & 3-19 with $\chi^2 = 4.20$ & $\chi^2 = 2.50$, respectively, both are below the critical value of 5.99).

On wild type background as well as on *ku70*$^{-/-}$ background, the Non-Mendelian segregation is due to the combination of the mutations. Since there are the same distortions observed in both genetic backgrounds, the Non-Mendelian segregation is not *KU*-dependent.

4.11.2.3. T-circles

As can be seen from table 3-14, *ku70*$^{-/-}$ *RAD51C*$^{+/-}$ *xrcc3*$^{-/-}$ could be obtained and this genotype was analyzed in a TCA. Figure 3-42 shows that even the strong impairment of the CX3 complex still leads to t-circle formation.

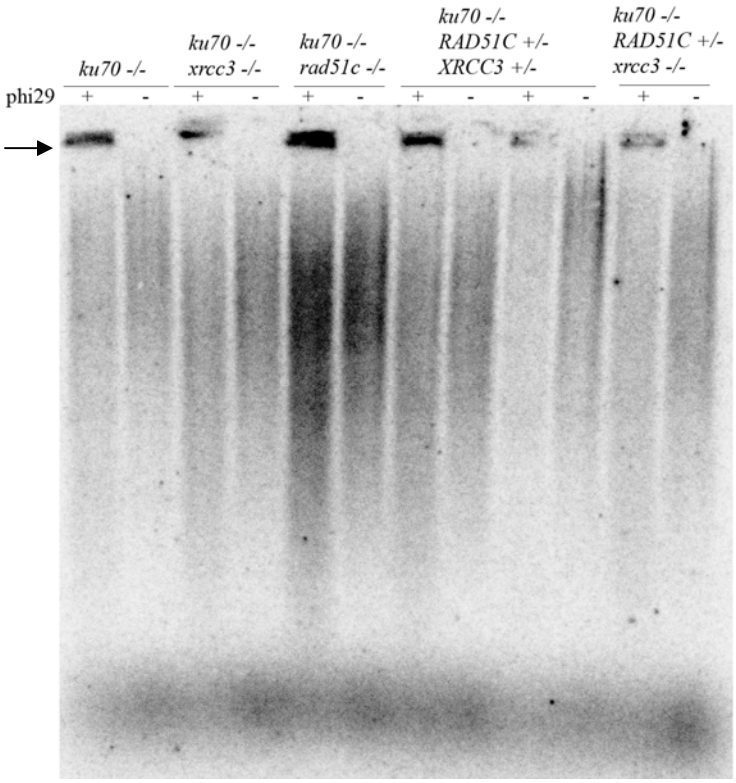

Fig. 3-42: TCA of obtained genotypes from the *ku70*$^{-/-}$ *RAD51C*$^{+/-}$ x *ku70*$^{-/-}$ *XRCC3*$^{+/-}$ cross. T-circles are present also in a plant containing 5 mutated alleles. -: no phi29 DNA polymerase added, serves as negative control. The arrow points towards the high molecular weight signal derived form t-circles. Smears seen below the high molecular weight signal are derived from TRFs.

4.11.2.4. Lethality of the Male Gametophyte

Why was it not possible to obtain a triple mutant? Our first hypothesis was that the CX3 complex is essential for survival and the *rad51c*$^{-/-}$ *xrcc3*$^{-/-}$ double mutant combination is therefore synthetically lethal. If this would be true, more *RAD51C*$^{+/+}$ *XRCC3*$^{+/+}$ plants should have been generated. This was not the case as can be seen from tables 3-14 and 3-17. Lethality of the *rad51c*$^{-/-}$ *xrcc3*$^{-/-}$ double and *ku70*$^{-/-}$ *rad51c*$^{-/-}$ *xrcc3*$^{-/-}$ triple mutant combination alone cannot explain the observed Non-Mendelian segregation pattern.

Nonetheless we wanted to know if lethality is involved. Therefore we utilized Alexander staining to check for pollen viability.

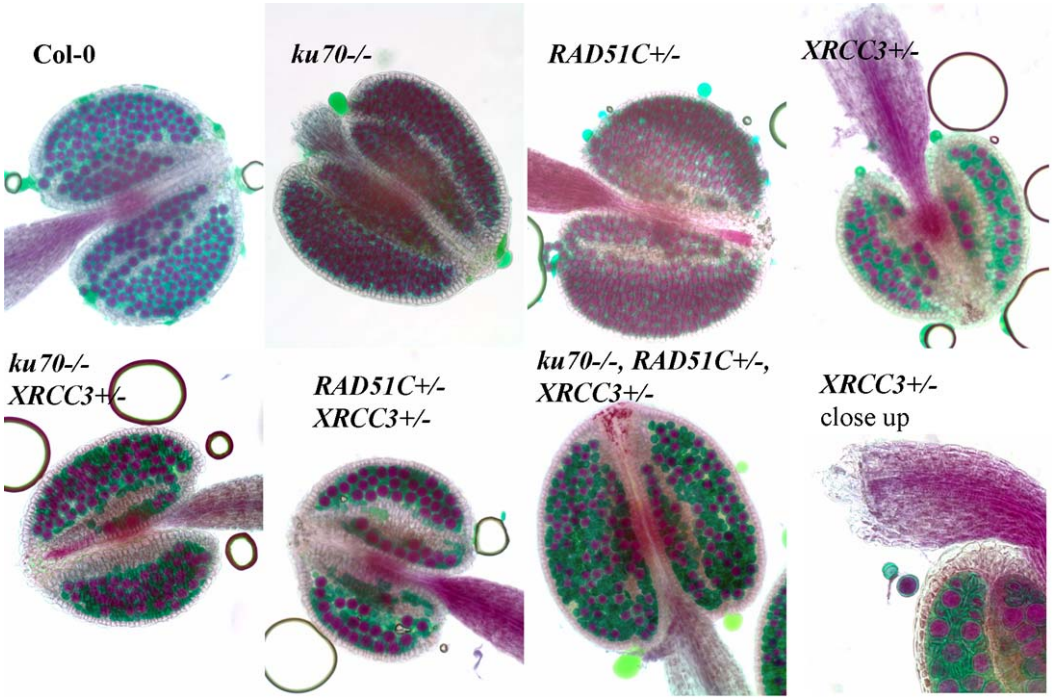

Fig. 3-43: Alexander staining of different genotypes of out-segregated plants from two different crossings. Genotypes as indicated. Purple – viable pollen, green – dead pollen

As can be seen in figure 3-43 all pollen are viable in Col-0 wild type plants, in *ku70*$^{-/-}$ and in *RAD51C*$^{+/-}$ plants. Detecting pollen lethality in *XRCC3*$^{+/-}$ was surprising, since those plants segregate Mendelian. If the *xrcc3-1*$^{-}$ allele is male gametophytically lethal, it would not be possible to segregate *xrcc3*$^{-/-}$ plants. Mendelian segregation from an *XRCC3*$^{+/-}$ plant could not be explained. This suggests that the observed lethality affects both the *xrcc3-1*$^{-}$ and the *XRCC3*$^{+}$ genotypes. This lethality also must be linked to the *XRCC3* gene, otherwise the lethality would be lost over generations.

RAD51C$^{+/-}$ *XRCC3*$^{+/-}$ plants also show pollen lethality, which is independent of *KU*. This is in correlation with the segregation analysis data. Counting viable pollen of all those genotypes and comparing it to the wild type situation lead to unsatisfying results. Anther size and number of pollen depends very much on the growth conditions. Differences on the same tray already have an effect. Nonetheless the results of this approach suggest no additive affect of *RAD51C*$^{+/-}$ onto *XRCC3*$^{+/-}$. Therefore pollen lethality in *RAD51C*$^{+/-}$ *XRCC3*$^{+/-}$ plants is due to pollen lethality of the *XRCC3*$^{+/-}$ plants. Still, an additive effect of the two mutations on pollen lethality cannot be excluded. Segregation analysis suggested no additive effect, since the wild type allele carrying genotypes *RAD51C*$^{+/+}$ *XRCC3*$^{+/-}$ and vice versa were as abundant as the mutant allele carrying genotypes *rad51c*$^{-/-}$ *XRCC3*$^{+/-}$ and vice versa.

4.11.2.5. DAPI Staining of Pollen from *XRCC3*$^{+/-}$ Plants

Since some pollen from *XCRR3*$^{+/-}$ plants were stained purple only partially, we wanted to know if this is due to dying of one of the three nuclei in mature pollen. Therefore I performed DAPI staining on pollen grains (fig. 3-44)

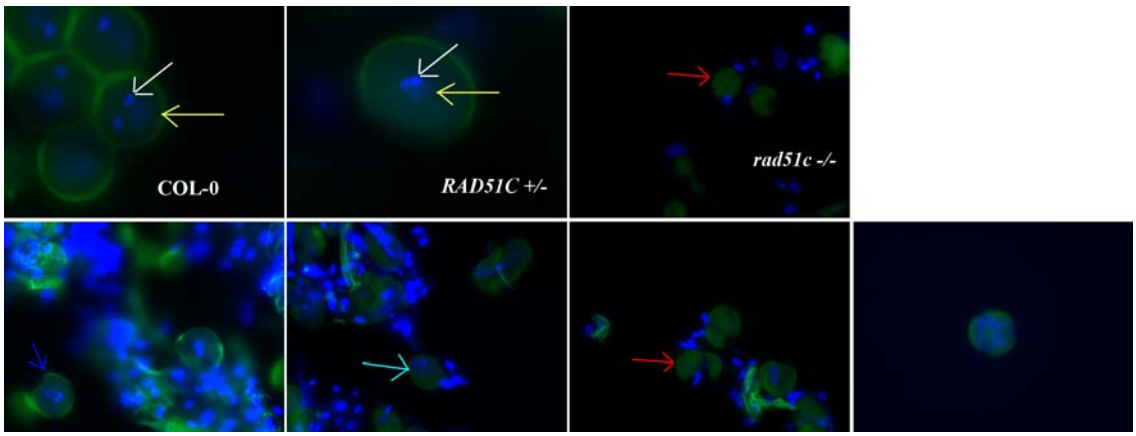

Fig. 3-44: DAPI staining of pollen. Genotypes are as indicated and the lower row only shows pollen from *XRCC3*$^{+/-}$ plants. The yellow arrow indicates the vegetative nucleus, the white arrow points out one sperm nucleus, the red arrow points towards a dead, empty pollen, the dark blue arrow shows a wild-type pollen, the light blue arrow indicates a pollen which only has a vegetative nucleus. The picture on the very right shows a pollen with fragmented nuclei. Blue – DAPI, green – auto-fluorescence of the pollen wall

In Col-0 wt pollen all three nuclei could be seen: 1 big one, the vegetative nucleus (yellow arrow in fig. 3-44), and two smaller, more densely staining nuclei, the two sperm nuclei (white arrow in fig. 3-44). The same was true for pollen from *RAD51C*$^{+/-}$ plants. In pollen from *rad51c*$^{-/-}$ plants, no nucleus was seen inside the pollen grain. These pollen are dead (red arrow in fig. 3-44). Several different situations can be found in pollen from *XRCC3*$^{+/-}$ plants (lower row of pictures in fig. 3-44). Some pollen showed all three nuclei (left picture, dark blue arrow), some only the vegetative nucleus (light blue arrow) and some pollen were ruptured and empty (red arrow). The fourth situation found was striking. Chromosome fragmentation was seen in these pollen (picture on the very right in fig. 3-44). These pollen were not viable and most likely about to die. They might be the ones observed to be staining purple only partially in Alexander staining.

The Non-Mendelian segregation pattern cannot be explained by pollen lethality alone. Still, it would be interesting to evaluate also the female gametophyte.

4.11.2.6. Linkage of RAD51C and XRCC3

By looking at the Mendelian segregation scheme of the 9:3:3:1 ratio, it became clear that the genotypes from heterozygous gametes were more abundant than the other ones (tables 3-14, 17 and 20).

	CX	**Cx**	**cX**	**cx**
CX	CCXX	CCXx	CcXX	CcXx
Cx	CCXx	CCxx	CcXx	Ccxx
cX	CcXX	CcXx	ccXX	ccXx
cx	CcXx	Ccxx	ccXx	ccxx

Table 3-20: Mendelian 9:3:3:1 segregation. Highlighted in yellow are the genotypes which are more abundant in the populations analyzed and their corresponding gametes. C – *RAD51C*, X – *XRCC3*, uppercase – wt allele, lowercase – mutant allele

A very clear pattern emerges, suggesting a physical linkage of those genes. Since *RAD51C* and *XRCC3* are on two different chromosomes (fig. 3-1), they should segregate independently, meaning Mendelian. But T-DNA insertion mutagenesis is not a very clean process. Usually several copies insert, also in inverted orientation. It is also possible, that a translocation event occurred during mutagenesis and physically linked the two genes of interest, *RAD51C* and *XRCC3* (fig. 3-45).

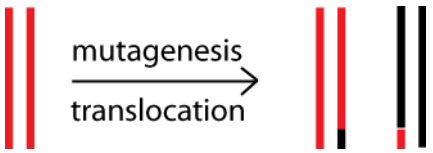

Fig. 3-45: Reciprocal translocation event during T-DNA mutagenesis.

I hypothesized that a translocation during T-DNA mutagenesis linked *RAD51C* and *XRCC3*.

Such a linkage by a translocation would result in gametes as shown in fig. 3-46. From this figure it can be seen that there are two gametes, which are missing one part of one chromosome (the two middle gametes). In *RAD51C*$^{+/-}$ *XRCC3*$^{+/-}$ plants the pollen lethality is roughly about 50% judged by eye and viable pollen counting. I assumed that the gametes which are missing one part of one chromosome result in the observed pollen lethality. This will then lead to one gamete carrying the physical linkage of the two genes, *RAD51C*$^{+}$ *xrcc3*$^{-}$. The other gamete carrying the two genes unlinked, with *rad51c*$^{-}$ on one chromosome and *XRCC3*$^{+}$ on the other one. From this gamete the two

genes can segregate independently. These are the two parental gametes (right and left gamete in fig. 3-46).

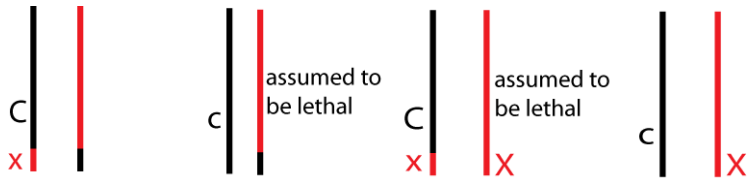

Fig. 3-46: Possible gametes segregating from a reciprocal translocation. Gametes assumed to result in lethality are indicated by text. C – *RAD51C*, X – *XRCC3*, uppercase – wt allele, lowercase – mutant allele, black – chromosome II, red – chromosome V

The other 11 genotypes found can be generated by a cross over event (fig. 3-47). The genotype selected for in the F1 generation is the parent (*RAD51C*$^{+/-}$ *XRCC3*$^{+/-}$). The two black chromosomes undergo a cross over event, unlinking the two wt alleles in one case and linking the two mutant alleles in the other case (right and left gamete in fig. 3-47). The two middle gametes are the parental ones, whereas the left and the right ones are the recombinant gametes. In fact, four more gametes would result from this situation, but as described above, those four gametes are unbalanced as the two middle ones in fig. 3-46, and are therefore assumed to be lethal.

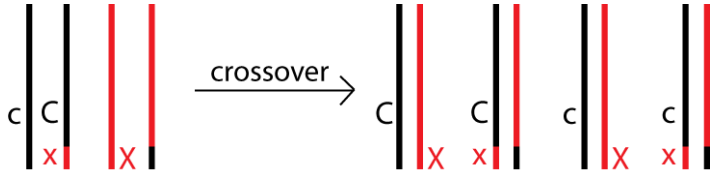

Fig. 3-47: Gametes generated after a cross over event between the black chromosomes. Gametes containing unbalanced chromosomes are assumed to be lethal and not shown. C – *RAD51C*, X – *XRCC3*, uppercase – wt allele, lowercase – mutant allele, black – chromosome II, red – chromosome V

4.11.2.7. Fluorescence *In Situ* Hybridization

To address the question of a translocation we decided to perform a Fluorescence *In Situ* Hybridization (FISH). Therefore we chose three Bacterial Artificial Chromosomes (BACs) for each gene, one BAC spanning the gene and the two flanking BACs. BACs for the locus of *XRCC3* on chromosome V were labelled with biotin and detected with a Texas-Red labelled antibody, producing red fluorescence. BACs for the locus of *RAD51C* on chromosome II were labelled with digoxigenin and detected with an Alexa labelled antibody, producing green fluorescence.

With the help of Ales Pecinka, a post doctoral fellow in the lab of Ortrun Mittelsten-Scheid at GMI, who had all the BACs necessary and the experience, I performed this FISH experiment.

To test the probes they were hybridized to pachytene chromosomes from wt Col-0 plants. As can be seen in fig. 3-48 the two signals (arrows) were far apart and most likely on two different chromosomes, which is hard to tell in pachytene. This is consistent with the current genome annotation of *A. thaliana*.

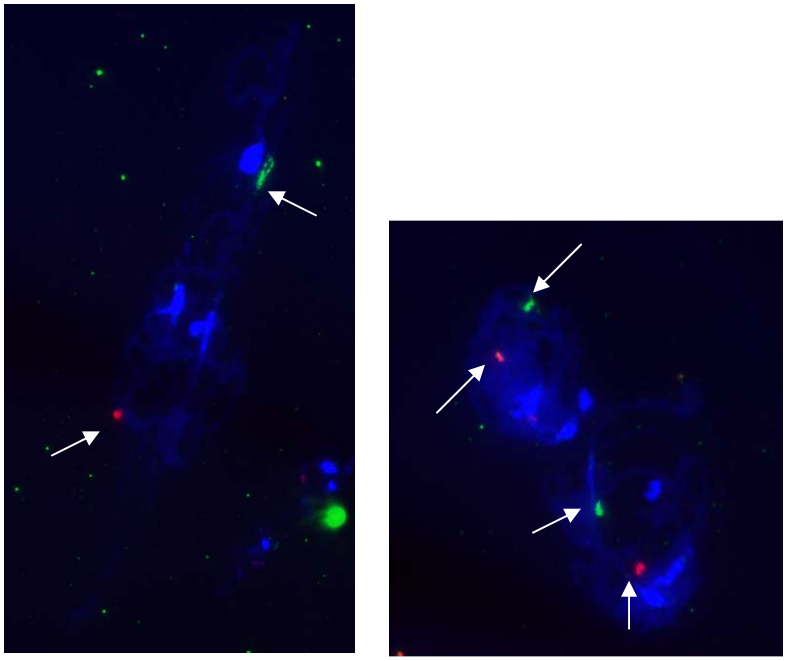

Fig. 3-48: FISH on pachytene chromosomes from wild type Col-0 plants. Arrows point to the specific FISH signals. Red – *XRCC3*, green – *RAD51C*, blue - DAPI

Fig. 3-49 shows two out-segregated *ku70*$^{-/-}$ *xrcc3*$^{-/-}$ nuclei at prometaphase. As can be clearly seen, the two signals were next to each other on one chromosome (white arrows in fig. 3-49). The reciprocal part of the translocation can also be seen (yellow arrows in fig. 3-49). These results proved the existence of a reciprocal translocation in the populations used for analysis.

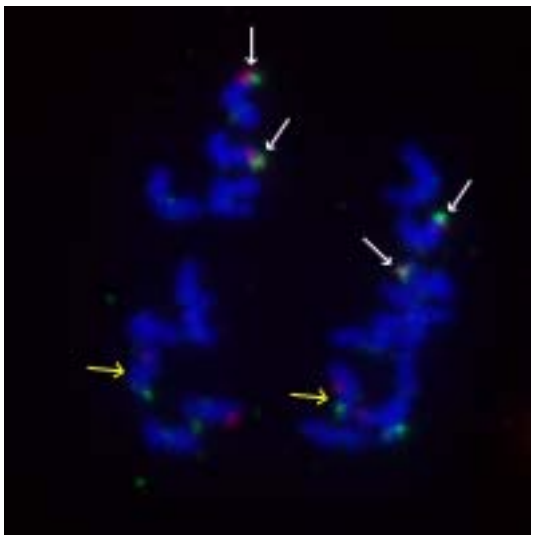

Fig. 3-49: FISH on prometaphase of two out-segregated *ku70*$^{-/-}$ *xrcc3*$^{-/-}$ nuclei. White arrows point to the linking translocation, yellow arrows point towards the chromosomes carrying the reciprocal part of the translocation. Red – *XRCC3*, green – *RAD51C*, blue - DAPI

We wanted to know which mutant line (*rad51c-1* or *xrcc3-1*) carries this translocation. Figure 3-50 shows FISH results from *RAD51C*$^{+/-}$ and *XRCC3*$^{+/-}$ plants. The pictures are quite noisy and the result is preliminary, but it suggests the SALK line for *xrcc3-1* (SALK_045564) and not the *rad51c-1* line as carrier.

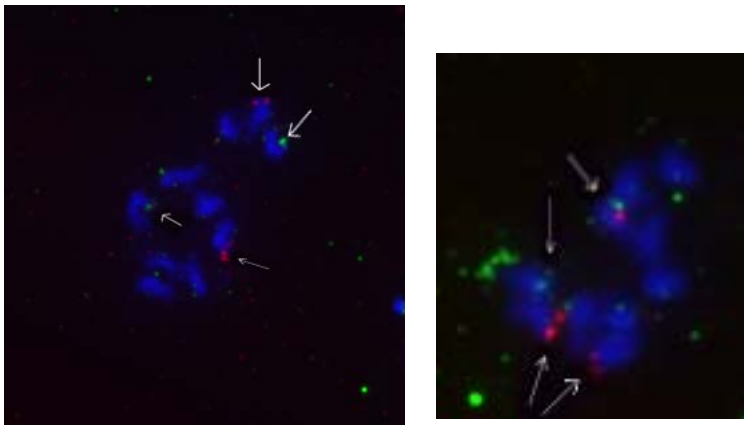

Fig. 3-50: FISH on *RAD51C*$^{+/-}$ (left) and *XRCC3*$^{+/-}$ (right). Arrows point out the specific signals. Red – *XRCC3*, green – *RAD51C*, blue – DAPI

The populations analyzed carry a translocation linking *RAD51C* and *XRCC3*. The SALK line for *XRCC3* seems to be the carrier of the translocation. This also fits the observation of pollen lethality in *XRCC3*$^{+/-}$ plants.

4.11.2.8. Genetic Distance between *RAD51C* and *XRCC3*

The segregation data enabled me to calculate the genetic distance between *RAD51C* and translocated *XRCC3*. Table 3-21 shows highlighted in yellow the parental gametes and genotypes. Recombinant genotypes are on white background. As can be seen from this table, *RAD51C*$^{+/-}$ *XRCC3*$^{+/-}$ plants (CcXx in table 3-21) can result from parental gametes, but also from recombinant gametes. I therefore did not include this genotype

in the calculation, since the ratio by which *RAD51C*$^{+/-}$ *XRCC3*$^{+/-}$ plants resulting from recombinant gametes is not known.

	CX	**Cx**	**cX**	**cx**
CX	CCXX	CCXx	CcXX	CcXx
Cx	CCXx	CCxx	CcXx	Ccxx
cX	CcXX	CcXx	ccXX	ccXx
cx	CcXx	Ccxx	ccXx	ccxx

Table 3-21: Mendelian 9:3:3:1 segregation. Highlighted in yellow are the parental genotypes and their corresponding gametes. C – *RAD51C*, X – *XRCC3*, uppercase – wt allele, lowercase – mutant allele

Since segregation of *RAD51C* with *XRCC3* is independent of *KU*, summing up of all populations analyzed, either on *ku70*$^{-/-}$ background or not, is possible (table 3-22). The yellow bars highlight the genotypes resulting from parental gametes, excluding *RAD51C*$^{+/-}$ *XRCC3*$^{+/-}$.

This results in 61 plants having a genotype resulting form recombinant gametes and 204 plants with a genotype resulting from parental gametes.

		Number of plants		**probability**	
n=510		**Mendel**	**Observed**	**Mendel**	**Observed**
RAD51C$^{+/+}$	***XRCC3***$^{+/+}$	31,88	2	0,063	0,004
RAD51C$^{+/+}$	***XRCC3***$^{+/-}$	63,75	18	0,125	0,035
RAD51C$^{+/-}$	***XRCC3***$^{+/+}$	63,75	17	0,125	0,033
RAD51C$^{+/-}$	***XRCC3***$^{+/-}$	127,50	245	0,250	0,480
rad51c$^{-/-}$	*XRCC3*$^{+/+}$	31,88	93	0,063	0,182
rad51c$^{-/-}$	***XRCC3***$^{+/-}$	63,75	10	0,125	0,020
RAD51C$^{+/+}$	*xrcc3*$^{-/-}$	31,88	111	0,063	0,218
RAD51C$^{+/-}$	***xrcc3***$^{-/-}$	63,75	14	0,125	0,028
rad51c$^{-/-}$	***xrcc3***$^{-/-}$	31,88	0	0,063	0,000

table 3-22: Summed up segregation pattern of the crosses *RAD51C*$^{+/-}$ x *XRCC3*$^{+/-}$, *XRCC3*$^{+/-}$ x *RAD51C*$^{+/-}$ and *ku70*$^{-/-}$ *RAD51C*$^{+/-}$ x *ku70*$^{-/-}$ *XRCC3*$^{+/-}$. Yellow bars highlight the two genotypes resulting from parental gametes used for calculation of the genetic distance.

The translocation resulted in a genetic distance between *RAD51C* and translocated *XRCC3* of 23.01 cM.

4.11.2.9. Summary of the *ku70*$^{-/-}$ *RAD51C*$^{+/-}$ x *ku70*$^{-/-}$ *XRCC3*$^{+/-}$ cross

I was not successful to obtain a *ku70*$^{-/-}$ *rad51c*$^{-/-}$ *xrcc3*$^{-/-}$ triple mutant, since first: The two genes became linked in the *XRCC3-1* mutant line, therefore reducing the possibility of obtaining the triple mutant to the probability of a cross over event. Secondly, a lethality of the *rad51c*$^{-/-}$ *xrcc3*$^{-/-}$ double and the *ku70*$^{-/-}$ *rad51c*$^{-/-}$ *xrcc3*$^{-/-}$ triple mutant

cannot be ruled out. In order to make a statement on this combination of mutants, the crosses need to be repeated with another allele of *XRCC3*, which needs to be tested for this particular translocation prior to use.

The following two tables summarize the analyses and experiments I performed in this thesis.

Gene	Allele	line	reference	Ecotype	multiplex set up	Designed primer	Seeds	Telomere length	t-Circles	Crossed to
AtKU70	-1		(Riha, Watson et al. 2002)	Ws	Yes	No	+/+ +/- -/-	n. d.	Present	*atmus81-2* $^{-/-}$ *AtMUS81-3* $^{+/-}$
AtMRE11	-3	SALK_054418	(Puizina, Siroky et al. 2004)	Col-0	Yes	No	+/-	n. d.	n. d.	*AtRAD51C* $^{+/-}$
AtRAD51	-1	GABI_134A01	(Li, Chen et al. 2004)	Col-0	Yes	no	no	n. d.	n. d.	
AtRAD51C	-1	SALK_021960	(Bleuyard, Gallego et al. 2005)	Col-0	Yes	Yes	+/-	n. d.	n. d.	*AtMRE11* $^{+/-}$ *AtXRCC3* $^{+/-}$
AtXRCC2	-1	SALK_029106	(Bleuyard, Gallego et al. 2005)	Col-0	yes	Yes	no	n. d.	n. d.	
AtXRCC3	-1	SALK_045564	(Bleuyard and White 2004)	Col-0	Yes	Yes	+/-	n. d.	n. d.	*AtRAD51C* $^{+/-}$
AtFAS1	-4		(Kirik, Pecinka et al. 2006)	C24	No genotyping	No genotyping	+/- -/-	Wt range	absent	
AtAPOLLO	-1	GABI_236D05		Col-0	Yes	Yes	+/- G1 -/-	Wt range	n. d.	
AtBARD1	-1	SALK_097601	(Reidt, Wurz et al. 2006)	Col-0	Not tested	Yes	Bags	n. d.	n. d.	*AtKU80* $^{+/-}$
	-2	SALK_031862		Col-0	Not tested	Yes	bags	n. d.	n. d.	*AtKU80* $^{+/-}$
AtMUS81	-2	SALK_107515	(Hartung, Suer et al. 2006)	Col-0	Not tested	Yes	-/-	n. d.	n. d.	*AtKU70* $^{+/-}$
	-3	SALK_002176		Col-0	yes	yes	+/-	n. d.	n. d.	*AtKU70* $^{+/-}$
AtWEX	-1	SALK_003278		Col-0	No	Yes	+/- -/-	n. d.	n. d.	

Table 3-23: Summary of Genes used and performed Analyses and crosses. n. d. – not determined

♀	♂	Seeds	Segregation	t-circles
AtRAD51C $^{+/-}$	*AtXRCC3* $^{+/-}$	F1, F2	Non-Mendelian	n. d.
AtXRCC3 $^{+/-}$	*AtRAD51C* $^{+/-}$	F1, F2	Non-Mendelian	n. d.
AtRAD51C $^{+/-}$	*AtMRE11* $^{+/-}$	F1, F2	n. d.	n. d.
AtMRE11 $^{+/-}$	*AtRAD51C* $^{+/-}$	F1, F2	n. d.	n. d.
AtBARD1-1 $^{+/-}$	*AtKU80* $^{+/-}$	F1	n. d.	n. d.
AtKU80 $^{+/-}$	*AtBARD1-1* $^{+/-}$	F1	n. d.	n. d.
AtBARD1-2 $^{+/-}$	*AtKU80* $^{+/-}$	F1	n. d.	n. d.
AtKU80 $^{+/-}$	*AtBARD1-2* $^{+/-}$	F1	n. d.	n. d.
atmus81-2 $^{-/-}$	*AtKU70* $^{+/-}$	F1, F2	Non-Mendelian	n. d.
AtKU70 $^{+/-}$	*atmus81-2* $^{-/-}$	F1, F2	n. d.	n. d.
AtMUS81-3 $^{+/-}$	*AtKU70* $^{+/-}$	F1	n. d.	n. d.
AtKU70 $^{+/-}$	*AtMUS81-3* $^{+/-}$	F1	n. d.	n. d.
atku70 $^{-/-}$*, AtRAD51C* $^{+/-}$	*atku70* $^{-/-}$*, AtRAD51* $^{+/-}$	F3	Mendelian	present
atku70 $^{-/-}$*, AtRAD51C* $^{+/-}$	*atku70* $^{-/-}$*, AtXRCC2* $^{+/-}$	F2	Mendelian	present
atku70 $^{-/-}$*, AtXRCC2* $^{+/-}$	*atku70* $^{-/-}$*, AtRAD51* $^{+/-}$	F2 triple heterozygote	Mendelian	present
atku70 $^{-/-}$*, AtMRE11* $^{+/-}$	*atku70* $^{-/-}$*, AtRAD51* $^{+/-}$	F3	Mendelian	present
atku70 $^{-/-}$*, AtMRE11* $^{+/-}$	*atku70* $^{-/-}$*, AtRAD51C* $^{+/-}$	F2, F3	Non-Mendelian	n. d.
atku70 $^{-/-}$*, AtRAD51C* $^{+/-}$	*atku70* $^{-/-}$*, AtXRCC3* $^{+/-}$	F3	Non-Mendelian	present

Table3-24: Summary of crosses and results of TCA. T-circles refers to results of the triple mutant, except for the *ku70*$^{-/-}$ *RAD51C*$^{+/-}$ x *ku70*$^{-/-}$ *XRCC3*$^{+/-}$ cross, where no triple mutant was obtained and the combinations *ku70*$^{-/-}$ *RAD51C*$^{+/-}$ *XRCC3*$^{+/-}$ and *ku70*$^{-/-}$ *RAD51C*$^{+/-}$ *xrcc3*$^{-/-}$ were tested. n. d. – not determined

Discussion

1. FAS1

As described, the *fas1-4* mutant has a very clear growth phenotype of fasciation and dwarfism. Using the published data by Kirik et al 2006 (Kirik, Pecinka et al. 2006) I designed primers for genotyping. But the first genotyping results showed, that even in the mutant plants, a wild type sized amplification product was yielded. This could mean that either the primers designed were misplaced, or that the insertion site was mapped wrong. As it turned out, the lab of Bernd Reiss also has no clear genotyping set up (personal communication between Karel Riha and Bernd Reiss). This might hint to the miss-mapping of the insertion. Since the *fas1-4*$^{-/-}$ plants showed such a clear phenotype and we were only interested in the mutants, we decided to pick the plants only according to their phenotype.

Our hypothesis that the hyperrecombinogenic phenotype of the loosened chromatin structure of *fas1-4*$^{-/-}$ mutants is sufficient for t-circle formation and/or change in telomere length was not correct. In fact telomeres are C24 wt length and I was unable to detect a clear t-circle signal. Taken together these results show that the T-loop is still protected even though the HR machinery is stimulated a 100 fold compared to wild type and the chromatin structure is loosened up.

2. *BARD1*

We chose the *bard1*$^{-/-}$ mutant since, in contrast to *fas1-4*$^{-/-}$, shows a hyporecombination phenotype (Reidt, Wurz et al. 2006). I hypothesized a reduction of t-circle formation in a *ku70*$^{-/-}$ *bard1*$^{-/-}$ double mutant. So far we have obtained seeds from the F1 plants but the F2 population has not been analyzed by the end of this thesis.

3. *MUS81*

MUS81 was chosen since it showed endonuclease activity on Holliday junctions (Constantinou, Chen et al. 2002; Blais, Gao et al. 2004). Two mutant *MUS81* alleles were crossed to *KU70*$^{+/-}$. One of the alleles, *mus81-3*, was not described before and *mus81-2* was characterized before (Hartung, Suer et al. 2006). Hartung et al. showed that the mutants only exhibited a phenotype under treatment with Mitomycin C (MMC).

In comparison to wt which showed a 23.6 fold induction of HR upon MMC treatment, *mus81-2*$^{-/-}$ plants only exhibited an 11.9 fold induction. MMC interferes with DNA synthesis. HR is a possible repair pathway for stalled replication forks. The sensitivity to MMC and the reduced induction of HR are in concurrence with the biochemical data on MUS81. MUS81 has been shown to have a strong endonuclease activity on 3' flap structures (Constantinou, Chen et al. 2002; Blais, Gao et al. 2004). Such structures occur in stalled replication forks.

Upon treatment with Bleomycin, a radiomimetic agent which introduces DNA DSBs, *mus81-2*$^{-/-}$ plants showed a 33.7 fold induction of HR compared to a 60.5 fold induction in wt plants (Hartung, Suer et al. 2006). This result implicates MUS81 in DNA DSB repair.

Our working hypothesis was that t-circles are the result of T-loop resolution by a homologous recombination event. If MUS81 is the long seeked eukaryotic Holliday junction resolvase, than we would expect to see suppression of t-circle formation in a *ku70*$^{-/-}$ *mus81*$^{-/-}$ double mutant.

The crossing of *mus81-2*$^{-/-}$ to *KU70*$^{+/-}$ plants was successful and one population of F2 plants was analyzed. Surprisingly only one *mus81*$^{-/-}$ plant was recovered. I also did not obtain a *ku70*$^{-/-}$ *mus81*$^{-/-}$ double mutant and therefore was unable to analyze the role of MUS81 in t-circle formation.

Since this population was grown at the very end of this thesis, this combination of mutants was not regrown. Analysis of more plants have do be done to verify the observed Non-Mendelian segregation and to try to obtain a double mutant to be tested for t-circle formation.

4. Genotyping of *RAD51C*

The SALK line SALK_021960 carries a T-DNA insertion that disrupts the gene *atRAD51C*. It was characterized in three different papers, Bleuyard et al. 2004 (Bleuyard, Gallego et al. 2005), Li et al. 2005 (Li, Yang et al. 2005) and Abe et al. 2005 (Abe, Osakabe et al. 2005). Bleuyard et al. and Abe et al. mapped the insertion at the end of exon three, whereas Li et al. mapped the insertion between exon 2 and exon 3 in intron 2. By testing several primers available in the lab, I could exclude the presence of the insertion in intron 2. The forward primer used had its binding site downstream of the

insertion site described in Li et al. (Li, Yang et al. 2005). I also sequenced the LBs from different amplification products, which were cut out of a gel. The sequencing result was not very clear; it seemed that more than one sequence was present in the sample. Nonetheless a read out of sufficient quality long enough was achieved to map the insertion to the site described by Bleuyard et al. and Li et al.

5. Triple Mutant *ku70*$^{-/-}$ *rad51c*$^{-/-}$ *rad51*$^{-/-}$

The presence of t-circles in the triple mutant not only excludes a resolvase activity of RAD51C and RAD51 as was shown before (Zellinger, Akimcheva et al. 2007), it also excludes redundancy between *RAD51* and *RAD51C*.

Knock out of *RAD51C* leaves a DX2 fragment of the BCDX2 complex. This DX2 complex was shown to have a very weak Holliday junction resolution activity similar to RuvC (Liu, Masson et al. 2004). In comparison, the BC fragment has a 5 fold higher activity and the complete BCDX2 complex an 8 fold higher Holliday junction resolution activity. These results suggest high redundancy of the proteins in this complex.

T-circles could still be formed due to endonuclease activity of one of the other proteins present in the BCDX2 and CX3 complexes.

6. Triple Mutant *ku70*$^{-/-}$ *rad51c*$^{-/-}$ *xrcc2*$^{-/-}$

Presence of t-circles in the triple mutant excludes Holliday junction resolvase activity by the BCDX2 complex. XRCC3 was shown to be essential for t-circle formation in human colon carcinoma cell line (Wang, Smogorzewska et al. 2004). With this triple mutant combination we cannot exclude the possibility that XRCC3 resolves the T-loop, and is therefore essential for t-circle formation.

The fact that I could not even detect reduction of the t-circle signal suggests the presence of a major endonuclease. This could be XRCC3 but also MUS81 or an unidentified endonuclease.

7. Triple Mutant *ku70*$^{-/-}$ *xrcc2*$^{-/-}$ *rad51*$^{-/-}$

In this triple mutant a BC complex and the complete CX3 complex are still present. Both have been shown to have a Holliday junction resolution activity (Liu, Masson et

al. 2004). T-circle formation in this triple mutant is not unexpected but we can exclude a major role of XRCC2 in t-circle formation. The results suggest non-redundancy between *RAD51* and *XRCC2*.

8. Triple Mutant *ku70$^{-/-}$ mre11-3$^{-/-}$ rad51$^{-/-}$*

T-circles are still formed in the triple mutant. This suggests that genes necessary for early steps in HR are not required for t-circle formation.

9. Combination of *ku70$^{-/-}$ mre11-3$^{-/-}$ rad51c$^{-/-}$*

No triple mutant was obtained. The population showed Non-Mendelian segregation. This was due to a bias against *mre11$^{-/-}$*. In contrast, *rad51c$^{-/-}$* plants were more abundant. The Non-Mendelian segregation of the population is due to Non-Mendelian segregation of both single loci. From the other combinations of mutants described above, we knew that the single loci usually show Mendelian segregation.

The severe growth phenotype of the two *ku70$^{-/-}$ mre11$^{-/-}$ RAD51C$^{+/-}$* plants obtained suggests haploinsufficiency of RAD51C in *mre11$^{-/-}$* mutants. It is therefore very likely that the triple mutant combination is synthetically lethal. RAD51C also seems to be important in repair of the chromosomal instabilities resulting of the *mre11$^{-/-}$* mutation. This is in concurrence with the role of RAD51C in DNA repair.

Alexander staining revealed pollen lethality in *MRE11$^{+/-}$ RAD51C$^{+/-}$* plants. It is possible that male gametophytes with the genotype *mre11^{-} rad51c^{-}* die. Staining of pollen from a *MRE11$^{+/-}$* plants also showed some pollen lethality. Additionally, pollen carrying the *mre11^{-}* allele might have a certain lethality rate.

We did not investigate the female gametophytes. Since we found genotypes which can only occur if a *mre11^{-} rad51c^{-}* gametophyte is involved, those gametophytes might be viable on the female side, but this is speculation.

The reason for the Non-Mendelian segregation is clearly a bias against *mre11$^{-/-}$*. Whether this is KU dependent or not is still unclear, since the control population was not analyzed by the end of this thesis. The cause of the observed pollen lethality is also still unclear.

Taken the results together they suggest a genetic interaction between *MRE11* and *RAD51C*. Further investigations on this combination will definitely bring interesting results.

10. Combination of *ku70*$^{-/-}$ *rad51c*$^{-/-}$ *xrcc3*$^{-/-}$

As with the combination of *ku70*$^{-/-}$ *MRE11*$^{+/-}$ *RAD51C*$^{+/-}$ the triple mutant was never obtained. The populations also showed Non-Mendelian segregation. But unlike the combination described above, the single loci exhibited Mendelian segregation. Therefore, the Non-Mendelian segregation was due to combining the two mutations. As it turned out the two loci got linked. The translocation which caused the linkage most likely happened during T-DNA mutagenesis. FISH analysis suggests a reciprocal translocation. Since we don't know anything about the size and the exact position of the translocation, all the lethality phenomena observed might be due to this translocation event. Pollen lethality and FISH analysis suggest the SALK line for *xrcc3-1*, SALK_045564, as the carrier of the translocation.

Therefore this cross needs to be repeated with another allele of *XRCC3*.

The TCA result on a *ku70*$^{-/-}$ *RAD51C*$^{+/-}$ *xrcc3*$^{-/-}$ plant revealed presence of t-circles. It seemed that there is no reduction in t-circle formation.

Taken these results together we cannot say anything about the genetics of the two genes and we cannot exclude a synthetic lethality of *rad51c*$^{-/-}$ *xrcc3*$^{-/-}$. Repeating the crosses with another *XRCC3* allele is definitely necessary to answer the question about genetics, synthetic lethality and t-circle formation.

11. Summary on Triple Mutant Combinations

The data presented in this thesis are the first genetic data on the BCDX2 and CX3 complexes. We could show that RAD51 and RAD51C are not redundant and we could also show that RAD51C and XRCC2, two members of the BCDX2 complex, are not redundant.

Several studies have shown that the CX3 complex does not only have an early role in HR, but also a late role (Liu, Masson et al. 2004; Wang, Smogorzewska et al. 2004; Liu, Tarsounas et al. 2007). Wang et al. have shown that XRCC3 is important for t-circle formation in human cell cultures by complementation and knock downs. The

biochemical study by Liu Yilun et al. has recently tested recombinant RAD51C and XRCC3 if they behave the same as the cell extracts do. The recombinant proteins fail to build the high molecular DNA-protein complex as bacterial RuvA does. But they still did not show any assay on Holliday junction cleavage with the reconstituted recombinant proteins. In their discussion they point out that attempts to show Holliday junction resolution activity with the reconstituted recombinant CX3 complex have failed so far (Liu, Tarsounas et al. 2007).

Therefore the triple mutant *ku70*$^{-/-}$ *rad51c*$^{-/-}$ *xrcc3*$^{-/-}$ would allow us to show two things: (1) If the t-circles are repressed we would know that the CX3 complex is the resolvase and (2) this would prove that the t-circles are formed due to a homologous recombination event.

It is necessary to repeat this cross with another *XRCC3* allele to try to obtain the triple mutant.

The Non-Mendelian segregation of the combination of *MRE11* and *RAD51C* was surprising. Future studies on this combination will provide interesting insights into the HR pathway. Also there is still no data on t-circle formation in this combination of mutants.

Taken all the results together suggest that the T-loop is a very special nucleoprotein structure which might need a cascade of endonucleases to be resolved. Loss of certain protein interactions might also be necessary to enable this cascade to start and/or to continue.

Future crosses and analysis of the last two discussed populations will definitely teach us something more about the HR pathway and about t-circle formation.

12. Postulation and Future Experiments

The structure of the T-loop can be drawn differently as depicted in figure 4-1. As reviewed in Haber and Heyer (Haber and Heyer 2001), the Mus81-Eme1 complex was shown biochemically to cut at the site indicated in figure 4-1 (orange arrow). Three studies suggest a resolving role for the CX3 complex (Liu, Masson et al. 2004; Wang, Smogorzewska et al. 2004; Liu, Tarsounas et al. 2007). Wang et al. have shown that XRCC3 is essential for t-circle formation in TRF2$^{\Delta B}$ cells. Liu et al. has shown that RAD51C and XRCC3 are found in fractions of a HeLa cell extract that exhibits

Holliday junction resolution activity (Liu, Masson et al. 2004). Recombinant CX3 complexes have failed to form a high molecular weight nucleoprotein complex as is the case with bacterial RuvA (Liu, Tarsounas et al. 2007). Data on Holliday junction resolution activity of this complex is missing.

In order to resolve the T-loop a second endonuclease would be necessary, since the Mus81-Eme1 complex only cuts one strand in this structure. Due to the three studies about RAD51C and XRCC3 involvement in t-circle formation and Holliday junction resolution, I postulate the CX3 complex to be the endonuclease cutting the second strand (black arrow in fig. 4-1).

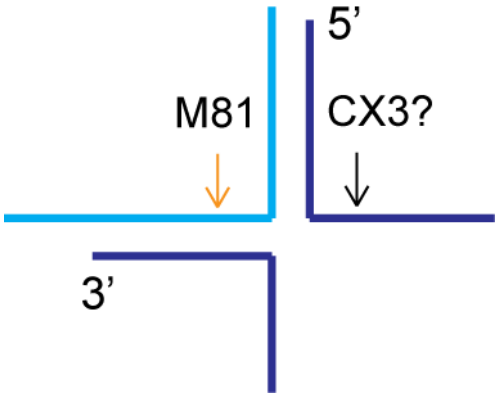

Fig. 4-1: Postulated model of the proteins necessary for T-loop resolution. 3' indicates the invaded 3' G-overhang. The orange arrow indicates the restriction site for the Mus81-Eme1 complex. The black arrow shows the second restriction site for T-loop resolution. I postulate the CX3 complex to be the endonuclease necessary. M81 – Mus81-Eme1 complex, CX3 – CX3 complex

In order to test this postulation, *ku70*$^{-/-}$ *mus81*$^{-/-}$ double mutants would need to be analyzed for presence of t-circles. In this thesis I failed to generate this required double mutant.

Secondly, a *ku70*$^{-/-}$ *rad51c*$^{-/-}$ *xrcc3*$^{-/-}$ triple mutant needs to be generated and tested for the presence of t-circles. The cross described in this thesis would need to be repeated with another *XRCC3* mutant allele to generate the triple mutant.

Materials and Methods

1. Plant materials

1.1. Insertion lines and growth conditions

Plants were grown on soil at 22°C with a 16h/8h light/dark photoperiod in an environmentally controlled growth chamber. When plants were about 3 weeks old, leaves were taken for DNA extraction for genotyping. At the age of about 6 weeks, DNA was extracted for TCA or TRF (see below). Inflorescences of plants for propagation were wrapped in paper bags when the first siliques became brown or dry. The seeds were then harvested in these bags and transferred to Eppendorf tubes and were stored at room temperature.

Table 1 gives a list of all T-DNA insertion lines used.

Allele	AGI code	Insertion line	reference
atku70-1	At1G16970	Wisconsin line	(Riha, Watson et al. 2002)
atku80-1	At1G48050	JF46-4	(Friesner and Britt 2003)
atmre11-3	At5G54260	SALK_054418	(Puizina, Siroky et al. 2004)
atrad51-1	At5G20850	GABI_134A01	(Li, Chen et al. 2004)
atrad51c-1	At2G45280	SALK_021960	(Bleuyard, Gallego et al. 2005)
atxrcc2-1	At5g64520	SALK_029106	(Bleuyard, Gallego et al. 2005)
atxrcc3-1	At5G57450	SALK_045564	(Bleuyard and White 2004)
atmus81-2	At4G30870	SALK_107515	(Hartung, Suer et al. 2006)
atmus81-3	At4G30870	SALK_002176	
atbard1-1	At1G04020	SALK_097601	(Reidt, Wurz et al. 2006)
atbard1-2	At1G04020	SALK_031862	(Reidt, Wurz et al. 2006)
atapollo-1	At1G27410	GABI_236D05	
atfas1-4	At1G65470		(Kirik, Pecinka et al. 2006)
atwex-1	At4G13870	SALK_003278	

Table 1: List of T-DNA insertion lines used

1.2. Crossings

As soon as the plants chosen for crossings flowered, siliques on the stem from mother-plants were removed and the largest, still closed floral buds were used for crossing. Smaller floral buds were removed. Under a preparative microscope those buds were carefully opened. Opened flowers from father-plants were taken and the pollen was put

onto the carpel of the opened floral buds of the mother-plant. The stem carrying the crossed buds was taped to a stick and marked. Silique formation was monitored and all seeds from those siliques were harvested. Seeds from the uncrossed part of the plant could also be collected on demand.

1.3. Fixation of Floral Buds for Cytology

Inflorescences were taken off the plant with forceps and put into 1 ml of 3:1 fixative (3 parts 96% ethanol, 1 part acetic acid) for 2 hours. Then the fixative was changed for incubation over night. If the fixative was greenish, it was changed again. Fixed inflorescences were stored directly in the fixative at -20°C.

2. DNA work

2.1. DNA extraction “PCR-grade”

2.1.1. Low throughput

Leaves from plants were grinded with pistils in 400 µl extraction buffer (0.2 M Tris.HCl pH-7.5, 0.25 M NaCl, 0.5% SDS, 25 mM EDTA), debris was spun down for 5 min at 16000g at room temperature. 350 µl of supernatant were mixed with 350 µl of 2-propanol. After 10 min at room temperature, DNA was spun down with 16000g for 5 min at room temperature. The pellet was washed once with 70% ethanol, air dried and re-suspended in 30 µl TE buffer (10 mM Tris.HCl pH-8.0, 1 mM EDTA) at 65°C for 20 min. The extracted DNA can then be stored at +4°C or for long term at -20°C.

2.1.2. High throughput

Juvenile leaves of plants were grinded two times with a metal bead in 500 µl extraction buffer (0.2 M Tris.HCl pH-7.5, 0.25 M NaCl, 0.5% SDS, 25 mM EDTA) at 30 Hz at room temperature in a microtiter plate. The debris was spun down with 3148g for 20 min at room temperature (20°C). 350µl supernatant was taken off and mixed with 350 µl 2-propanol in a fresh microtiter tube. DNA was precipitated for about 20 min and spun down with 3148g for 20 min at room temperature (20°C) followed by washing once with ice cold 70% ethanol and dried at 55°C for 15 min. The pellet was then re-suspended in 30 µl TE buffer (10 mM Tris.HCl pH-8.0, 1 mM EDTA) at 65°C for 20 min. The DNA can then be stored at +4°C and for long term at -20°C. 2 x 96 samples could be handled in parallel with this method.

2.2. Genotyping

The PCR reaction mix contained 2 µl of the “PCR grade” extracted DNA, 1x PCR buffer (500 mM KCl, 200 mM Tris.HCl pH-8.3, 1.7 mg BSA/ml), 0.2 mM of each dNTP, 1.5 mM $MgCl_2$, and 1 µM of each primer and 0.2µl of homemade taq-polymerase. The list of primer combinations, annealing temperatures and numbers of cycles for genotyping is given in table 2.

Allele	Wt – allele	LB1	LB 2	Annealing temperature [°C]	# of cycles
atku70-1	ku_2, ku_11 (939bp)	ku_11, LB-cd6 (639bp)	n.p.	60	35-40
atku80-1	ku80_20, ku80_21 (630bp)	ku80_20, Gus1 (1150bp)	n.t.	55	35
atmre11-3	mre_1, mre_3 (701bp)	mre_1, LBc-1 (470bp)	mre_3, LBc-1 (490bp)	60	35-40
atrad51-1	rad51_1, rad51_2 (912bp)	rad51_1, rad51T-DNA (295bp)	n.t.	58	35
atrad51c-1	rad51c_5, rad51c_8 (639bp)	rad51c_5, LBc-1 (807bp)	n.d.	60	30
atxrcc2-1	xrcc2_7, xrcc2_8 (531bp)	xrcc2_7, LBc-1 (607bp)	xrcc2_8, LBc-1 (205bp)	55	35
atxrcc3-1	xrcc3_3, xrcc3_8 (230bp)	n.d.	xrcc3_2, LBc-1 (365bp)	60	30
atmus81-2	mus81_1, mus81_2 (961bp)	mus81_1, LBc-1 (960bp)	mus81_2, LBc-1 (379bp)	50	40
atmus81-3	mus81_3, mus81_4 (853bp)	mus81_3, LBc-1 (806bp)	mus81_4, LBc-1 (503bp)	55	35
atbard1-1	bard_1, bard_2 (1025bp)	bard_2, Lbc-1 (816bp)	n.t.	60	35
atbard1-2	bard_1, bard_2 (1025bp)	bard_2, Lbc-1 (551bp)	n.t.	60	35
atapollo-1	apollo_1, apollo_2 (991bp)	apollo_1, Gabi_1 (655bp)	apollo_2, Gabi_1 (1262bp)	60	35
atwex-1	wex_1, wex_2 (876bp)	wex_1, Lbc-1 (250bp)	wex_2, LBc-1 (900bp)	60	30

Table 2: Primer combinations used for genotyping n.p. – not present, n.d. – not detected with this set up, n.t. – not tested

The standard PCR programme was 94°C for 3 min, each cycle following ran 94°C for 15 sec, annealing temperature for 30 sec, 72°C for 1 min and after finishing the last cycle 5 min at 72°C were added before the reaction was stopped by cooling to 8°C until the sample was used.

Table 3 lists all primers used.

name of primer	sequence
LB-cd6	GAA CAT CGG TCT CAA TGC AA
LBc-1	TGG ACC GCT TGC TGC AAC TCT
Gabi-1	GAT GTT AGG CCA GGA CTT TGA A
GUS1	TCC CAC CAA CGC TGA TCA AT
rad51TDNA	CCC ATT TGG ACG TGA ATG TAG ACA C
ku_2	ACT CAG ACA AAG CCG TGA TGG TT
ku_11	ACT TGG GAT AGC TCT TCC ACA GTA
rad51c_5	ACT TGG GAT AGC TCT TCC ACA GTA
rad51c_8	GGA GAT GAC ATA CCA ATC TCT
rad51c_4	GAT AAC ATT TTG GGC GGT G
rad51c_7	GAT TTG CTC GGT GTA ACT GCA
xrcc3_2	CTA CGC TTG AAC CGC ACA AAT C
xrcc3_8	GTT GTT CCT TCT TTA GGC TTG
xrcc3_3	GGA TTT GGT TGA AAC TTC TGA TGG
xrcc3_5	GCT CTG TAC CCA ACT TCC GAT TT
xrcc3_6	TAA CCA AGA GGA GGA ATC CGA AAA
Ku80_20	CAA CAA TTC CAA CTT CAT CAT ACT T
Ku80_21	TCT TCC AGC ACA ACT CCT CA
pcr_rad51_1	GGT TCC ATC ACG GAG TTA TAT GG
pcr_rad51_2	ACG CAT GAT ATT CCC ACC AAT C
xrcc2_7	ATC TAG CAA GCT GAC AGG AAG AAT T
xrcc2_8	GGA AGT TTG AGA TGA AGC GAC TAT A
mre_1	CCA ATG GAT GAG GCC TGA AGT T
mre_3	GTC TGC CAC CAC CAT AAC AT
mre11_12	CCA TTC CAG ATA CCT CCT TCA A
apollo_1	CCA TCG ATG CTC ACC ACT GT
apollo_2	GAC ACC ACA ATT CCT TTC ATG C
wex_1	CTC ACC ATT TGA TTC GAA TTC C
wex_2	CAA TAA GAT GTT GGA GAC TTT GAG G
bard_1	TAT TCA CAT TTT CTC CCG CTT AAT C
bard_2	GGC AGC ATC ATA CTC TGA TTC AAA
mus81_1	CCT TAT GGT GCC CTT GAC TTG TAT T
mus81_2	TGG TTC CAT CTG ATG CCA ACT ATA
mus81_3	CAT ACG TTT TTG GTT CCC GTT AA
mus81_4	CCC TTT CTC TGG CCT AGT CAA AA

Table 3: List of primers used

2.3. Gel electrophoresis

0.8 – 1.6% agarose gels were used for analysis of PCR products and TRF (see below). According amounts of agarose were weighted and boiled in 1x TAE in the microwave. The mixture was cooled down to approximately 60°C, 0.5 µl ethidiumbromide (1 g/100 ml stock)/100 ml gel were added and the gel was poured into a prepared tray in an electrophoresis chamber. After solidification the gel was put into 1x TAE (40 mM Trisacetate, 1 mM EDTA) in the electrophoresis chamber, combs were pulled out and the samples were loaded after mixing them with 6x loading buffer (60% glycerol, 10 mM Tris.HCl pH-7.5, 60 mM EDTA, 0.03% Bromphenolblue), together with a marker.

I usually used 5 µl of the Fermentas GeneRuler™ 1kb DNA ladder. Bands were visualized using the Eagle Eye GelDoc System from BioRad.

2.4. DNA extraction “high grade”

2.4.1. Ren’s Protocol

2-3 plants of the same genotype were shock frozen and grinded in liquid nitrogen. The fine powder was then transferred into 50 ml Falcon tubes containing 30 ml of pre-cooled extraction buffer (63.77 g Sorbitol/l, 100 mM Tris.HCl pH-7.5, 5 mM EDTA), mixed and centrifuged at 2424g for 10 min at 4°C. The supernatant was discarded and the pellet was resuspended in 1.25 ml of extraction buffer and transferred into a fresh 15 ml Greiner tube. 1.75 ml of nuclei lysis buffer (200 mM Tris.HCl pH-8, 50 mM EDTA, 2 M NaCl and 2 g CTAB/100 ml) as well as 0.6 ml of 5% sarcosyl (L-Lauroyl, w/V) were added, mixed, and after addition of 40 µl of 10 mg RNase/ml, RNA was digested for 25 min at 65°C in a waterbath. After RNA digest 7.5 ml of a 24:1 $CHCl_3$ – Isoamylalcohol mixture was added for DNA extraction. Phases were separated by centrifuging with 2424g for 10 min at room temperature. The aqueous phase was transferred into a fresh 15 ml Greiner tube and DNA was precipitated by addition of 2 ml 2-propanol. DNA was pelleted by centrifugation at 2424g for 10 min at room temperature. The pellet was washed once with 70% ethanol and transferred into an Eppendorf tube, where it was air dried. DNA was resuspended in 400 µl H_2O and extracted with a 25:24:1 Tris.HCl pH-8.0 buffered phenol/$CHCl_3$/Isoamylalcohol mixture until a clear phase border was observed. DNA was then precipitated from the aqueous phase by adding 800 µl 96% ethanol and 40 µl of CH_3COONa at -20°C for at least 30 min. By centrifugation at 16100 g for 10 min at room temperature, the DNA was pelleted, then washed once with 70% ethanol, air dried and resuspended in 100 µl TE (10 mM Tris.HCl pH-8, 1 mM EDTA). DNA could then be stored short term at +4°C or at -20°C for long term. Usually 1 µl was checked for quality and quantity on a 0.8% agarose gel.

2.4.2. CTAB extraction method

Single plants were shock frozen and grinded in liquid nitrogen. The fine powder was transferred into a 15 ml Greiner tube containing 4 ml of 2x CTAB buffer (1.4 M NaCl, 0.2 g CTAB/10 ml, 100 mM Tris.HCl pH-8, 20 mM EDTA), mixed and incubated at 65°C for 30 min. DNA was then extracted with an equal amount of 25:24:1 Tris.HCl pH-8.0 buffered phenol/$CHCl_3$/Isoamylalcohol mixture, and precipitated from the aqueous phase with 0.8 volumes of 2-propanol. By centrifuging at 3148g for 30 min at room temperature DNA was pelleted and washed with 70% ethanol. The pellet was resuspended in 200 µl TE (10 mM Tris.HCl pH-8, 1 mM EDTA). DNA could then be stored short term at +4°C or at -20°C for long term.

3. Enzymatic treatments

3.1. Restriction digest with *Tru1*I

Approximately 500 ng of CTAB extracted DNA was digested with 20 units of Tru1I from Fermentas in buffer R™ over night at 65°C in a total volume of 100 µl. Digested DNA was precipitated with 100 µl 96% ethanol and 10 µl 3 M CH_3COONa at -20°C for at least 30 min. The pellet was washed once with 70% ethanol and resuspended in a corresponding volume of H_2O.

3.2. Restriction digest with *Alu*I

Approximately 500 ng of Ren's extracted DNA was digested with 20 units of AluI from Fermentas in buffer Tango™ over night at 37°C in a total volume of 100 µl. Digested DNA was precipitated with 100 µl 96% ethanol and 10 µl 3 M CH_3COONa at -20°C for at least 30 min. The pellet was washed once with 70% ethanol and resuspended in a corresponding volume of H_2O.

4. Telomere assays

4.1. Terminal Restriction Fragment (TRF)

CTAB extracted DNA was Tru1I digested and resuspended in 20 µl of H_2O. A long (>20 cm) 0.8% agarose gel was poured and the DNA was loaded onto the gel after mixing with 6x loading buffer (60% glycerol, 10 mM Tris.HCl pH-7.5, 60 mM EDTA, 0.03% Bromphenolblue). Gels were run over night at about 70 V (2 V/cm). The gel was stained in an ethidiumbromide solution and a picture was taken using the Eagle Eye GelDoc System from BioRad to check for equal loading. The gel was analysed in a Southern blot (see below).

4.2. Telomeric Circle Amplification (TCA)

4.2.1. Primer annealing and phi29 reaction

Ren's extracted DNA was digested with AluI and resuspended in 15.5 µl H_2O. For primer annealing this DNA was mixed with 2.5 µl of 10 µM 5'-Thio-$(CCCTAAA)_3$ oligo and 2 µl of 10x annealing buffer (200 mM Tris.HCl pH-7.5, 200 mM KCl, 1 mM EDTA) in a PCR tube. The annealing mixture was heated for 5 min at 96°C to denature DNA and annealing occurred during cool down to room temperature. The annealing mixture is then split into two PCR tubes. To both parts of the sample 9.5 µl of a premix (1x Phi buffer (Fermentas), 0.1 mM dNTPs) were added. To one part 0.5 µl (5 units) phi29-DNA-Polymerase (Fermentas) was added, whereas the other part was substituted with 0.5 µl of H_2O. The phi29 reaction was carried out in a PCR cycler for 16 h at 30°C followed by 20 min at 65°C for enzyme inactivation.

4.2.2. Alkaline gel electrophoresis

1.2 g of agarose were boiled with 150 ml H_2O in the microwave and the gel was brought to 55°C in a waterbath. For alkalization 750 µl of 10 M NaOH and 300 µl of 0.5 M EDTA were added and the gel was poured in an appropriate electrophoresis chamber. After solidification The electrophoresis chamber was filled with alkaline running buffer (50 mM NaOH, 1 mM EDTA pH-8) and samples were loaded after mixing with 6x alkaline loading buffer (50 µl of 6x loading buffer + 1.5 µl 10 M NaOH and 0.6 µl of 0.5 M EDTA). The gel was run for 15-17 h at 25V. The gel was analysed in a Southern blot.

5. Detection methods

5.1. Southern Blot

The TRF or TCA gel is soaked in 0.25 M HCl for 10 min, rinsed with water and then soaked in denaturizing solution (1.5 M NaCl, 0.5 M NaOH) for 30 min. After rinsing

with water the gel is neutralized with neutralizing solution (1.5 M NaCl, 0.5 M Tris.HCl pH-7.0) for 15 min. 3 MM filter papers (Wattman) and the membrane (Hybond NX, Amersham Biosciences) were equilibrated in 10x SSC (1.5 M NaCl, 150 mM sodium citrate) prior to setting up the transfer pyramid. One filter paper was placed onto a stack of paper towels together with the wet, marked membrane. The neutralized gel was placed on top of the wet membrane and bubbles were removed. Two additional filter papers were placed bubble free onto the gel and a 10x SSC wet sponge was put on top. DNA was transferred for 4-6h and then cross-linked to the membrane in a Strata cross linker.

5.2. Southern Hybridization

5.2.1. Labelling of an oligonucleotide probe

For detection of telomeric sequence a G-strand probe (a C-strand was generated in a TCA) $(TTTAGGG)_4$ was end-labelled with γ-^{32}P (>3000 Ci/mmol). Therefore 10 pmol of the oligo was mixed with 1 unit of PNK (Fermentas) in 1x PNK buffer™ (Fermentas) and 5 µl of γ-^{32}P (>3000 Ci/mmol) in 20 µl reaction volume. The reaction was run at 37°C for 20 min. The labelled oligo was purified by the Nucleotide Removal Kit from Qiagen following the company's protocol.

5.2.2. Hybridization

For hybridization the membrane was pre-hybridized for 30 min to 2 h in 20 ml of hybridization buffer (0.25 M Na-phosphate buffer, 7% SDS and 0.1 g BSA) at 55°C in the hybridization oven. The labelled oligo was then added and hybridization was run over night. After hybridization buffer containing the labelled probe was poured into a 50 ml Falcon tube and frozen for further use. The membrane was then washed twice for 10 min at 55°C with 2x SSC (300 mM NaCl, 30 mM sodium citrate) containing 0.1 % SDS. Stringent washing at 55°C for 30 min followed with 0.2x SSC (30 mM NaCl, 3 mM sodium citrate) containing 0.1% SDS. The membrane was then wrapped into Saran foil and checked with a Geiger counter for presence and intensity of a radioactive signal.

5.2.3. Detection

The wrapped and checked membrane was then placed with the radioactive side up into a photographic cassette and an erased Kodak Phosphor Screen (Amersham) was placed with the white side down onto the membrane and the cassette was closed. Depending on the intensity of the radioactive signal exposure could last from a few hours to several days. The detected signals were then visualized with a Phospho Imager (Biorad) and the screen was then erased by light exposure.

6. Cytology

6.1. Alexander Staining

Floral buds which were just about to open were taken off the plant and put into Alexander stain (10 ml 96% ethanol, 1 ml 1% malachite green in ethanol, 50 ml of distilled water, 25 ml glycerol, 5 g phenol, 5 g chloral hydrate, 5 ml 1% acid fuchsin in water, 0.5 ml of 1% orange G in water, 4 ml glacial acetic acid just before usage) and anthers were dissected. A cover slip was applied bubble-free and fixed with fixing gum.

Slides were kept in the dark over night for differential staining to develop. Alexander stain also worked as a fixative and slides could be stored at room temperature in the dark.

6.2. DAPI staining of Pollen

Inflorescences were washed 2x with water followed by washing in 1x citrate buffer (4 mM citric acid, 6 mM tri-sodium citrate) pH 4.6 two times for 5 min. Anthers were dissected from fixed floral buds, if possible from opened ones. 20 µl of enzymatic solution (0.5% cellulase, (Sigma), 0.5% pectolyase (Sigma) in 1x citrate buffer) were put onto the dissected anthers and incubated for 10 min at 37°C in a wet chamber. The reaction was stopped by replacement of the enzyme mix and addition of cold 1x citrate buffer. Citrate buffer was removed and 45% acetic acid was added and when the white colour of the anthers was gone, a cover slip was applied, a piece of filter paper put on top and the slide was squashed slightly with the rubber end of a pencil to release the pollen from the anthers. The slide was shock frozen in liquid nitrogen, the cover slid chopped off and the slide was post-fixed in 3:1 fixative for 10 min. After air drying 8 µl of DAPI solution (2 mg/ml Vectashield®) was applied and the slide was analysed under an epi-fluorescent microscope.

6.3. Fluorescence In Situ Hybridization (FISH)

Table 4 lists the BACs (Bacterial Artificial Chromosomes) used for FISH analysis and the affiliated gene.

BAC	Gene	Antibiotic	Label	Antibody label
$T_{14}P_1$	upstream of *RAD51C*	Chloramphenicol	Digoxigenin	Alexa 488 ex: 499 nm em: 520 nm
F_4L23	*RAD51C*	Kanamycin		
$F_{17}K_2$	downstream of *RAD51C*	Kanamycin		
MJB24	upstream of *XRCC3*	Kanamycin	Biotin	Texas Red ex: 596 nm em: 613 nm
MSF19	*XRCC3*	Kanamycin		
MUA2	downstream of *XRCC3*	Kanamycin		

Table 4: BACs used, their antibiotic selector and corresponding labels. ex – excitation wave length, em – emission maximum wave length

6.3.1. Isolation of BACs

Bacteria transformed with BACs from a glycerol stock were taken and plated onto LB – medium (1% peptone, 0.5% yeast extract, 1% NaCl, 1.5% agar-agar) containing the selection antibiotic (30 mg chloramphenicol/l, 50 mg kanamycin/l). Plates were incubated upside down over night at 37°C. Until further use, plates were stored at +4°C. Single colonies were picked and put into 3 ml of LB medium containing 150 µg of the corresponding selection antibiotic. Tubes were incubated over night at 250 rpm and 37°C. Cells were harvested by centrifugation at 12000g for 1 min at +4°C. The cell pellet was resuspended in 100 µl ice cold solution 1 (50 mM glucose, 25 mM Tris.HCl pH-8, 10 mM EDTA pH-8) and 200 µl freshly prepared solution 2 (0.2 M NaOH,

1% SDS) were added for alkaline cell lysis and the mixture was incubated for 5 min on ice. 150 µl of ice cold solution 3 (3 M CH_3COOK, 20 mM CH_3COOH, pH-6.9) were added, mixed and incubated for another 5 min on ice. DNA was extracted with 450 µl phenol:$CHCl_3$ 1:1 and phases were separated by centrifugation at 12000g for 5 min at +4°C. 420 µl of supernatant were transferred into a new Eppendorf tube and DNA was precipitated by addition of 840 µl of 96% ethanol for 2 min. DNA was pelleted by centrifugation at 12000g for 5 min at +4°C. The pellet was washed once with 1 ml of 70% ethanol and air dried for 10 – 30 min. DNA was resuspended in 35 µl of H_2O containing 10 µg RNase/ml and the mixture was incubated at 37°C for 10 – 30 min for RNA digestion. The sample was then stored at -20°C until further use.

6.3.2. Labelling of BAC probes

The amount of DNA isolated from each BAC was estimated in a gel electrophoresis. Always three BACs (table 4) were labelled for one gene. 1 µg of each BAC was mixed with 5 µl NT buffer (0.5 M Tris.HCl pH-7.5, 50 mM $MgCl_2$, 0.05% BSA), 5 µl 0.1 M mercaptoethanol, 5 µl of dNTP mix (0.5 mM dATP, dGTP, dCTP, 0.1 mM dTTP), 1 µl DNase (1:250 dilution), 1 µl PolI and 4 µl of the corresponding labelled dUTP (Biotin label for *XRCC3* affiliated BACs, Digoxigenin for *RAD51C* affiliated BACs) in a total reaction volume of 50 µl. The reaction mix was incubated for 1.5 h at 16°C and the efficiency of the digestion was checked on an agarose gel. If digestion was sufficient the enzyme was inactivated at 65°C for 10 min and DNA was precipitated over night with 115 µl 96% ethanol and 4.5 µl 3 M CH_3COONa. DNA was pelleted by centrifugation at 16100g for 30 min at +4°C, washed once with 70% ethanol and taken up in 30 µl of 100% deionised foramide.

6.3.3. Slide preparation

Fixed floral buds were rinsed twice for 5 min with sterile water followed by washing in 1x citrate buffer (4 mM citric acid, 6 mM tri-sodium citrate) pH 4.6 two times for 5 min. The floral buds were then incubated with an enzyme mixture (0.3% cellulase, 0.3% pectylase, 0.3% cytohelicase in citrate buffer) for 1.5h in a moist chamber at 37°C. One floral bud of appropriate size was then put onto a clean slide and chopped with a needle until a milky suspension was produced. 2x 15 µl of 60% acetic acid were put onto the slide and the mixture was stirred carefully without touching the surface of the slide on a hot block at 45°C for 40 – 60 sec. Then, 2x 100 µl of 3:1 fixative were placed around the droplet of acetic acid and the excessive solution was removed by tilting the slide. The slide was then dried with a cold air blowing hair drier and the preparation checked under a phase contrast microscope. Good preparations were post-fixed for 10 min in 4% formaldehyde in water. Slides were air dried and stored at +4°C until further usage.

6.3.4. Pepsin treatment of slides

Slides were DAPI stained and the quality of the slide was checked under an epi-fluorescence microscope. Slides were chosen and digestion time with Pepsin was estimated. For Pepsin treatment immersion oil was washed off with water and the slides were put into 2x SSC (300 mM NaCl, 50mM sodium citrate) until the cover slip fell off. Then, slides were washed twice for 5 min in 2x SSC. Slides were put into the Pepsin solution (250 µl Pepsin (10mg/ml) in 50 ml 10 mM HCl) for 2-5 min at 38°C in a waterbath. Slides were then washed twice for 5 min in 2x SSC, followed by post-fixation for 10 min in 4% formaldehyde in 2x SSC at room temperature. Slides were

again washed twice for 5 min in 2x SSC and dehydrated in an ethanol row of 70%, 90% and 96% ethanol and were air dried.

6.3.5. Hybridization

10 µl of the pool of three labelled BACs affiliated with one gene were mixed with 10 µl 20% dextransulfate in 4x SSC. 20 µl of this mixture were placed on large cover slips which were taken up with the pepsin treated slide and put on the hot block for 2 min at 80°C for denaturation. Hybridization was performed over night in a wet chamber at 37°C.

6.3.6. Detection

Cover slips were thrown off the slides with a slight movement and slides were rinsed three times for 5 min at 42°C in SF50 (50% formamide in 2x SSC pH-7.0), followed by washing twice for 5 min in 2x SSC at 42°C. After a 5 min washing step at 42°C in 4T (4x SSC, 0.05% Tween-20) the slides were incubated for 30 min in blocking buffer (5% BSA, 0.2% Tween-20, 4x SSC) at 37°C in a wet chamber. After the blocking step the slides were again rinsed for 5-10 min in 4T at 42°C and were then incubated with Avidin~Texas Red (1:1000 in blocking buffer) at 37°C for 30 min. Slides were rinsed twice for 5 min in 4T at 42°C, followed by washing for 5 min in TNT (100 mM Tris.HCl pH-7.5, 150 mM NaCl, 0.05% (v/v) Tween-20). Primary antibodies goat-anti-avidin~biotin (1:200 in incubation buffer (1% BSA, 4x SSC, 0.1% Tween-20)) and mouse-anti-digoxigenin (1:250 in incubation buffer) were incubated on the slides at 37°C for 30 min in a wet chamber. Slides were rinsed 3 times 5 min in TNT at 42°C. Slides were then incubated with Avidin~Texas Red (1:1000 in incubation buffer) and the secondary antibody goat-anti-mouse Alexa 488 (1:200 in incubation buffer) for 30 min at 37°C in a wet chamber. Slides were again rinsed 3 times 5 min in TNT at 42°C and dehydrated in an ethanol series of 70%, 90% and 96% for 2 min each and air dried. Slides were DAPI stained and analysed under an epi-fluorescence microscope.

6.4. Microscopy

Slides were analyzed under a Zeiss Axio epi-fluorescence microscope. Pictures for FISH were taken with a 1.4 Megapixel single channel camera (Visitron Systems) at 1000x magnification and were merged using the Colour Align tool of the MetaVue software version 7.0r3. For Alexander stainings a three channel camera (Visitron Systems) was utilized also under a Zeiss Axio epi-fluorescence microscope at 40x magnification.

7. Statistics

To examine differences between expected and observed segregation patterns we utilized the χ^2 – Test (chi^2 test). The Chi-Square test is a statistical test which computes the probability that there is no significant difference between the expected frequency of an occurrence with the observed frequency of that occurrence (source: http://www.brendan.com/glossary.html#c).

$$\chi^2_{n-1} = \sum_{i=1}^{n} \frac{(O_i - E_i)^2}{E_i}$$

n total number of observations

n-1 degrees of freedom

O_i Observed number of trait i

E_i Expected number of trait i

H_0 states that there is no difference between the observed and the expected distribution.

For segregation analysis of 2 loci there are 8 degrees of freedom (9 possible genotypes). For an error probability of 5% (α=0.05) the critical value for the χ^2 – Test is 15.51 (http://de.wikibooks.org/wiki/Mathematik:_Statistik:_Tabelle_der_Chi-Quadrat-Verteilung).

For analysis of 1 Locus, there are 2 degrees of freedom (3 possible genotypes). For α=0.05 the critical value for the χ^2 – Test is 5.99.

If the the χ^2 – value is above the critical value H_0 is discarded, meaning that there is a significant difference between the observed and the expected distribution.

Acknowledgements

I thank Karel Riha for giving me the opportunity to do my diploma thesis in his lab. I also thank Barbara Zellinger for her patient supervision and proofreading of this manuscript. Further I'd like to thank Ales Pecinka for his help with the FISH experiments. My thank goes also to all members of the Riha lab who were all very helpful and open for discussions.

Appendix I: Zusammenfassung

Telomere sind die Enden von linearen Chromosomen. Ihre Hauptfunktion ist zu verhindern, dass die Enden als DNS DoppelStrangBrüche (DSB) erkannt werden. In höheren Eukaryonten geschieht dies durch die T-loop Struktur. Bei dieser Struktur invasiert das einzelsträngige 3' Chromosomenende die doppelsträngige telomerische DNS. Es wird angenommen, dass dazu die Maschinerie der Homologen Rekombination (HR) benötigt wird. Anders als bei einem DNS Reperaturereignis wird der T-loop jedoch nicht aufgelöst. Wie dieses unterschiedliche Verhalten entsteht wird noch nicht verstanden. Proteine der HR Maschinerie, wie der MRN Komplex (MRE11-RAD50-NBS1) sind auch am Telomer zu finden. RAD51 und die BCDX2 (RAD51B-RAD51C-RAD51D-XRCC2) und CX3 (RAD51C-XRCC3) Komplexe sind notwending für den Schritt der Stranginvasion während der HR. Manche Studien schlagen auch eine Rolle der BCDX2 and CX3 Komplexe in der Auflösung der Zwischenstrukturen der HR vor. Doch obwohl es biochemische Daten zu diesen zwei Komplexen gibt, sind keine genetischen Daten vorhanden. Die Rolle der beiden Komplexe im Stoffwechsel des T-loops sind unbekannt. In dieser Diplomarbeit verwendete ich *Arabidopsis thaliana* als Modellorganismus, um genetische Grundlagen der telomerischen Rekombination zu untersuchen. Mutaten in einem der fünf Gene, welche die BCDX2 and CX3 Komplexe bilden sind in Pflanzen vital. In Mäusen hingegen sind Mutationen in *RAD51C* und *XRCC2* embryolethal. In dieser Diplomarbeit presentieren wir die ersten Daten über genetische Interaktionen zwischen den Genen, die für die Proteine der BCDX2 and CX3 Komplexe kodieren. Weiters untersuchten wir die Rolle von RAD51 und MRE11 im Stoffwechsel des T-loops. Um auf funktionelle Redundanzen innerhalb der BCDX2 and CX3 Komplexe zu testen, erzeugten wir Tripelmutanten mit *ku70*$^{-/-}$. In dieser Mutante enstehen extrachromosomale, telomerische Ringe (t-circles), welche zur Betrachtung der HR an Telomeren verwendet werden können. Ich testete sechs verschiedene Mutantenkombinationen und konnte vier davon erzeugen. In diesen vier Tripelmutanten waren t-circles vorhanden. Ich scheiterte daran *rad51c-1 xrcc3-1 ku70-1* und *mre11-3 rad51c-1 ku70-1* Tripelmutanten zu erzeugen. Die Segregationsanalyse enthüllte Nicht-Mendelische Segregation der F2 Populationen beider Mutantenkombinationen. Weitere Analysen brachten eine Translokation zum Vorschein, welche für das Nicht-Mendelische Verhalten der *rad51c-1 xrcc3-1* Mutantenkombination verantwortlich war. Diese Translokation verband die beiden

Gene physisch. Im Falle der *mre11-3 rad51c-1* Mutantenkombination kennen wir den Grund für das Nicht-Mendelische Verhalten noch nicht. Um dies zu erklären werden weitere Experimente benötigt.

Appendix II: References

Abe, K., K. Osakabe, et al. (2005). "Arabidopsis RAD51C gene is important for homologous recombination in meiosis and mitosis." Plant Physiol **139**(2): 896-908.

Alexander, M. P. (1969). "Differential staining of aborted and nonaborted pollen." Stain Technol **44**(3): 117-22.

Aravind, L. and E. V. Koonin (2001). "Prokaryotic homologs of the eukaryotic DNA-end-binding protein Ku, novel domains in the Ku protein and prediction of a prokaryotic double-strand break repair system." Genome Res **11**(8): 1365-74.

Baer, R. and T. Ludwig (2002). "The BRCA1/BARD1 heterodimer, a tumor suppressor complex with ubiquitin E3 ligase activity." Curr Opin Genet Dev **12**(1): 86-91.

Bennett, B. T. and K. L. Knight (2005). "Cellular localization of human Rad51C and regulation of ubiquitin-mediated proteolysis of Rad51." J Cell Biochem **96**(6): 1095-109.

Blais, V., H. Gao, et al. (2004). "RNA interference inhibition of Mus81 reduces mitotic recombination in human cells." Mol Biol Cell **15**(2): 552-62.

Bleuyard, J. Y., M. E. Gallego, et al. (2005). "Differing requirements for the Arabidopsis Rad51 paralogs in meiosis and DNA repair." Plant J **41**(4): 533-45.

Bleuyard, J. Y. and C. I. White (2004). "The Arabidopsis homologue of Xrcc3 plays an essential role in meiosis." Embo J **23**(2): 439-49.

Bundock, P. and P. Hooykaas (2002). "Severe developmental defects, hypersensitivity to DNA-damaging agents, and lengthened telomeres in Arabidopsis MRE11 mutants." Plant Cell **14**(10): 2451-62.

Cesare, A. J., N. Quinney, et al. (2003). "Telomere looping in P. sativum (common garden pea)." Plant J **36**(2): 271-9.

Constantinou, A., X. B. Chen, et al. (2002). "Holliday junction resolution in human cells: two junction endonucleases with distinct substrate specificities." Embo J **21**(20): 5577-85.

D'Amours, D. and S. P. Jackson (2002). "The Mre11 complex: at the crossroads of dna repair and checkpoint signalling." Nat Rev Mol Cell Biol **3**(5): 317-27.

de Lange, T. (2004). "T-loops and the origin of telomeres." Nat Rev Mol Cell Biol **5**(4): 323-9.

de Lange, T. (2005). "Shelterin: the protein complex that shapes and safeguards human telomeres." Genes Dev **19**(18): 2100-10.

Downs, J. A. and S. P. Jackson (2004). "A means to a DNA end: the many roles of Ku." Nat Rev Mol Cell Biol **5**(5): 367-78.

Fisher, T. S. and V. A. Zakian (2005). "Ku: a multifunctional protein involved in telomere maintenance." DNA Repair (Amst) **4**(11): 1215-26.

Friesner, J. and A. B. Britt (2003). "Ku80- and DNA ligase IV-deficient plants are sensitive to ionizing radiation and defective in T-DNA integration." Plant J **34**(4): 427-40.

Griffith, J. D., L. Comeau, et al. (1999). "Mammalian telomeres end in a large duplex loop." Cell **97**(4): 503-14.

Haber, J. E. (1998). "The many interfaces of Mre11." Cell **95**(5): 583-6.

Haber, J. E. and W. D. Heyer (2001). "The fuss about Mus81." Cell **107**(5): 551-4.

Hanahan, D. and R. A. Weinberg (2000). "The hallmarks of cancer." Cell **100**(1): 57-70.

Hartung, F., S. Suer, et al. (2006). "The role of AtMUS81 in DNA repair and its genetic interaction with the helicase AtRecQ4A." Nucleic Acids Res **34**(16): 4438-48.

Joenje, H. and K. J. Patel (2001). "The emerging genetic and molecular basis of Fanconi anaemia." Nat Rev Genet **2**(6): 446-57.

Kanaar, R., J. H. Hoeijmakers, et al. (1998). "Molecular mechanisms of DNA double strand break repair." Trends Cell Biol **8**(12): 483-9.

Kirik, A., A. Pecinka, et al. (2006). "The chromatin assembly factor subunit FASCIATA1 is involved in homologous recombination in plants." Plant Cell **18**(10): 2431-42.

Kuznetsov, S., M. Pellegrini, et al. (2007). "RAD51C deficiency in mice results in early prophase I arrest in males and sister chromatid separation at metaphase II in females." J Cell Biol **176**(5): 581-92.

Lenain, C., S. Bauwens, et al. (2006). "The Apollo 5' exonuclease functions together with TRF2 to protect telomeres from DNA repair." Curr Biol **16**(13): 1303-10.

Li, B., S. P. Jog, et al. (2008). "WRN controls formation of extrachromosomal telomeric circles and is required for TRF2{Delta}B-mediated telomere shortening." Mol Cell Biol.

Li, B. and A. J. Lustig (1996). "A novel mechanism for telomere size control in Saccharomyces cerevisiae." Genes Dev **10**(11): 1310-26.

Li, W., C. Chen, et al. (2004). "The Arabidopsis AtRAD51 gene is dispensable for vegetative development but required for meiosis." Proc Natl Acad Sci U S A **101**(29): 10596-601.

Li, W., X. Yang, et al. (2005). "The AtRAD51C gene is required for normal meiotic chromosome synapsis and double-stranded break repair in Arabidopsis." Plant Physiol **138**(2): 965-76.

Lin, Z., H. Kong, et al. (2006). "Origins and evolution of the recA/RAD51 gene family: evidence for ancient gene duplication and endosymbiotic gene transfer." Proc Natl Acad Sci U S A **103**(27): 10328-33.

Liu, Y., J. Y. Masson, et al. (2004). "RAD51C is required for Holliday junction processing in mammalian cells." Science **303**(5655): 243-6.

Liu, Y., M. Tarsounas, et al. (2007). "Role of RAD51C and XRCC3 in genetic recombination and DNA repair." J Biol Chem **282**(3): 1973-9.

Masson, J. Y., M. C. Tarsounas, et al. (2001). "Identification and purification of two distinct complexes containing the five RAD51 paralogs." Genes Dev **15**(24): 3296-307.

Miller, K. A., D. Sawicka, et al. (2004). "Domain mapping of the Rad51 paralog protein complexes." Nucleic Acids Res **32**(1): 169-78.

Mimori, T., M. Akizuki, et al. (1981). "Characterization of a high molecular weight acidic nuclear protein recognized by autoantibodies in sera from patients with polymyositis-scleroderma overlap." J Clin Invest **68**(3): 611-20.

Puizina, J., J. Siroky, et al. (2004). "Mre11 deficiency in Arabidopsis is associated with chromosomal instability in somatic cells and Spo11-dependent genome fragmentation during meiosis." Plant Cell **16**(8): 1968-78.

Reidt, W., R. Wurz, et al. (2006). "A homologue of the breast cancer-associated gene BARD1 is involved in DNA repair in plants." Embo J **25**(18): 4326-37.

Ridgway, P. and G. Almouzni (2000). "CAF-1 and the inheritance of chromatin states: at the crossroads of DNA replication and repair." J Cell Sci **113 (Pt 15)**: 2647-58.

Riha, K. and D. E. Shippen (2003). "Ku is required for telomeric C-rich strand maintenance but not for end-to-end chromosome fusions in Arabidopsis." Proc Natl Acad Sci U S A **100**(2): 611-5.

Riha, K., J. M. Watson, et al. (2002). "Telomere length deregulation and enhanced sensitivity to genotoxic stress in Arabidopsis mutants deficient in Ku70." Embo J **21**(11): 2819-26.

Schlacher, K. and M. F. Goodman (2007). "Lessons from 50 years of SOS DNA-damage-induced mutagenesis." Nat Rev Mol Cell Biol **8**(7): 587-94.

Shen, X., H. Xiao, et al. (2003). "Modulation of ATP-dependent chromatin-remodeling complexes by inositol polyphosphates." Science **299**(5603): 112-4.

Thacker, J. and M. Z. Zdzienicka (2004). "The XRCC genes: expanding roles in DNA double-strand break repair." DNA Repair (Amst) **3**(8-9): 1081-90.

van Gent, D. C., J. H. Hoeijmakers, et al. (2001). "Chromosomal stability and the DNA double-stranded break connection." Nat Rev Genet **2**(3): 196-206.

van Nocker, S. (2003). "CAF-1 and MSI1-related proteins: linking nucleosome assembly with epigenetics." Trends Plant Sci **8**(10): 471-3.

van Overbeek, M. and T. de Lange (2006). "Apollo, an Artemis-related nuclease, interacts with TRF2 and protects human telomeres in S phase." Curr Biol **16**(13): 1295-302.

Wang, R. C., A. Smogorzewska, et al. (2004). "Homologous recombination generates T-loop-sized deletions at human telomeres." Cell **119**(3): 355-68.

Watson, J. M. and D. E. Shippen (2007). "Telomere rapid deletion regulates telomere length in Arabidopsis thaliana." Mol Cell Biol **27**(5): 1706-15.

West, S. C. (2003). "Molecular views of recombination proteins and their control." Nat Rev Mol Cell Biol **4**(6): 435-45.

Wu, L., A. S. Multani, et al. (2006). "Pot1 deficiency initiates DNA damage checkpoint activation and aberrant homologous recombination at telomeres." Cell **126**(1): 49-62.

Zellinger, B., S. Akimcheva, et al. (2007). "Ku suppresses formation of telomeric circles and alternative telomere lengthening in Arabidopsis." Mol Cell **27**(1): 163-9.

Zellinger, B. and K. Riha (2007). "Composition of plant telomeres." Biochim Biophys Acta **1769**(5-6): 399-409.

Christian Sailer
Kirchengasse 76
A-7052 Müllendorf
+43676 950 87 76
christian.sailer@gmx.at

EDUCATION

2006 – 2007 **Gregor Mendel Institute** Vienna, Austria

- Diploma Thesis in Karel Rihas lab: "Genetic Analysis of Homologous Recombination at *A. thaliana* Telomeres"

2001 – Present **University of Vienna** Vienna, Austria

- Studying Molecular Biology and Ecology

1996 – 2001 **Secondary College for Chemical Industry, Rosensteingasse** Vienna, Austria

- Graduated with "excellent success" with majors in biochemistry, biotechnology and genetic engineering

2000 – 2001 **University of Vienna** Vienna, Austria

- Diploma Work at Institute for Medical Biochemistry, to graduate the secondary college in practical terms in a team of three candidates for graduation. Topic: "Cloning of a GFP – tagged ERAD Substrate"

WORK EXPERIENCE

1/2005 – 6/2005 **CO-OP Student** at Genome Science Centre Vancouver, Canada

- Working with hazardous blood samples in a biological safety cabinet
- Performing PCR and gel electrophoresis in a high throughput manner
- Literature research, journal club

Summer 2000 – 2002 **Laboratory assistant** at BEIERSDORF GmbH Vienna, Austria

- Quality assurance

2002 – 2004 **Private tutor** Vienna, Austria

- High School Students
- University Students
- Chemistry, mathematics, biochemistry

Summer 1999 **Laboratory assistant** at Water supervision of the Northern Burgenland
Wulkaprodersdorf, Austria

- Testing water samples and calculating water quality

Summer 1998 **Laboratory assistant** at ISOSPORT Eisenstadt, Austria

- In – Line controlling and quality assurance of thermoplastics